Well-to-Wheel Energy, Emissions, and Cost Analysis of Electricity and Fuel Used in Conventional and Electrified Vehicles, and Their Connection to a Sustainable Energy Infrastructure

By

Bryan Anthony Strecker

Submitted to the graduate degree program in Mechanical Engineering and the Graduate Faculty of the University of Kansas in partial fulfillment of the requirements for the degree of Master of Science.

Chair: Dr. Christopher Depcik

Dr. Ronald L. Dougherty

Dr. Bedru Yimer

Dr. Terry Faddis

Defended: November 29, 2012

The Thesis Committee for Bryan Strecker certifies that this is the approved version of the following thesis:

Well-to-Wheel Energy, Emissions, and Cost Analysis of Electricity and Fuel Used in Conventional and Electrified Vehicles, and Their Connection to a Sustainable Energy Infrastructure

By

Bryan Anthony Strecker

Chair: Dr. Christopher Depcik

Acceptance Date

Abstract

Recent legislation by the United States Environmental Protection Agency (EPA) requires record low vehicle tailpipe emissions, necessitating research and development in the areas of lowering conventional (i.e., internal combustion engine) vehicle emissions rates while facilitating the widespread introduction of electrified vehicles. Currently, the EPA views Battery Electric Vehicles as having zero emissions. However, a number of studies illustrate this is not the case when considering the emissions produced in creating the electricity through a full Life Cycle Analysis. As a result, proper comparison of electrified and conventional vehicles must include a complete Well-to-Wheel (WtW) study including the emissions generated through production and use of liquid petroleum and biofuels. As a result, this work provides a full WtW investigation into fuel, electricity, and production analysis of conventional and electrified vehicles. This is supported by a thorough literature review of current and projected future technology, extrapolating to a fleet analysis, as well as applying the technology to an advanced electricity infrastructure.

In the following effort, the first chapter simply provides a background into these different areas in order to help set the stage. Chapter 2 explores conventional vehicle emissions profiles predicting future requirements of engine and catalytic exhaust aftertreatment technologies. Findings illustrate that low temperature climates and aging both adversely affect a vehicle's ability to perform proper emissions reductions. This chapter additionally demonstrates an improvement in the fuel use emissions profiles of Argonne National Laboratories' Greenhouse Gases, Regulated Emissions, and Energy Use in Transportation (GREET) model through the update of embedded time-sheet

emissions lookup tables using EPA's Motor Vehicle Emissions Simulator (MOVES). This simulation package utilizes a statistical database of over 3000 counties in the continental United States in calculating the emissions profile of various vehicle and fuel type combinations, updating the current tables utilized in GREET.

Chapter 3 utilizes these efforts in performing a life cycle analysis of a 1974 Volkswagen Super Beetle converted to a plug-in series hybrid. This work utilizes GREET in exploring the WtW fuel use emissions profile, as well as estimating the energy and emissions savings through reusing a number of stock vehicle components in the conversion. A vehicle dynamics model supports this analysis, calculating the average fuel use in a typical city/highway drive cycle.

The fourth chapter expands upon this work, analyzing an 800+ vehicle fleet in a comparative analysis between electrified vehicles and their conventional counterparts. This work utilizes four simplified vehicle dynamics models, focusing on ten vehicles with various powertrains and fuel use algorithms. These models calculate the average fuel consumption of these vehicles, employing the GREET model in calculating the emissions profiles on a per-mile and yearly total basis. Furthermore, a full cost analysis of fuel and vehicle combinations demonstrates the economic impacts of electrifying the vehicle fleet.

Finally, Chapter 5 seeks to support future research into electrified vehicles for vehicle-to-grid technology, energy storage, and infrastructure control through the design and construction of a small-scale smart grid in collaboration with a previous University of Kansas EcoHawks senior design team. This design consists of a renewable and conventional energy source, a grid load, bulk and dynamic grid storage, and a full

sensory and control system. The final design meets the two requirements of a smart grid set forth by the Department of Energy: decentralization of energy production and storage, and providing two-way communication from end users or appliances and the energy network.

Words: 546.

Table of Contents

Table of Figures

Table of Tables

1.0: Introduction

Since the establishment of the United States Environmental Protection Agency (EPA) in 1970, increasingly stringent regulations on vehicle exhaust emissions have put pressure on automotive manufacturers to explore methods of lowering tailpipe emissions [1]. The most recent regulations include the EPA's Tier 2 emissions standards, which utilize a tiered system in categorizing vehicles by their emissions profiles, as well as introducing a fleet nitrogen oxides (NO_x) requirement [1]. To this end, technological improvements work toward reducing the emissions profiles of conventional internal combustion engine (ICE) powered vehicles, including exploration of novel combustion regimes and the use of exhaust aftertreatment devices. However, continued lowering of regulations from both the EPA and the California Air Resource Board (CARB) make it difficult for even the most technologically advanced ICEs to meet emissions standards. This is because the chemical combustion of fuels including the effects of dissociation will result in emissions, regardless of the combustion process employed (e.g., Low Temperature Combustion).

As a result, the industry is looking toward the electrified vehicle (EV) to reduce tailpipe emissions through the utilization of electricity from batteries effectively reducing or eliminating the use of combustion for propulsion. In this effort, the nomenclature EV refers to any vehicle that contains a battery pack for propulsion purposes. Recent studies on the emissions produced in creating electricity for charging EVs show high emission rates from conventional power plants, such as Gagnon et al.'s investigation of a variety of electricity sources, focusing on emissions profiles and land requirements of hydroelectricity through the use of reservoirs [2]. Furthermore, the introduction of plug-

in hybrid electric vehicles (PHEV) and battery electric vehicles (BEV) are a cause for concern for the current electricity infrastructure and its ability to handle the necessary power grid for charging a large number of EVs [3]. Thus, the efforts in this thesis explore the effects and future requirements of internal combustion engine (ICE) vehicles, EVs, and the required improvements in the energy infrastructure.

2.0: Background

Improvements in ICE vehicles dedicated towards lowering emissions include engine technologies such as exhaust gas recirculation, improvements in engine timing, heightened control over the combustion process, and the use of catalytic aftertreatment devices such as the widely employed three-way catalyst [4]. Because combustion will always result in emissions, the use of the three-way catalyst in spark-ignition engines is critical for reduced exhaust species levels. This device operates by oxidizing carbon monoxide (CO), converting total unburned hydrocarbons (THC), and reducing NO_x to nitrogen and oxygen simultaneously. However, the abilities of the three-way catalyst and many other exhaust aftertreatment device technologies are dependent largely upon two factors: the age of the catalyst, and the light-off temperature required for supporting the chemical reactions of the catalyst (i.e., the temperature at 50% conversion of the chemical species under study) in converting the exhaust emissions to less harmful counterparts [5-8]. Thus, research with these aftertreatment devices include efforts toward reducing aging effects and decreasing the time required to reach the light-off temperature from cold-start [5, 6, 9, 10]. However, even the most recent improvements may not be able to keep up with the emission reduction rates required by the EPA or

CARB. Thus, many manufacturers are introducing EVs in order to meet the future clean transportation requirements.

The simplest EV powertrain is the BEV, which consists of an electric motor, a transmission, and a high-voltage battery pack that stores the electricity. Examples of this type of vehicle include the Nissan LEAF and the Ford Transit Connect EV. Other EV powertrains include both parallel and series hybrid vehicles, which utilize a combination of an electric motor and ICE. Series hybrids, or extended range electric vehicles (EREV), employ an electric motor for vehicle traction, while a small, high efficiency ICE acts as a generator, charging the vehicle's battery pack augmenting the range of the vehicle. This use of an ICE relieves a common hesitation towards BEVs regarding range anxiety [11]. An example of an EREV is the Chevrolet Volt that actively promotes the extended range capability of the vehicle in order to dispel the notion of range anxiety (“electric when you want it, gas when you need it” [12]).

While an EREV acts to utilize the electric motor as the sole means for vehicle movement, parallel hybrids implement a sophisticated electronically continuously variable transmission (ECVT) in utilizing both an electric motor and an ICE for tractive efforts. This technology reduces the torque requirements of ICE in city driving while improving the overall fuel economy of the vehicle. An ICE requires increased rotational speed to generate torque, often resulting in lower fuel efficiency and a slow response time for city driving. Hence, parallel hybrids utilize the electric motor, capable of instantaneous torque, to accelerate the vehicle from a complete stop. Furthermore, the ability of the electric motor to act as a generator allows regenerative braking to recover energy typically dissipated as heat by standard braking systems. Common examples of

parallel hybrids include the Toyota Prius, the Chevrolet Silverado Hybrid, and the Ford Fusion Hybrid. It is important to note that when manufacturers add the designation "plug-in" prior to "hybrid", this simply means that the consumer can plug the vehicle into a standard wall socket or commercial charging station in order to recharge the vehicle's battery pack.

These vehicles boast increased fuel efficiency and reduced use of the ICE, thus lessening total tailpipe emissions. Furthermore, the EPA often views a BEV as a zero emissions vehicle since it does not employ an ICE [13]. However, recent research efforts look into the total emissions produced in creating the electricity for charging from conventional and renewable sources, as well as studying the emissions produced in creating vehicles and their associated components. One example of this Life Cycle Analysis (LCA) is a program created by Argonne National Laboratory(ANL); Greenhouse Gases, Regulated Emissions, and Energy Use in Transportation (GREET) [14]. The GREET 1 series simulates a complete Well-to-Wheels (WtW) fuel analysis, capable of analyzing the fuel cycle from the extraction, refining, and transportation of the fuel feedstock all the way through the combustion of the fuel in the vehicle. Furthermore, GREET investigates the electricity production process, providing an estimated emissions profile of EVs on a grams-per-mile basis [15]. In addition, the GREET 2 series analyzes the creation of the vehicle components (including standard and lightweight materials), EV batteries, and the final assembly processes of the vehicles and their battery packs [16].

ANL separates the GREET fuel analysis into two main areas: Well-to-Pump (WtP), and Pump-to-Wheels (PtW). The WtP analysis simulates the feedstock

extraction, refining, transportation, and fuel production processes, while the PtW analysis models the fuel use in the vehicle. Periodic GREET updates focus largely on the WtP segment while alternatively relying on a relatively stagnant statistical database for the PtW calculations. In particular, this database comes from an older EPA program, MOBILE6.2 [15]. The EPA has since replaced MOBILE6.2 with a new simulation tool, the EPA's Motor Vehicle Emissions Simulator (MOVES) [17]. This simulation package utilizes an emissions database collected from over 3000 counties in the United States [18]. This program is capable of calculating over 30 different emissions from 13 sources, 13 vehicle types, and six fuel types, focusing on fuel use in driving the vehicle [17]. This newest version contains the most recent emissions measurements from across the country, and thus the PtW analysis in GREET is slightly outdated. As a result, this work seeks to improve this GREET PtW analysis with updated emissions profiles developed in MOVES2010b.

Finally, as stated previously, the recent increase in BEVs and PHEVs are a cause for concern for the current energy infrastructure. In particular, the rapid increase in demand for vehicle charging could cause localized power outages. Studies illustrate the ability to reduce this risk through using smart electric metering and smart grid technology, such as Erol-Kantarci's study using a home gateway controller to modulate electricity usage in order to avoid overloading neighborhood transformers [19]. Likewise, studies on the utilization of vehicle-to-grid (V2G) technology demonstrate significant reductions in peak electricity demand by using PHEVs and BEVs as auxiliary power sources during times of high demand [20]. Other studies explore the ability of V2G technology to provide auxiliary renewable energy storage in times of low demand,

saving this clean energy for later use [21]. This work seeks to support this research at the University of Kansas through the creation of a small-scale smart grid capable of meeting the Department of Energy's requirements for a Smart Grid. Furthermore, this effort provides a baseline proof of concept design for a large-scale, building-wide implementation of smart grid technology.

3.0: Previous Efforts at KU

Mechanical Engineering Assistant Professor Dr. Christopher Depcik oversees a mechanical engineering senior design program called the KU EcoHawks, focusing on five tenets of sustainability, referred to as the five E's: Energy, Environment, Economics, Education, and Ethics [22]. This well-rounded view of sustainability provides a foundation for research at the University of Kansas in the areas of automobiles and energy infrastructure. The program utilizes two converted Electrified Vehicles (including a 1974 Volkswagen Super Beetle PHEV and a 1997 GMC Jimmy BEV) as a means for sustainable automotive research. Furthermore, the EcoHawks improve the sustainability of the fuel sources for these vehicles through the utilization of a biodiesel generator in the Beetle and a solar photovoltaic fueling station for recharging both vehicles' battery packs. Thus, the desire exists to explore the emissions profiles of these vehicles on a full WtW basis, as well as to study the energy and emissions savings in utilizing converted vehicles as opposed to manufacturing new vehicles. Furthermore, there is need for research and development in the area of smart grid technology, including system sensing and control, and the implementation of V2G architecture. This thesis documents research in these areas utilizing a thorough

literature review of the technologies currently available, a vehicle and fleet fuel, emissions, and cost analysis, and the development of smart grid technology.

4.0: Thesis Focus

Chapter 2 of this thesis outlines the utilization of the EPA's MOVES package for two efforts: improving the GREET PtW fuel analysis through the creation of new time-sheet emissions databases, and the prediction of future requirements of engine and catalytic aftertreatment technologies in order to keep up with the increasingly stringent vehicle exhaust emissions regulations. Furthermore, this work investigates the effects of catalyst aging and climate on the vehicle's overall emissions profiles along with the ability of the engine and aftertreatment system to work properly. This work provides a baseline for future work with MOVES and GREET in exploring the emissions profiles of future vehicles and fuels at the University of Kansas.

Chapter 3 of this thesis utilizes the information gathered in Chapter 2 in performing a LCA of the recycled components of the EcoHawks Beetle and the fuel used from the various sources available. This study employs a vehicle dynamics model created by Austin Hausmann [23] in calculating the fuel use in a typical city/highway drive cycle. Subsequently, the author of this thesis performed the calculations required in GREET 1 for the full energy and emissions analysis of this fuel and electricity use from the 100% biodiesel generator, the conventional electricity grid, and the EcoHawks solar photovoltaic fueling station. Furthermore, the author utilized GREET 2 in analyzing the emissions and energy saved in reusing a number of stock vehicle components of the 1974 Volkswagen Super Beetle, including the transaxle, body, chassis, and a number of other minor components.

Chapter 4 expands upon this single vehicle dynamics model through the creation of a full commercial (company name withheld for privacy reasons) fleet analysis of ten conventional and electrified vehicles, utilizing four baseline vehicle dynamics models in calculating the typical fuel use for mixed city/highway drive cycles. The vehicles in this study include the Chevrolet Impala, Chevrolet Silverado (1500 and 2500), Chevrolet Uplander, Nissan LEAF, Chevrolet Volt, Chevrolet Silverado Hybrid, Ford Fusion Hybrid, Toyota Prius, and Ford Transit Connect EV, as well as a typical medium-duty line truck (not modeled due to lack of experimental data available). Each of these vehicles requires unique fuel and energy use algorithms, developed by the author based on a thorough literature review. This work utilizes GREET 1 in calculating the fuel use emissions profiles for a full WtW analysis, expanding these profiles to the entire fleet based on the average distance traveled each year by the various vehicles.

Finally, Chapter 5 outlines the design and construction of the EcoHawks Smart Grid. This Smart Grid consists of sources, energy storage, an energy load, and a sensory and control system. The electricity sources consist of a solar photovoltaic panel representing a renewable energy source, and a gasoline generator acting as the conventional energy source. The design uses two bulk energy storage systems in the form of deep cycle lead acid batteries, as well as a dynamic energy storage system in the form of a lithium BEV battery pack, supporting the exploration of V2G technology. A popcorn maker represents the load on the electric grid, utilized for its known power usage and short use cycle for ease of testing. Finally, the smart grid implements a control system written in LabVIEW, supported by a National Instruments data acquisition chassis in order to sense power flow in all directions, calculating efficiencies

of components along with power storage and use capabilities. The author contributed to this team effort through the creation of a student-built solar panel, the construction and assembly of the smart grid communications and power transfer infrastructure, performing system testing with the help of Jonathan Mattson and Nicholas Surface, and calculating the emissions profiles of the fuel sources based in GREET.

5.0: References

1. United States Environmental Protection Agency. *Summary of Current and Historical Light-Duty Vehicle Emission Standards*. 2010 3/7/2012; 6/21/2012 [Available from: http://www.epa.gov/greenvehicles/detailedchart.pdf.
2. Gagnon, L., C. Bélanger, and Y. Uchiyama, *Life-Cycle Assessment of Electricity Generation Options: The Status of Research in Year 2001.* Energy policy, 2002. **30**(14): pp. 1267-1278.
3. Hadley, S.W. *Evaluating the impact of Plug-in Hybrid Electric Vehicles on regional electricity supplies*. in *Bulk Power System Dynamics and Control - VII. Revitalizing Operational Reliability, 2007 iREP Symposium*. 2007.
4. Mooney, J.J. *An AIChE Mini History of John Mooney*. 2012; Available from: http://chemicaleng.njit.edu/news/JMooney.php.
5. Andrews, G.E., Zhu, G., Lu, H., Simpson, A., Wylie, J.A., Bell, M., Tate, J., *The Effect of Ambient Temperature on Cold Start Urban Traffic Emissions for a Real World SI Car*, 2004, SAE International.
6. Koltsakis, G.C. and D.N. Tsinoglou, *Thermal Response of Close-Coupled Catalysts During Light-Off*, 2003, SAE International.
7. Shen, H., Shamim, T., Sengupta, S., Adamczyk, A.A., *An Investigation of Catalytic Converter Performances During Cold Starts.* 1999, SAE International.
8. He, Z., Shao, Q., Li, Y., Jing, Z., Duan, Q., *Study on the Aging Test Methods and the Properties of the Three-Way Catalysts.* 2003, SAE International.
9. Farrauto, R.J. and R.M. Heck, *Catalytic Converters: State of the Art and Perspectives.* Catalysis Today, 1999. **51**(3-4): pp. 351-360.
10. Kaspar, J., P. Fornasiero, and N. Hickey, *Automotive catalytic converters: current status and some perspectives.* Catalysis Today, 2003. **77**(4): p. 419-449.
11. Grathwaite, J., *Range Anxiety: Fact or Fiction?* 2011, National Geographic News. [Available from: http://news.nationalgeographic.com/news/energy/2011/03/110310-electric-car-range-anxiety/]
12. General Motors, *Chevrolet Volt.* 2012, [Available from: http://www.chevrolet.com/volt-electric-car.html].
13. United States Department of Energy, *EPA Approves California's Zero Emissions Vehicle Program.* 2007, [Available from: http://www1.eere.energy.gov/femp/news/news_detail.html?news_id=10492].
14. Wang, M., *Argonne National Lab's Greenhouse Gases, Regulated Emissions, and Energy Use in Transportation Model.* Center for Transportation Research, Energy Systems Division, Argonne National Laboratory, Iowa, 2011.
15. Wang, M., Y. Wu, and A. Elgowainy, *Operating Manual for GREET: version 1.7.* Center for Transportation Research, Energy Systems Division, Argonne National Laboratory, Ames, Iowa, 2007: p. 119.
16. Burnham, A., Wang, M., and Wu, Y., *Development and Applications of GREET 2.7 -- The Transportation Vehicle-Cycle Model.* Argonne National Labs, Ames, Iowa, 2006 [Available from: http://www.transportation.anl.gov/pdfs/TA/378.PDF].
17. United States Environmental Protection Agency, *MOVES (Motor Vehicle Emission Simulator)*, 2010, [Available from: http://www.epa.gov/otaq/models/moves/index.htm].
18. United States Environmental Protection Agency. *Motor Vehicle Emission Simulator (MOVES): User Guide for MOVES2010a*. 2010 August 2010 [EPA-420-B-10-036; August 2010, [Available from: http://www.epa.gov/otaq/models/moves/MOVES2010a/420b10036.pdf.

19. Erol-Kantarci, M. and H.T. Mouftah. *Management of PHEV batteries in the smart grid: Towards a cyber-physical power infrastructure*. *Wireless Communications and Mobile Computing Conference (IWCMC), 2011 7th International*. Cagliari, Sardinia, Italy. 2011.
20. Guille, C. and G. Gross. *Design of a Conceptual Framework for the V2G Implementation*. *Energy 2030 Conference, 2008. ENERGY 2008. IEEE*. Atlanta, GA. 2008.
21. Lund, H. and W. Kempton, *Integration of renewable energy into the transport and electricity sectors through V2G.* Energy policy, 2008. **36**(9): pp. 3578-3587.
22. Depcik, C. *A Message from Assistant Professor Chris Depcik*. 2012 [cited 2012 12/3/2012]; Available from: http://groups.ku.edu/~ecohawks/.
23. Hausmann, A., *Advances in Electric Drive Vehicle Modeling with Subsequent Experimentation and Analysis*, *Department of Mechanical Engineering* 2012, University of Kansas. M.S. Thesis. p. 171.

Macroscopic Study of Projected Catalytic Converter Requirements

Bryan Strecker and Christopher Depcik

Department of Mechanical Engineering - University of Kansas, Lawrence, Kansas (United States)

Abstract

Software packages including Argonne National Lab's Greenhouse Gases, Regulated Emissions, and Energy Use in Transportation (GREET) model and the EPA's Motor Vehicle Emissions Simulation (MOVES) model are useful in analyzing the emissions profiles of light-duty vehicles. In particular, GREET performs a detailed life cycle fuel energy and emissions analysis, while MOVES focuses on energy and emissions during vehicle operation. This study uses MOVES2010b in the creation of emission trends in order to predict future emissions regulations and the subsequent aftertreatment device areas of improvement required to meet these standards. A second objective was to create four time sheet tables in order to update the base vehicle operation emission profiles used in GREET. The simulation results depict the balance between nitrous oxide and hydrocarbon emissions, the dependency upon climate effects, and areas for potential improvement given recent engine design trends.

Words: 140.

Keywords: GREET; MOVES; life cycle analysis;

Nomenclature

Variable	Description	Units
D	Distance driven	[miles]
E	Petroleum used by all vehicles	[MMBtu]
LHV	Lower heating value of the fuel at hand	[MJ/kg]
m	Mass	[kg]
ρ	Density	[kg/m^3]

1.0: Introduction

The United States Environmental Protection Agency (EPA) has been regulating vehicle exhaust emissions since its establishment in 1970. In that year, amendments to the United States' Clean Air Act included the first federal regulations on vehicle exhaust emissions. Since then, increasingly stringent emission regulations have gradually progressed toward the current standards, with the most recent regulations being phased in between 1999 and 2008 [1, 2]. To date, the EPA and the California Air Resource Board (CARB) hold regulations on five main criteria pollutant emissions: carbon monoxide (CO), oxides of nitrogen (NO_x), particulate matter in sizes less than ten microns (PM_{10}) and less than 2.5 microns ($PM_{2.5}$), hydrocarbons in the form of formaldehyde (HCHO), and non-methane organic gases (NMOG) [3]. In order to comply with regulations, Mooney and Keith in 1974 developed the three-way catalytic converter to lower CO, NO_x, and total hydrocarbons (THC) emissions [4]. Subsequent improvements to this original design have led to its use in nearly every gasoline vehicle in production.

To aid in the study of these regulated emissions, a number of vehicle emission simulation tools are available including Argonne National Lab's Greenhouse Gases, Regulated Emissions, and Energy Use in Transportation (GREET) model. The GREET model performs a Well-to-Wheels (WtW) emissions and energy use analysis studying

the extraction, enrichment, production, and transportation of fuels (Well-to-Pump: WtP), as well as the burning of these fuels in various vehicle types (Pump-to-Wheels: PtW). Since its creation, numerous studies have used GREET for its detailed WtP analysis of the fabrication of conventional fuels and biofuels. For example, Rosseau et al.'s [5, 6] investigation of fuel cell vehicles, and Atkins and Koch's [7] multiple vehicle comparative analysis.

GREET focuses on three basic vehicle types: the passenger car (or light-duty vehicle: LDV) and the light-duty truck, classes 1 and 2 (LDT1 and LDT2, respectively). In performing the PtW analysis, GREET uses two programs to track criteria pollutant emissions: CARB's EMFAC2002 motor vehicle emissions factor model and EPA's MOBILE6.2 model. Argonne used these programs in 2007 in order to create a set of emissions factors, organizing them into reference time sheets based on the model year of the vehicle under study [8]. Of importance, Argonne has not updated these emission factors in the subsequent versions of GREET, while the EPA replaced MOBILE6.2 with the updated Motor Vehicle Emissions Simulator (MOVES) series. The newest version at the time of this study, MOVES2010b, uses a default database of emissions factors from various sources including EPA research studies, Census Bureau vehicle surveys, Federal Highway Administration travel data, and other federal, state, local, industrial, and academic sources [9].

The focus of this effort is to perform a macroscopic analysis of vehicle exhaust emission profiles using MOVES2010b in order to update the greenhouse gas, criteria pollutant, and toxic air emission factors used in the GREET model. The authors created four time sheets in order to predict future EPA regulations in an attempt to demonstrate

possible design requirements of catalytic converters over the next ten to twenty years. In particular, this study analyzes the past regulations of the EPA and CARB in order to find trends that could carry into the future. Moreover, this work uses the calculations found in MOVES2010b in order to create future projections of these emission profiles, backed by a literature review. Finally, the authors analyze these future possibilities in order to mitigate some of the trends found. The results are intended to help guide future research in the area of catalytic exhaust aftertreatment. Predicting future emission requirements and catalyst weaknesses will provide a head start in the development of the next generation of catalytic converters. The next sections describe first how GREET and MOVES perform their simulations, as well as how the simulations run in order to create these emissions profiles.

2.0: GREET

As stated previously, GREET is an automobile fuel use and emissions model created by Argonne National Lab's Dr. Michael Wang [10]. The purpose of this model is to perform a WtW analysis, studying not only the burning of fuel in internal combustion engines, but the creation of these fuels, as well. This model is broken down into these two areas: WtP, which includes the extraction, enrichment, and transportation of the fuels to the end user, and PtW that consists of using and burning the fuels in the vehicle at hand. GREET is most commonly used for its WtP analysis, as in Rousseau and Sharer's comparative analysis of conventional and alternative sport utility vehicles (SUV) wherein they compare conventional fuels to the use of fuel cells [6].

GREET's ability to analyze every step of the fuel creation process makes it an invaluable tool for automobile studies [5]. For example, one can analyze the effects of

improving the refining efficiency of petroleum fuels, or through changing the distance between the oil drilling point and the fuel refinery. Moreover, it provides for a comparison of the total energy use and emissions produced based on the type of feedstock used in biodiesel production. The PtW capabilities are also formidable in their ability to compare different vehicle types holding the production process constant. For example, one can study the efficiency of a conventional vehicle run on ethanol and compare this to a flex-fuel vehicle designed for ethanol use. In addition, the model allows for evaluation of vehicles of the same type from different model years. These are just a few of the many options available in GREET. Although extremely important, the WtP category is out of the scope of this study. Rather, the focus is on the PtW analysis.

In comparison, MOVES utilizes a default set of emissions statistics to calculate emissions and fuel use profiles based on vehicle parameters including vehicle type, fuel type, geographic location, and study year, among many others. Of utmost importance to this paper is the study year and fuel type. A set of time-series reference tables like the one shown in Table 1 aid in calculating the baseline emissions profile for emissions for conventional gasoline (CG) and conventional diesel (CD) [10]. The emissions studied in this table include volatile organic compounds (VOC), both from running the vehicle as well as evaporative emissions during filling up and spillage, carbon monoxide (CO), oxides of nitrogen (NO_x), particulate matter both smaller than 10 microns (PM_{10}) and smaller than 2.5 microns ($PM_{2.5}$), methane (CH_4), and nitrous oxide (N_2O). PM_{10} and $PM_{2.5}$ both have two sources: the exhaust and tire and brake wear (TBW). These values represent emissions of vehicles that are five years old during the target year. For example, if the target year for the study is 2010, the vehicle at hand is of the model

year 2005. This is because the values are deemed to be at the halfway point in the vehicle's ten-year lifespan, giving an average value for the vehicle's lifetime [8]. This will be a potential area of improvement in the analysis. However, the sources of these values requires further examination.

Argonne developed the default emissions profiles for GREET including the future projections through the year 2020 using a combination of the EPA's MOBILE 6.2 vehicle model, and CARB's EMFAC2002 motor vehicle emissions factor model [8]. Argonne created a separate profile each for the six baseline vehicles, including gasoline and diesel counterparts for LDV, LDT1, and LDT2. GREET calculates the profiles for simulations involving alternative fuels and using percentage increases or decreases based on the default specifications; thus, amplifying any inaccuracies in the baseline profile. GREET allows the user to perform stochastic simulations as well in order to address some of the uncertainties in the GREET time-sheet tables through applying probability distributions to the model inputs, although this is outside the scope of this study [10, 11].

The EPA now utilizes a new MOVES vehicle model series which superscedes the calculation of these initial baseline factors, but the emissions factors used in GREET have not been updated. Thus, one of the two goals of this study is to update these factors in order to get a more representative set of baseline profiles through using a national average simulation in MOVES. Developing the future projections required of the catalytic aftertreatment devices will help to accomplish this objective. The following section contains a description of the software and a detailed explanation of the simulation specifications used in MOVES.

3.0: MOVES

The US EPA developed MOVES as a replacement for the previous MOBILE 6.2, focusing on cars, trucks, and motorcycles. MOVES uses a set of default emissions databases in order to calculate the fuel use and emissions of 78 combinations of fuels and vehicles [9]. A majority of these are out of the scope of this study, as the only combinations desired are those six previously mentioned in GREET (CG LDV, LDT1, and LDT2, as well as CD LDV, LDT1, and LDT2). This default database comes from EPA research studies, Census Bureau vehicle surveys, Federal Highway Administration travel data, and other federal, state, local, industry, and academic sources [9].

Table 1: Time sheet for criteria pollutant emissions found in Argonne's GREET2011 model for a gasoline LDV [10]. All units are in grams of emissions per mile driven.

Model Year	MPG	VOC (Exhaust)	VOC (Evap.)	CO	NO_x	PM_{10} (Exhaust)	PM_{10} (TBW)	$PM_{2.5}$ (Exhaust)	$PM_{2.5}$ (TBW)	CH_4	N_2O
1990	22.10	0.881	0.527	14.056	1.285	0.0131	0.0205	0.0124	0.0073	0.0883	0.067
1995	21.70	0.533	0.382	8.356	0.657	0.0096	0.0205	0.0089	0.0073	0.0582	0.030
2000	22.00	0.154	0.073	5.210	0.300	0.0088	0.0205	0.0081	0.0073	0.0221	0.012
2005	23.40	0.122	0.058	3.745	0.141	0.0081	0.0205	0.0075	0.0073	0.0146	0.012
2010	24.81	0.095	0.057	3.492	0.069	0.0081	0.0205	0.0075	0.0073	0.0106	0.012
2015	27.20	0.094	0.057	3.482	0.069	0.0081	0.0205	0.0075	0.0073	0.0104	0.012
2020	29.45	0.093	0.057	3.460	0.069	0.0081	0.0205	0.0075	0.0073	0.0102	0.012

This database takes information from each of the over 3000 counties in the United States. The user has the ability to change the input database, but this work utilizes the default values [9].

In running each simulation, the user creates a specification profile called the RunSpec. Within each RunSpec are ten categories defining the vehicles, emissions, road types, and time periods desired for the simulation [12]. A majority of the RunSpecs created in this study are similar, only changing a small number of specifications for each calculation. The following subsections describe the RunSpec used in some detail, as well as the alternatives available.

3.1: Scale

The scale specification defines the domain and calculation type of the simulation. In Domain, there are three options: National, County, and Project. The County option allows the simulation to investigate one single county in the United States. Likewise, the Project option allows the user to add specific studies with detailed input databases when desired. Individual states utilize these custom databases for regional conformity analyses and State Implementation Plans (SIP), and thus are out of the scope of this study as this study is merely calculating general trends. The remaining option is the National scale, which uses the default statistical databases which include generalized state and local allocation factors. This is the option used here in order to obtain a national average emissions profile [9].

The two calculation types available are the Inventory and Emission Rates options. Inventory simply gives total mass and energy use within a desired region and time span, while the Emission Rates option calculates these outputs per unit of distance traveled or energy consumed [9]. In order to have more control over the post-processing of the information found, this work utilizes the Inventory option.

3.2: Time Spans

The Time Spans subsection defines the length of time included in the study. The first option is the choice of Time Aggregation Level, which the user can select to be year, month, day, or hour. With each step in further detail, the simulation run time increases, enhancing the amount of detail and the respective accuracy. The user can then choose the year of study, as well as which of the twelve months, days in each week, and hours in the day are included in the RunSpec [9]. These options are important in performing studies as a function of temperature or time of the week (such as just looking at weekends or weekdays), and thus the authors are considering them for future efforts. However, for the purposes of the yearly profiles desired, this work utilizes the year aggregation level for all years between 1990 and 2040, including all twelve months, the entire week, and all hours of the day. As an example inclusion in this study, this work uses the "Month" aggregation level in order to take into account the differences in weather patterns throughout each year.

3.3: Geographic Bounds

The Geographic Bounds subsection defines the region included in the RunSpec, with options including the entire Nation, individual states, counties, or a custom domain defined by the user in the input database. In order to obtain a national average, this work utilizes the Nation option. However, another example provided includes the state option in order to obtain the average profiles for Kansas, Minnesota, and Florida, studying the effects of different climates on the performance of the powertrain [9].

3.4: Vehicles/Equipment

This subsection defines what fuels and vehicles the RunSpec includes. The options for fuels include Compressed Natural Gas (CNG), diesel, gasoline, electricity, Liquefied Petroleum Gas (LPG), or a custom fuel type defined in the input database. The options for vehicles, or source use types, include combination long- and short-haul trucks, intercity buses, light commercial trucks, motor homes, motorcycles, passenger cars, passenger trucks, refuse trucks, school buses, single unit long- and short-haul trucks, and transit buses. Any combination of these vehicles and fuel types may be used, but as stated previously, only diesel and gasoline passenger cars and trucks have been chosen for this study, with light-duty trucks 1 and 2 being lumped together in the passenger truck selection [9]. This LDT1 and LDT2 combination reflects the "passenger truck" vehicle category available in MOVES, categorized by driving style as opposed to gross vehicle weight. This change reflects the EPA's shift to the new Tier 2 emission standards in which the same standards regulate all vehicle weight classes [9].

3.5: Road Type

There are five road types available for study, including rural and urban areas, both restricted and unrestricted, as well as off-network roads. This work utilizes all five in order to obtain a complete and well-rounded investigation. However, one can use the urban versus rural studies to determine the respective amounts of emissions produced. The authors considered this for possible future work since it is outside the scope of this study.

3.6: Pollutants and Processes

This subsection is where the user defines what emissions and pollutants the RunSpec includes in each simulation. The options include 39 different emission types from 13 sources. Thus, the user has complete control over the outputs, and can create extremely detailed studies [9]. In order to create the full emissions profile, the emissions included in this study are found in Table 2 (regulated emissions are denoted with a *). Note that the authors utilized separate simulations for evaporative emissions for hydrocarbons and organic gases, as well as the tire and brake wear particulates, since these require a time aggregation at the detailed by-hour level, though the results section contains all of this output data.

Table 2: Bulk emissions selected for the used RunSpec.

Total Gaseous Hydrocarbons	Non-Methane Hydrocarbons (NMHC)	Non-Methane Organic Gases (NMOG) *
Volatile Organic Compounds (VOC)	Carbon Monoxide (CO) *	Sulfur Dioxide (SO_2)
Nitrogen Oxide (NO)	Nitrogen Dioxide (NO_2)	Oxides of Nitrogen (NO_x) *
Total Primary Exhaust PM_{10} *	Total Primary Exhaust $PM_{2.5}$ *	Total Energy Consumption
Petroleum Energy Consumption	Fossil Fuel Energy Consumption	Methane (CH_4)
Nitrous Oxide (N_2O)	Atmospheric Carbon Dioxide (CO_2)	Carbon Dioxide Equivalent (CO_{2eq})
Formaldehyde (HCHO) *	Total Organic Gases (TOG)	Ammonia (NH_3)
Nitrous Acid (HONO)	Benzene	Additional Air Toxics
Polycyclic Aromatic Hydrocarbons (PAH)	Dioxins and Furans	

It is important to note the difference between THC, NMHC, Total Organic Compounds (TOG), NMOG, and VOC. THC encompasses all hydrocarbons emitted from the exhaust, while TOG includes THC and all oxidized compounds, most importantly alcohols and aldehydes. The reason is because these oxygenated compounds form ozone. However, methane is far less reactive than many of the other

hydrocarbons present, and thus NMHC and NMOG do not include methane. Furthermore, ethane is relatively dormant as well, and is thus excluded from VOC [13].

3.7: Manage Input Data Sets

This subsection allows the user to define an input database for the simulation to replace some or all of the default database [9]. SIP and conformity studies require user-defined databases, but for the purposes of this study, choice of this option is unnecessary.

3.8: Strategies

The strategies subsection allows for two main functions: studying the effects of vehicle retrofits and disabling the effect of any Clean Air Act Amendments in the simulation results. One can use the on-road retrofit subsection to import an input database defining the progress of vehicle emission reduction performance in current and future years, simulating theoretical future trends. Alternatively, if the Rate-of-Progress option is used, 1993 model year emission rates are applied to all post-1993 vehicles. This can be used to simulate Reasonable Further Progress SIP requirements [9]. Both of these options are out of the scope of this study, and are unused.

3.9: Advanced Performance Features

This subsection allows the user to exclude certain studies or information sources from the simulation. For example, one can command the program not to execute the final aggregation and summation calculations, decreasing the simulation run time [9]. These options create simulations far too specific for a national average, and thus are outside the scope of this study.

3.10: Output

The Output subsection is where the user defines an output database for simulation results. In this subsection, the user defines the output units for mass, energy, and distance. For the purposes of this study, the RunSpec utilizes the generic options kg, MMBtu, and miles for ease of post-processing. In addition the user can use the General Output tab to decide what activities are to be followed, including the distance traveled, the population of each area, and the number of vehicle starts, among others [9]. The population is simply the number of vehicles included in the study, useful in finding the average effect per vehicle. Likewise, the distance traveled is of utmost importance in obtaining emissions factors in the desired units of grams per mile. This total distance option was utilized in order to match the time-sheet table units in GREET. The number of starts can also be useful in determining the effects of the length of each drive cycle on the effectiveness of the catalyst, and thus the authors consider this for future efforts.

In the Output Emissions Detail sub-tab, aggregation levels for time span and vehicles are considered [9]. For example, one may use the time span option of performing the study by month, but may only want the year-long total. MOVES performs these post-processing operations according to the selections on this page. For the purposes of this study, the RunSpec includes the year and nation aggregation levels, separating out the vehicles studied by model year. This allows for a well-rounded national average while analyzing specific aged vehicles.

Moreover, this section allows the user to categorize the results according to the following parameters: model year, fuel type, and emission process. At this time, the

specific emission processes, although informative, are outside the scope of this study as the focus is a broad emission profile generalization. Fuel type is also a useful analysis, but GREET handles the alternative fuel and vehicle types, so this aggregation is not required in updating the time-sheet reference tables. However, model year is important since the age of the vehicle will help categorize the emissions results according to the EPA exhaust standards. MOVES separates the vehicles for each year into the following age groups: zero to three years, four to five, six to seven, eight to nine, 10 to 14, 15 to 19, and over 20 years. Each of these age groups has an increasing amount of emissions, taking into account the deterioration of the catalytic device and other powertrain components. This is calculated based on a logarithmic slope factor, growing the emission rate profiles based on the zero-to-three year age group [14].

3.11: MOVES Data Importer GUI

As stated, MOVES allows the user to import a number of different input databases, defining properties of the vehicle fleet such as the age distribution, the vehicle miles traveled, fuel details, and meteorological data, among others. Of importance to this paper is the Fueltype and Technologies tab, wherein one can define the ratios of vehicle types identified in the simulation. For example, the ratios changed for the purposes of this study are the number of diesel-powered trucks versus diesel-powered passenger cars. The reason for this revision is that the default number of diesel passenger cars influenced the outcomes of the simulation for model years 1986 through 2000. In particular, the ratio defaults to 100% LDT with 0% of the population driving a diesel LDV. The ratio utilized in this RunSpec matches the 1985 ratio in order to obtain trends for these years. This adjustment occurred under the direction of David

Brzezinski from the EPA's MOBILE group [15]. However, this adversely affected the outcomes of the diesel trends as discussed in a later section.

4.0: Results

The results from the simulations that were run in MOVES2010b provide a set of emissions trends for gasoline and diesel-powered LDV and LDT. The following sections describe the data obtained and how it influences the two desired outcomes: new GREET time-sheet tables, and emissions regulations trends and the requirements for catalysts held therein.

4.1: Criteria Pollutant Future Projections

Periodically, since its establishment in 1970, the US EPA has passed regulations requiring further lowered emission levels. Driven by this, the technology behind catalytic exhaust aftertreatment devices has increased dramatically in order to meet these specifications. However, the exhaust conversion requirements vary depending on local climate. For example, CARB has different requirements than the rest of the continental US, and these localized requirements are primarily stricter than EPA levels. Likewise, the New England area follows a set of requirements that are similar to CARB [3]. The general trend is that EPA regulations lag behind the CARB requirements by a few years. However, in order to support and test this assumption, this work utilizes simulations run in MOVES as a second opinion, providing a better idea of future regulations. The following subsections describe, in some detail, the current and historical emissions regulations by CARB and the EPA, the calculations used in processing the MOVES output data, using this data to make viable projections, and a comparison of these findings with CARB and New England regulations.

4.1.1: EPA and CARB Regulations: Historical and Current

EPA regulations are organized into a tiered system wherein the lower the tier, the older the vehicle model year that is regulated. The original regulations, covering the years through 1972, used testing procedures that are vastly different from the current system, enough so that the standards are not comparable [3]. Although these procedures changed again in 1975, those used in 1973 and 1974 were close enough that the historical trends can include these years [3]. Thus, beginning with model year 1973 vehicles, NO_x, CO, and THC levels are comparable to current levels [3]. The year 1982 brought the advent of Particulate Matter (PM) regulations [3]. These emission levels changed yearly until the Tier 0 regulations went into effect starting with 1987 vehicles. Appendix A1 lists these early requirements [3].

After 1993, the imposed Tier 1 program resulted in regulations that are more stringent. Moreover, the EPA then separated gasoline and diesel vehicles, as well as LDV and the four tiers of LDT, through separate emissions standards. The Tier 1 standards also brought the first national regulations on NMOG. These Tier 1 regulations lasted until 2004 when the EPA began phasing in the Tier 2 standards. The Tier 2 program consists of eight permanent and three temporary bins. Within each bin is a different set of regulations, each one more stringent than the previous. The eight permanent bins are still in use today, while the three temporary bins lasted until 2007 (the end of the phasing of the new system). In addition, the Tier 2 program applies the same regulations to vehicles of all weights and fuel types, letting the vehicles fall into one of the eleven bins. However, a manufacturer must meet a fleet average NO_x standard of 0.07 grams per mile. Thus, a single vehicle may produce more than this

level, but this excess NO_x must be compensated for by lower emissions from the other vehicles in the fleet [16]. Appendix A1 lists the Tier 1 and 2 emissions.

Beginning in 2001, California and the Northeastern states adopted the Low Emissions Vehicle, or LEV I CARB program [3]. These regulations were in effect for model year vehicles from 2001 through 2006 and classified vehicles into Low (LEV), Transitional-Low (TLEV), Inherently-Low (ILEV), Ultra-Low (ULEV), and Super-Ultra-Low Emissions Vehicles (SULEV) [3]. With the advent of the LEV II program came the introduction of the Zero Emissions Vehicle (ZEV) and the Partial-Zero Emissions Vehicle (PZEV). Table A1-3 lists these CARB emission standards for LDV and LDT [3].

4.1.2: Calculations and Post-Processing

The RunSpecs profile developed performs a majority of the post-processing required in order to obtain emissions trends throughout the past few decades according to the target and model years of the vehicles specified. However, in order to have more control over post-processing, as well as to decrease simulation run time, the RunSpec utilizes the "Inventory" scale parameter. As a result, the simulation calculates the total emissions, energy allotments, and distances driven, leaving only basic calculations left to the user. A majority of these calculations follow Equation 1 in order to obtain emissions in units of grams of emission per mile driven. In this equation, *m* is the total mass of the emissions produced by all vehicles in [kg], and *D* is the total distance driven by all vehicles in [miles]. These are the same metrics used in EPA and CARB regulations allowing for a simple comparative analysis[17]:

$$Emission\ Factor\ \left[\frac{g}{mile}\right] = \frac{m}{D} * 1000\ \left[\frac{g}{kg}\right]. \quad (1)$$

The remaining calculation finds the average fuel economy according to Equation 2. In this equation, *E* is the total amount of petroleum energy used by all vehicles [MMBtu], *D* is the total distance driven by all vehicles [miles], *ρ* is the density of the fuel [kg/m^3], and *LHV* is the lower heating value of the fuel [MJ/kg] (either gasoline or diesel):

$$MPG = \left\{ \left[\begin{matrix} \frac{E}{\rho * LHV} * 1055.87 \left[\frac{MJ}{MMBtu}\right] * \dots \\ 264.17 \left[\frac{gallons}{m^3}\right] \end{matrix} \right] / D \right\}^{-1} . \quad (2)$$

using the constants indicated in order to obtain the correct units.

From these results, the following section indicates projections for future requirements on the five currently regulated emissions and the total hydrocarbons.

4.1.3: MOVES Projections

Through the simulations run in MOVES, this work calculates a series of future projections through the year 2040 in order to determine an estimate for vehicle emission profiles (CO, NO_x, PM, HCHO, and NMOG) given the current regulations. Figures 1 through 5 illustrate the trends on a logarithmic scale for current-year CG vehicles, ten-year-old (10YO), and twenty-year-old (20YO) models for the years 1990 through 2040. For example, for the target year 2010, the current-year vehicle would be of the model year 2010, the 10YO vehicle would be model year 2000, and the 20YO vehicle would be model year 1990.

Figures 1 through 5 show vehicle emissions profiles as they come off the manufacturing line, at ten years, and then twenty years of their lives. One can follow the aging of the vehicles by moving vertically, up for older vehicles, down for younger vehicles. For example, in Figure 1, the 2010 current year CG LDV produces 1.88

grams of CO per mile; at ten years old, it produces 4.81 grams of CO per mile, and at twenty years old, it produces 6.52 grams of CO per mile. Appendix A2 contains similar trends for ultra-low sulfur diesel (ULSD) or CD-powered vehicles. MOVES calculates emission trends for future years using emissions standards and regulations affecting vehicles of model year 2012 and later. The user has the ability to utilize the Data Importer GUI to alter default assumptions about future regulations and changes to the vehicle fleet, studying the possible effects of more stringent regulations; however, these efforts are not included in this study [9].

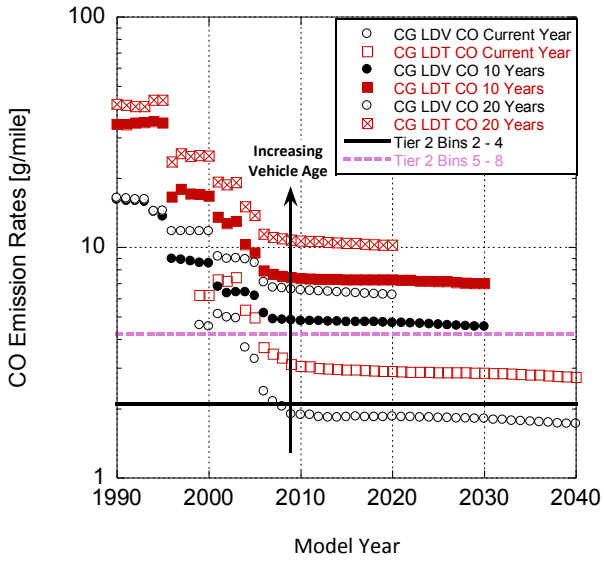

Figure 1: CG CO emission levels for new, ten-year, and twenty-year old LDV and LDT.

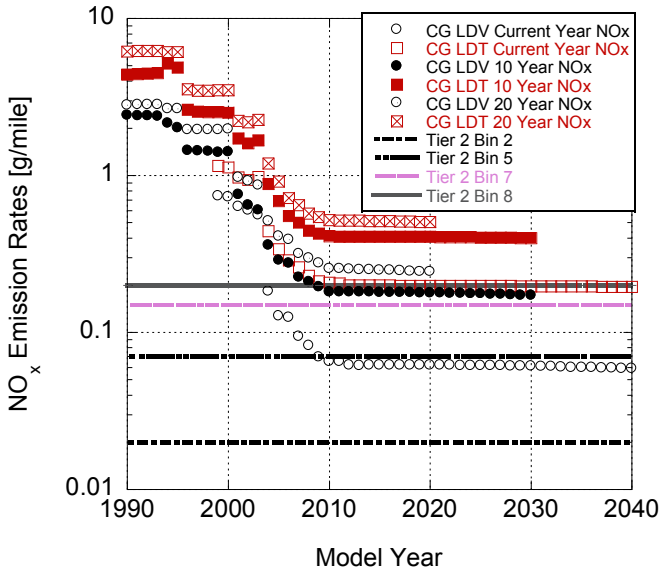

Figure 2: CG NO_x emission levels for new, ten-year, and twenty-year old LDV and LDT.

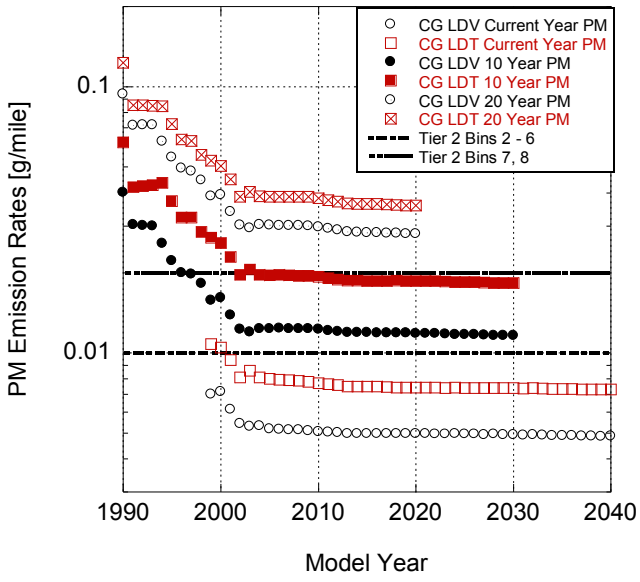

Figure 3: CG PM emission levels for new, ten-year, and twenty-year old LDV and LDT.

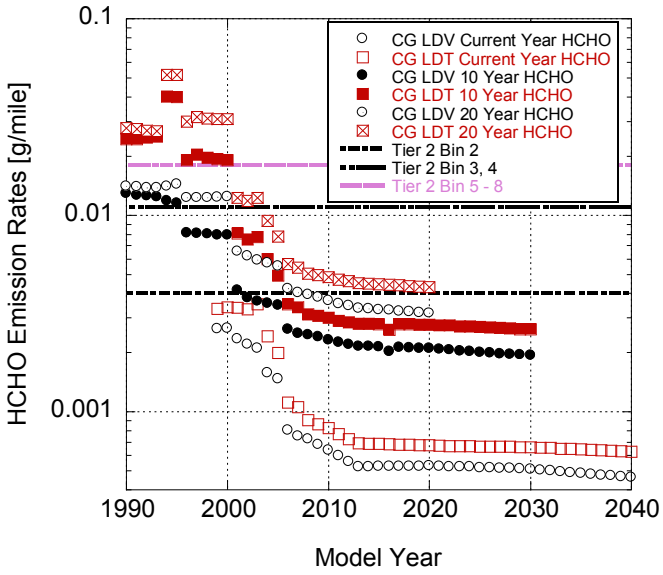

Figure 4: CG HCHO emission levels for new, ten-year, and twenty-year old LDV and LDT.

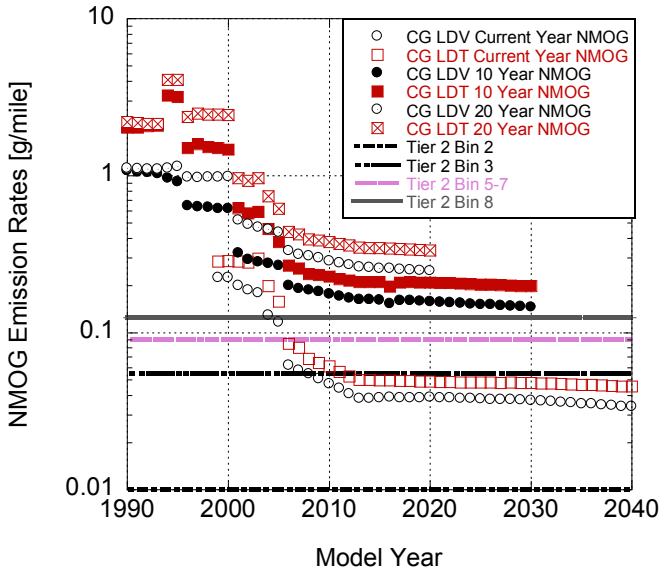

Figure 5: CG NMOG emission levels for new, ten-year, and twenty-year old LDV and LDT.

It is important to first indicate which current year vehicles meet the Tier 2 standards as manufactured since they would not have yet seen the detrimental effects

of catalyst or engine aging. CG LDVs meet the Bin 5 CO standard beginning in target year 2004, going on to meet the Bin 2 CO standard in target year 2008. Likewise, CG LDTs meet the Bin 5 CO standard in target year 2006, but LDTs do not meet the Bin 2 CO standard. Furthermore, current-year CG LDVs meet the Bin 7 standard for NO_x beginning in target year 2005, going on to meet the Bin 5 standard in target year 2009.

All current year CG LDVs meet the Bin 2 PM standard for all target years studied, with new CG LDTs meeting the Bin 2 PM standard beginning in target year 2001. Similarly, all new CG LDTs and LDVs meet the Bin 2 HCHO standard in all target years. However, in the case of NMOG, new CG LDVs only meet Bin 8 in target year 2005, meeting Bin 5 standards the next year, and meeting Bin 3 in target year 2008. New CG LDTs also meet the Bin 5 standard in 2006, but these LDTs are a bit delayed relative to LDVs, not meeting the Bin 3 standard until 2012.

This analysis shows that newly manufactured vehicles (e.g., those built in the year of the study) generally fall within Tier 2 Bin 5 standards except for NO_x and CG LDTs. The trend is similar for CD LDVs and LDTs, as current-year CD LDVs only meet the Bin 7 NO_x standard beginning in 2010. As a result, it seems unlikely that a fleet will meet the NO_x Bin 5 average requirement set forth by the EPA unless completely comprised of new CG LDVs (note that 42.5% of light-duty automobiles sold in the US fall within the LDT category for 2011 [18]). This trend may be exacerbated given increasing engine trends such as direct injection and boosting, which moves combustion towards a leaner air-fuel mixture regime for fuel economy improvement [19]. Thus, vehicle manufacturers will continue to face significant challenges in reducing lean NO_x emission levels in the coming years. Direct injection can also detrimentally affect a

vehicle's ability to meet PM emission standards due to fuel concentration variability within the spray stream [20]. However, combining proper tuning of direct injection with engine strategies, such as exhaust gas recirculation (EGR), can potentially help to lower HC, CO, and NO_x emission levels [21, 22].

Once these vehicles age ten years, the emissions trends change significantly. For example, neither 10YO LDVs nor LDTs meet any of the Tier 2 CO standards. Likewise, neither 10YO LDVs nor LDTs meet any of the Tier 2 NMOG standards. In the case of NO_x, only the 10YO CG LDVs meets the Bin 8 standard in the target year 2009. PM emissions rise such that 10YO CG LDV only meet the Bin 7 standard beginning in target year 1997, and 10YO CG LDT do not meet the Bin 7 standard until 2002, and again in 2004. Finally, HCHO emissions trends are not affected as much, with 10YO CG LDV meeting the Bin 5 standard in all target years studied, going on to meet the Bin 3 standard in target year 1996, then the Bin 2 standard in target year 2002. However, 10YO CG LDTs only begin to meet the Bin 3 HCHO standard in target year 2001, going on to meet Bin 2 in target year 2006.

Finally, 20YO vehicles suffer the greatest detriment as they never meet any of the CO, NO_x, PM, or NMOG standards, with CG LDVs only meeting the HCHO Bin 3 standard in 2001, going on to meet the Bin 2 standard in 2008. Likewise, 20YO CG LDTs meet the Bin 5 standard in target year 2001, going on to meet the Bin 3 standard in target year 2004.

These trends show the magnitude of the effects of engine and catalyst aging. Another detrimental effect on the efficiency of catalytic aftertreatment devices is low ambient temperature.

4.2: Climate Effects

In order to demonstrate the effects of climate on the emissions produced and the performance of catalytic converters over their lifetime, the authors have run a number of simulations in MOVES2010b utilizing a monthly aggregation focusing on three different states: Minnesota, Florida, and Kansas. These represent cold, hot, and moderate climates, respectively. Focusing on CG LDV, Figures 6 through 10 depict emission trends for comparing current year and ten-year-old vehicles. Appendix A4 contains similar trends for CDLDT. These simulations are important as they show that although the emissions are slightly higher in Minnesota, the difference is far less drastic than that of a gasoline vehicle.

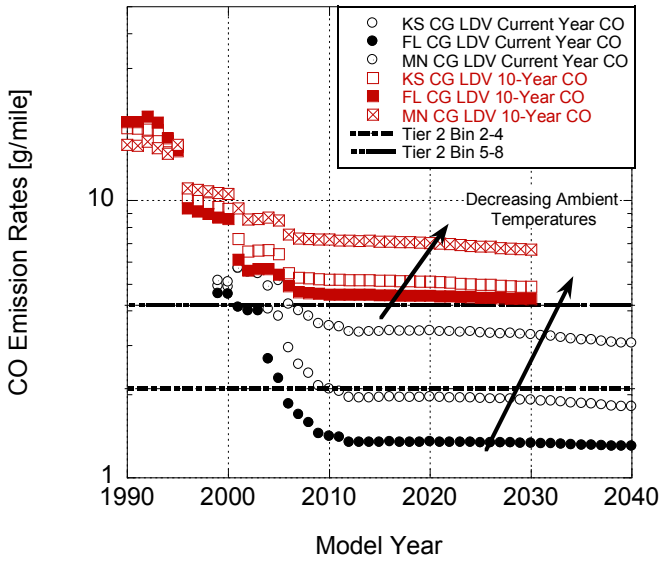

Figure 6: CG LDV CO emission rates by climate and model year

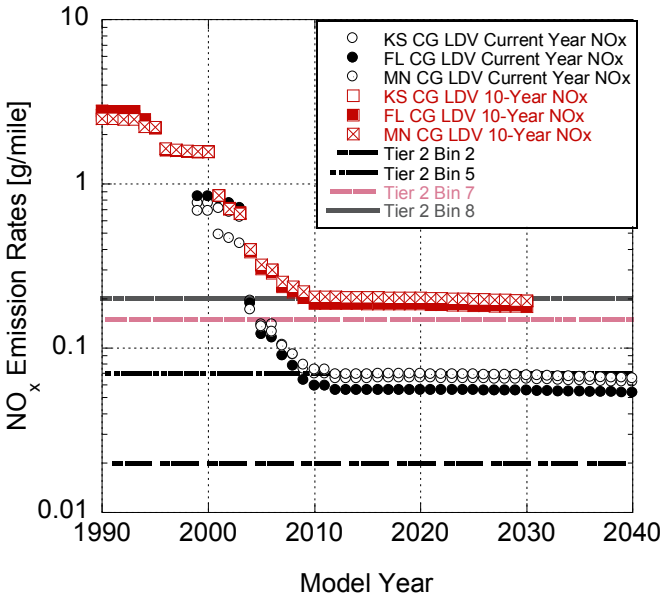

Figure 7: CG LDV NO_x emission rates by climate and model year.

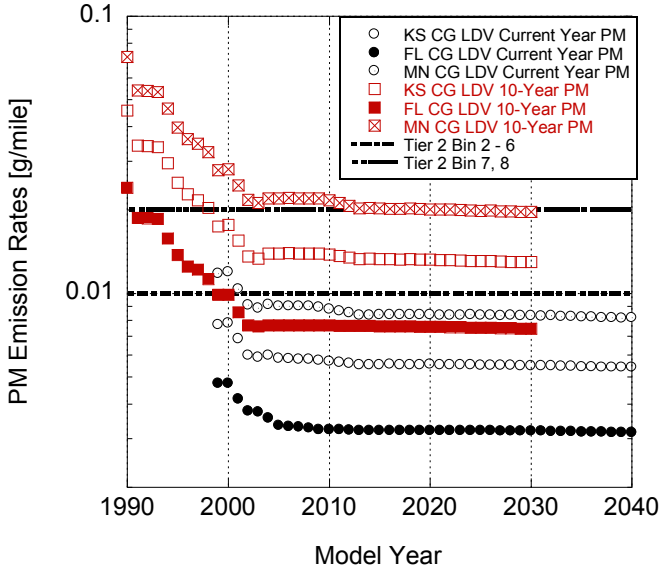

Figure 8: CG LDV PM emission rates by climate and model year

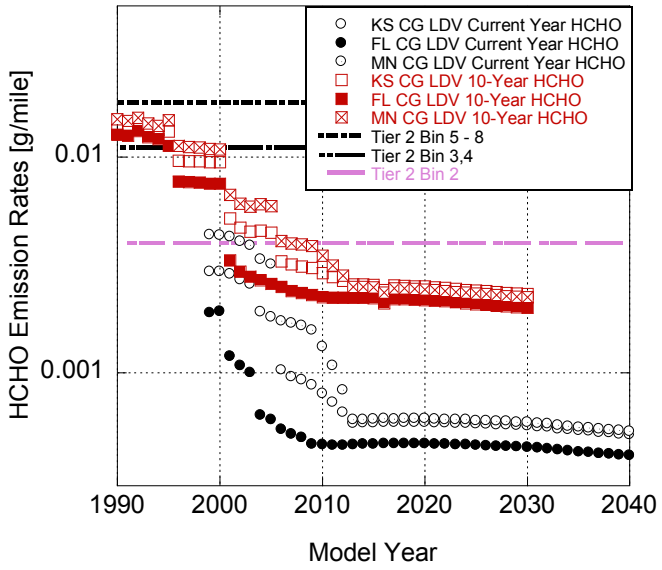

Figure 9: CG LDV HCHO emission rates by climate and model year

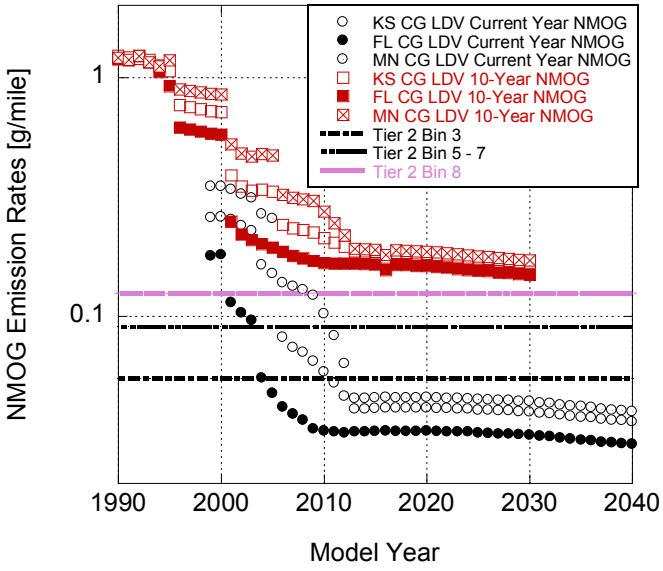

Figure 10: CG LDV NMOG emission rates by climate and model year

Figure 6 shows these effects as new CG LDV in Florida meet the Bin 5 CO standards in 2006, while the same vehicles in Minnesota never meet the Bin 5 CO standard. Figure 7 shows the effects of ambient temperatures on NO_x production and conversion as new CG LDV in Florida meet the Bin 5 NO_x standard for the first time in

target year 2009, while the same vehicles in Minnesota do not meet the Bin 5 standard until three years later, in target year 2012. Furthermore, once aged for ten years, the vehicles never meet the higher Bin 7 NO_x requirements, and LDVs in Florida only meet the Bin 8 standard starting in 2010. Overall, the detrimental effects on NO_x production and conversion are far less severe than the effects on CO and PM. Figure 8 shows the effects on PM emissions as new CG LDVs in Florida meet and exceed the Bin 2 PM standard by over 50% in target year 1999; whereas, CG LDVs in Minnesota do not meet this same standard in 1999.

Figures 9 and 10 show a similar trend for HCHO and NMOG, wherein the effects of low ambient temperature are greatly reduced by the projected model year 2013. All current year FL and KS CG LDVs meet the Bin 2 HCHO standard, with Minnesota-based CG LDVs meeting the Bin 2 HCHO standard in 2003. Minnesota-based 10YO CG LDVs meet the Bin 2 HCHO standard beginning in year 2007, with all 10YO CG LDVs meeting the Bin 5 HCHO standard in all years studied. For NMOG, current year vehicles all fall below the Bin 5 standard starting in 2004 for FL, 2006 for KS, and 2011 for MN. However, none of the 10YO-aged vehicles meet any of the bins for NMOG. This illustrates another challenge of aged catalysts moving forward.

It is important to study the effects of climate on vehicle emissions since the light-off temperature is a vital factor in the performance of a catalyst. In particular, low ambient temperatures lead to a delay in the catalyst reaching this value (i.e., temperature at 50% conversion of the chemical species under study). From these simulation results, it is apparent this greatly influences CO, HC, and PM emission rates, while NO_x emission rates are relatively uniform regardless of the weather conditions.

The consistency of NO_x is due to the fact that NO_x is created in an engine through the thermal NO mechanism when temperatures are sufficiently high enough allowing for the oxidation of nitrogen in the intake air [23]. Low ambient temperatures lead to a lower peak combustion temperature due to a lower starting combustion temperature, as well as increased heat transfer to the cooler engine walls and coolant. This lower combustion temperature reduces the production of NO_x. Furthermore, it leads to the engine producing cooler exhaust gas, reducing the heat transferred to the catalyst, further delaying light-off. As the engine heats up, producing more NO_x, the catalyst increases in temperature as well, increasing the conversion efficiency to N_2. Thus, increases in NO_x emissions as a function of lower ambient temperatures are not as drastic due to a balance between lower engine-out emissions and the reduced effectiveness of the catalyst [24].

On the other hand, CO, HC, and PM emissions are much higher in regions of colder ambient temperature. At cold start, an engine typically increases the amount of fuel injected into the engine, creating a rich air-to-fuel ratio in order to ensure sufficient vaporization of the liquid fuel, most notably for Port Fuel Injected (PFI) engines. A majority of current gasoline SI engines are PFI, whereas diesel engines utilize direct injection (DI) in order to control combustion timing. This may explain some of the differences between CG and CD emission profiles. The discussion section further addresses the differences between PFI and DI engines. Moreover, a degradation in combustion efficiency occurs due to colder engine jacket cooling water, lubricating oil, and piston temperatures at start-up. This rich, inefficient burn produces a larger amount of HC, CO, and PM emissions [24]. Furthermore, at these lower temperatures CO

cannot be sufficiently oxidized in the catalyst, thus less is converted to CO_2 [25]. This delay in reaching the catalyst's light-off temperature is due to a lower exhaust gas temperature (mentioned before), as well as the fact that more CO is produced acting as a strong inhibitor on the catalyst surface. Likewise, similar trends can be found for NMOG, as found by Christenson et al. [25].

Efforts toward reducing cold-start CO and HC emissions include a rise in the implementation of close-coupled catalysts. This process involves placing the catalytic converter directly after the exhaust manifold on the engine. In this way, the exhaust gas does not have as much time to cool down while traveling to the catalyst, reducing the time it takes to reach the light-off temperature. However, this process can lead to detrimental aging effects (subsequently seen in the 10YO results), including non-uniform aging, as studied by Koltsakis and Tsinoglou [26]. Further development of this technology may lead to improvements in aging uniformity, or overall reductions in aging effects.

4.3: GREET Time-Sheet Tables

As stated previously, GREET uses six principle time-sheet tables as a baseline for all PtW criteria pollutant emissions estimates for conventional vehicles, adjusting these numbers in the cases of alternative fuels and advanced powertrains. This study utilizes four time sheets to replace the six original tables, with MOVES lumping LDT1 and LDT2 into a bulk category under passenger trucks, categorizing these vehicles by driving style as opposed to vehicle weight. Tables 3, 4, 5, and 6 contain these trends. These tables show five-year-old technology in order to reproduce the calculations originally embedded within GREET. Thus, if the target year for the GREET simulation is

2010, the vehicle model year 2005 will be selected, giving proper mid-life emissions estimates. Note the numbers in red, highlighting leaps in trends that may be erroneous values calculated by insufficient statistical data. These values may change in the future with updates to the MOVES package.

Table 3: CG LDV emissions estimates for GREET2011. All emissions are in units of grams per mile driven [10].

Target Year	Model Year	MPG	VOC (Ex.)	VOC (Evap.)	CO	NO_X	PM_{10} (Ex.)	PM_{10} (TBW)	$PM_{2.5}$ (Ex.)	$PM_{2.5}$ (TBW)	CH_4	N_2O
2000	1995	24.65	0.439	0.615	7.839	1.346	0.0124	0.0181	0.0115	0.0046	0.038	0.0290
2005	2000	24.53	0.238	0.059	5.162	0.798	0.0087	0.0181	0.0080	0.0046	0.018	0.0158
2010	2005	24.21	0.147	0.041	4.230	0.164	0.0066	0.0181	0.0061	0.0046	0.018	0.0062
2015	2010	24.59	0.079	0.042	3.073	0.099	0.0066	0.0181	0.0060	0.0046	0.010	0.0063
2020	2015	29.18	0.068	0.041	3.085	0.099	0.0064	0.0181	0.0059	0.0046	0.011	0.0042
2025	2020	30.99	0.067	0.040	3.053	0.099	0.0064	0.0181	0.0059	0.0046	0.011	0.0041
2030	2025	31.02	0.066	0.036	3.023	0.098	0.0064	0.0181	0.0059	0.0046	0.010	0.0041
2035	2030	31.08	0.063	0.036	2.953	0.096	0.0063	0.0181	0.0058	0.0046	0.010	0.0039
2040	2035	31.13	0.061	0.035	2.896	0.094	0.0063	0.0181	0.0058	0.0046	0.009	0.0038

Table 4: CG LDT emissions estimates for GREET2011. All emissions are in units of grams per mile driven [10].

Target Year	Model Year	MPG	VOC (Ex.)	VOC (Evap.)	CO	NO_X	PM_{10} (Ex.)	PM_{10} (TBW)	$PM_{2.5}$ (Ex.)	$PM_{2.5}$ (TBW)	CH_4	N_2O
2000	1995	18.55	0.867	0.66604	15.657	2.698	0.0231	0.0259	0.0213	0.0067	0.070	0.0684
2005	2000	17.42	0.460	0.27327	8.091	1.359	0.0167	0.0259	0.0154	0.0067	0.041	0.0531
2010	2005	16.80	0.200	0.06094	6.293	0.414	0.0125	0.0259	0.0115	0.0067	0.039	0.0128
2015	2010	18.63	0.097	0.00005	4.570	0.250	0.0123	0.0259	0.0113	0.0067	0.022	0.0124
2020	2015	23.04	0.082	0.00005	4.515	0.249	0.0119	0.0259	0.0110	0.0067	0.023	0.0070
2025	2020	24.28	0.081	0.00005	4.457	0.248	0.0118	0.0259	0.0109	0.0067	0.023	0.0069
2030	2025	24.28	0.082	0.00004	4.439	0.247	0.0118	0.0259	0.0109	0.0067	0.021	0.0069
2035	2030	24.32	0.080	0.00004	4.356	0.246	0.0117	0.0259	0.0108	0.0067	0.021	0.0067
2040	2035	24.36	0.077	0.00004	4.273	0.244	0.0117	0.0259	0.0107	0.0067	0.020	0.0064

Table 5: Diesel LDV emissions estimates for GREET2011. All emissions are in units of grams per mile driven [10].

Target Year	Model Year	MPG	VOC (Ex.)	VOC (Evap.)	CO	NO_X	PM_{10} (Ex.)	PM_{10} (TBW)	$PM_{2.5}$ (Ex.)	$PM_{2.5}$ (TBW)	CH_4	N_2O
2000	1995	25.70	0.156	0.0132	0.314	0.921	0.1304	0.0181	0.1266	0.0046	0.000	0
2005	2000	25.79	0.147	0.0066	0.292	0.891	0.1261	0.0181	0.1223	0.0046	0.000	0
2010	2005	25.79	0.146	0.0066	0.291	2.615	0.0047	0.0181	0.0046	0.0046	0.001	0.0007
2015	2010	25.51	0.050	0.0067	2.311	0.196	0.0037	0.0181	0.0036	0.0046	0.069	0.0007
2020	2015	34.71	0.050	0.0049	2.313	0.196	0.0037	0.0181	0.0036	0.0046	0.069	0.0007
2025	2020	36.86	0.049	0.0046	2.301	0.194	0.0037	0.0181	0.0036	0.0046	0.068	0.0007
2030	2025	36.88	0.048	0.0046	2.286	0.191	0.0037	0.0181	0.0035	0.0046	0.066	0.0006
2035	2030	36.93	0.046	0.0046	2.251	0.185	0.0036	0.0181	0.0035	0.0046	0.063	0.0006
2040	2035	36.98	0.044	0.0046	2.219	0.178	0.0036	0.0181	0.0035	0.0046	0.060	0.0006

Table 6: Diesel LDT emissions estimates for GREET2011. All emissions are in units of grams per mile driven [10].

Target Year	Model Year	MPG	VOC (Ex.)	VOC (Evap.)	CO	NO_X	PM_{10} (Ex.)	PM_{10} (TBW)	$PM_{2.5}$ (Ex.)	$PM_{2.5}$ (TBW)	CH_4	N_2O
2000	1995	17.64	0.904	0.0189	4.196	5.696	0.6368	0.0259	0.6177	0.0067	0.002	0.0026
2005	2000	17.15	0.863	0.0103	4.025	4.572	0.3062	0.0259	0.2970	0.0067	0.002	0.0026
2010	2005	13.84	0.626	0.0122	2.888	5.398	0.2355	0.0259	0.2285	0.0067	0.002	0.0027
2015	2010	14.84	0.061	0.0113	1.176	1.027	0.0118	0.0259	0.0114	0.0067	0.083	0.0027
2020	2015	15.92	0.060	0.0105	1.166	1.019	0.0107	0.0259	0.0103	0.0067	0.082	0.0027
2025	2020	16.07	0.059	0.0104	1.159	1.011	0.0106	0.0259	0.0103	0.0067	0.081	0.0027
2030	2025	16.08	0.059	0.0104	1.156	1.009	0.0106	0.0259	0.0103	0.0067	0.080	0.0027
2035	2030	16.09	0.057	0.0104	1.143	0.998	0.0106	0.0259	0.0103	0.0067	0.078	0.0026
2040	2035	16.11	0.056	0.0104	1.129	0.986	0.0106	0.0259	0.0103	0.0067	0.076	0.0026

It is important to note the large variances in the diesel tables indicated by red font. Specifically, N_2O shows zero emissions for diesel LDVs for the model years 1995 and 2000, the large jumps in CO and CH_4 from model year 2005 to 2010, and the spike in NO_x for model year 2005 diesel LDVs are all inconsistent. The increase in CH_4 is similar to that of the diesel LDTs, but the trends do not match for CO, NO_x, or the absence of N_2O emissions. Likewise, the trends produced for the diesel LDVs do not resemble the default timesheet table in GREET2011 (See Appendix A3). These changes are somewhat justified for a number of reasons, including the introduction of ULSD in this timeframe [27], the increased restrictions on NO_x as the Tier 2 program neared the end of the phasing period [3], and possibly issues with MOVES itself and the way it handles changing the Fueltype and Technologies importer. For these reasons, although the trends can still be helpful for future efforts, this study will not utilize the two diesel timesheets tables until the MOVES package is further developed.

5.0: Discussion

The results show that when compared to the previous GREET estimates, the updated MOVES calculations are similar in magnitude, aside from the few instances in the diesel simulations as stated previously. However, the projections created using MOVES are a rough estimate for future emissions levels. Inevitably, increasingly strict requirements will be set in order to continue to lower the emission levels of all vehicles. At this point, LDV and LDT generally meet these requirements at their initial production, aside from NO_x, which requires a vast improvement to meet the current fleet standard. However, once aged, these vehicles no longer meet the average Bin 5 EPA standards, and do not meet any of the NMOG standards. Thus, it appears that catalytic converter

manufacturers have room for improvement under the current standards, and more research should be targeted towards understanding and modeling the aging effect of catalysts. The tiered bin system will result in the higher bins becoming outdated, requiring vehicles to meet lower bin levels. For example, in the case of NO_x, one can assume that once vehicle fleets are meeting the set 0.07 g/mile standard, the required bin could be lowered to Bin 4 or further. ZEV and Bin 1 will always be the final level, as one cannot drop below zero emissions, but tiers that are more detailed are also likely.

Current technologies such as EGR and low temperature combustion (LTC) will lead to lower NO_x emission levels. EGR acts to lower NO_x by acting as a non-combustible heat sink in the cylinder. Cooled EGR, especially in the case of diesel engines and turbocharged engines, can further reduce in-cylinder temperatures, allowing for leaner combustion ratios with lower NO_x production. LTC engines may lead to lowered requirements for aftertreatment devices as this technology has shown to provide NO_x emission levels which meet EPA standards at the engine outlet. This is illustrated by Ojeda et al. who used partially premixed charge compression ignition (PCCI) technology combined with variable valve timing [28]. Due to high mixing requirements in PCCI and homogeneous charge compression ignition (HCCI) engines, there is not a direct method for initializing combustion. However, a study performed by Yao et al. describes techniques for controlling this combustion, including precise use of EGR in gasoline engines and controlled mixing in diesel engines [29]. This study also supports the need for further computer modeling of the combustion process through the development of five numerical models [29]. Other current issues with HCCI include a narrow operating range, issues with cold starts (further exaggerated by low ambient

temperatures), and techniques for homogeneous mixture preparation, crucial for efficient combustion resulting in low HC and PM emissions [29]. Further research in these areas, supported by improved understanding of fuel combustion and numerical modeling, will help to enhance the projection capabilities of MOVES for NO_x.

Of importance, the number of vehicles equipped with direct injection is growing steadily [30]. This technology reduces cold-start and general fuel consumption through better modulation along with the use of lean air-to-fuel (AF) mixtures in conjunction with a higher compression ratio. In fact, the average compression ratio in gasoline spark-ignition engines has risen from 9.6 in 2000 to 10.3 in 2008 [30]. This results in lowering brake-specific fuel consumption, providing better fuel economy and lower CO_2 emission rates. Enhanced fuel control through DI technologies also reduces engine-out CO and HC emissions. However, direct injection leads to higher PM engine-out emissions from the combustion of a rich fuel core spray from the injector. Furthermore, the lean global AF ratio combined with the higher compression ratio (thus higher in-cylinder pressures and combustion temperatures) leads to increased NO_x production. Future revisions of MOVES may need to include the option to study emissions from DI vs. PFI engines, investigating the effects of this technology.

This study has also shown the effects of a relatively cold climate on the performance of the catalyst. From Christenson and Loiselle's study of temperature effects on commercial vehicles, one can see that the trends created by MOVES follow real-world experimentation [25]. Automobile cold-starts, especially in areas of low ambient temperature, can lead to a large increase in HC, CO, and PM emissions. Part of this degradation is due to heat loss from the exhaust traveling to the catalyst from the

exhaust manifold. Over the past ten years, car manufacturers have begun to implement close-coupled catalysts in order to reduce exhaust heat losses in traveling to the catalyst. A computer model developed by Koltsakis and Tsinoglou shows that this technology can vastly reduce the time required to reach the catalyst light-off temperature, often times reaching this critical point within 20 seconds [26]. However, this practice can lead to effects, as stated previously, such as non-uniform aging. As studied, rapid aging can be extremely detrimental to the conversion efficiency of the catalyst, and thus is an area of concern. However, future developments may lead to changes that improve the uniformity of the exhaust flow, mitigating this effect.

This study shows the effects of aging through studying current-year, 10YO, and 20YO vehicle models, showing that, in order to meet the current EPA standards, vehicle manufacturers must improve the performance of the catalyst system at the full life of the vehicle. A number of studies investigate this fact, including He and Shao's study of the test methods used to analyze the aging effects on three-way catalysts [31]. In that study, they describe two testing methods: one based on time aging, the other investigating driving distance aging. The results therein show that in general, the catalysts tested pass the EURO I and II regulations after 80,000 km and 100 hours aging [31]. Kaspar et al. determine that in addition to improved aging and low ambient temperature cold-start emissions, future catalyst systems must have extreme thermal stability and be able to handle temperatures exceeding 1100 °C [32].

6.0: Future Efforts

Moving forward using MOVES, one can model vehicle start-up emissions as a methodology to stress the importance of a lower light-off temperature in catalytic

converters, or improvements to heating the aftertreatment devices. Although MOVES does not model or report the light-off temperatures, it can analyze the number and duration of starts, thus making this a possibility for future work. Future work may also include studying the effects of extended idle conditions on the performance of the catalytic converters. This information is important in looking at city driving at times of high traffic, typical of many daily commuters.

The results provide a baseline for future experimentation with biofuels, their exhaust constituents, and the subsequent effects on the performance of catalytic aftertreatment devices. The recent influx of biofuels, including ethanol and various biodiesels, will affect the aftertreatment system as shown in Fathali and Ekstrom's study of three-way catalysts in E85 fueled vehicles [33]. In this study, Fathali and Ekstrom depict the production of methane gas through catalysis of ethanol exhaust gas. Likewise, studies of NO_x production from biodiesel use can be analyzed similar to that of Eckerle et al. study who used methyl ester biodiesel blends to augment NO_x emission levels [34]. Furthermore, studying the effects caused by different climates could lead to developing trends to help identify emission constituents based on temperature.

7.0: References

1. United States Environmental Protection Agency. *History of the Clean Air Act*. 2012; February 17, 2012 [Available from: http://epa.gov/oar/caa/caa_history.html.
2. United States Environmental Protection Agency. *Mobile Source Emissions - Past, Present, and Future: Milestones*. 2012 January 3, 2012; January 3, 2012 [Available from: http://www.epa.gov/otaq/invntory/overview/solutions/milestones.htm.
3. United States Environmental Protection Agency. *Summary of Current and Historical Light-Duty Vehicle Emission Standards*. 2010 3/7/2012; 6/21/2012 [Available from: http://www.epa.gov/greenvehicles/detailedchart.pdf.
4. Mooney, J.J. *An AIChE Mini History of John Mooney*. 2012; Available from: http://chemicaleng.njit.edu/news/JMooney.php.
5. Rousseau, A.; Ahluwahlia, R.; Deville, B.; Zhang, Q.; *Well-to-Wheels Analysis of Advanced SUV Fuel Cell Vehicles.* 2003, SAE International.
6. Rousseau, A. and P. Sharer, *Comparing Apples to Apples: Well-to-Wheel Analysis of Current ICE and Fuel Cell Vehicle Technologies.* 2004.
7. Atkins, M.J. and C.R. Koch, *A Well-to-Wheel Comparison of Several Powertrain Technologies.* 2003.
8. Wang, M.; Y. Wu; and A. Elgowainy; *Operating manual for GREET: Version 1.7.* Center for Transportation Research, Energy Systems Division, Argonne National Laboratory, Iowa, 2007: p. 119.
9. United States Environmental Protection Agency. *Motor Vehicle Emission Simulator (MOVES): User Guide for MOVES2010a*. 2010 August 2010 [cited EPA-420-B-10-036; August 2010 [Available from: http://www.epa.gov/otaq/models/moves/MOVES2010a/420b10036.pdf.
10. Wang, M., *Argonne National Lab's Greenhouse Gases, Regulated Emissions, and Energy Use in Transportation Model.* Center for Transportation Research, Energy Systems Division, Argonne National Laboratory, Iowa, 2011.
11. Subramanyan, K. and U.M. Diwekar, *User Manual for Stochastic Simulation Capability in GREET.* Argonne National Laboratory: Argonne, IL, 2005.
12. United States Environmental Protection Agency, *MOVES (Motor Vehicle Emission Simulator)*, 2010.
13. United States Environmental Protection Agency, *Conversion Factors for Hydrocarbon Emission Components.* 2005. **EPA420-R-05-015**.
14. United States Environmental Protection Agency. *Final Report: Development of Emission Rates for Light-Duty Vehicles in the Motor Vehicle Emissions Simulator (MOVES2010)*. 2011 [EPA-420-R-11-011; August 2011 [Available from: http://www.epa.gov/otaq/models/moves/documents/420r11011.pdf.
15. Brzezinski, D., *Via Electronic Mail*, April 4, 2012, United States Environmental Protection Agency.
16. Diesel Net. *Emission Standards: USA: Cars and Light-Duty Trucks - Tier 2*. 2006; 2006 [Available from: http://www.dieselnet.com/standards/us/ld_t2.php.
17. United States Environmental Protection Agency. *Light-Duty Vehicle and Light-Duty Truck -- Tier 0, Tier 1, National Low Emission Vehicle (NLEV) and Clean Fuel Vehicle (CFV) Exhaust Emission Standards*. 2010; August 5, 2010 [Available from: http://www.epa.gov/otaq/standards/light-duty/tiers0-1-ldstds.htm.
18. U.S. Department of Energy Alternative Fuels Data Center, *Light-Duty Vehicles Sold in the U.S.*, 2012.

19. Sougawa, Y.; Koseki, K.; Kawaguchi, K.; Nishimura, J.; Namiyama, K.; Yamagishi, Y.; Ogawa, Y.; *Improvement of Repeatability in Tailpipe Emission Measurement with Direct Injection Spark Ignition (DISI) Vehicles*, 2002, SAE International.
20. Zhang, S. and W. McMahon, *Particulate Emissions for LEV II Light-Duty Gasoline Direct Injection Vehicles.* SAE Int. J. Fuels Lubr., 2012. **5**(2): pp. 637-646.
21. Sadakane, S.; Sugiyama, M.; Kishi, H.; Abe, S.; Harada, J.; Sonoda, Y.; *Development of a New V-6 High Performance Stoichiometric Gasoline Direct Injection Engine*, 2005, SAE International.
22. Hashimoto, K.; Kagi, Y.; Arai, M.; Tamura, M.; *Effects of Fuel Properties on the Stratified-Charge Combustion of Direct-Injection Gasoline Engine with EGR*, 2003, SAE International.
23. Theis, J.R.; Ura, J.A.; Li, J.J.; Surnilla, G.G.; Roth, J.M.; Goralski, C.T.; *NOx Release Characteristics of Lean NOx Traps During Rich Purges.* 2003.
24. Andrews, G.E.; Zhu, G.; Li, H.; Simpson, A.; Wylie, J.A.; Bell, M.; Tate, J.; *The Effect of Ambient Temperature on Cold Start Urban Traffic Emissions for a Real World SI Car*, 2004, SAE International.
25. Christenson, M.; Loiselle, A.; Karman, D.; Graham, L.A.; *The Effect of Driving Conditions and Ambient Temperature on Light Duty Gasoline-Electric Hybrid Vehicles (2): Fuel Consumption and Gaseous Pollutant Emission Rates.* 2007.
26. Koltsakis, G.C. and D.N. Tsinoglou, *Thermal Response of Close-Coupled Catalysts During Light-Off*, 2003, SAE International.
27. United States Environmental Protection Agency, *EPA Enforcing Diesel Fuel Pump Label Requirements*, 2007.
28. Ojeda, W.d.H., K.; Taylor, S.; *Low-Temperature Combustion Demonstrator for High Efficiency Clean Combustion.* U.S. Department of Energy's FY 2009 Progress Report for Advanced Combustion Engine Research and Development, 2009. **December 2009**.
29. Yao, M.; Z. Zheng; and H. Liu; *Progress and recent trends in homogeneous charge compression ignition (HCCI) engines.* Progress in Energy and Combustion Science, 2009. **35**(5): pp. 398-437.
30. Heywood, J.B. and O.Z. Welling, *Trends in Performance Characteristics of Modern Automobile SI and Diesel Engines.* SAE Int. J. Engines, 2009. **2**(1): p. 1650-1662.
31. He, Z.; Shao, Q.; Li, Y.; Jing, Z.; Duan, Q.; *Study on the Aging Test Methods and the Properties of the Three-Way Catalysts.* 2003.
32. Kaspar, J.; P. Fornasiero; and N. Hickey; *Automotive catalytic converters: current status and some perspectives.* Catalysis Today, 2003. **77**(4): p. 419-449.
33. Fathali, A. and M. Ekström, *Methane Production over Three-Way Catalysts in E85-Fuelled Vehicles.* 2011.
34. Eckerle, W.A.; Lyford-Pike, E.J.; Stanton, D.W.; LaPointe, L.A; Whitacre, S.D; Wall, J.C; *Effects of Methyl Ester Biodiesel Blends on NOx Emissions.* SAE Int. J. Fuels Lubr., 2008. **1**(1): p. 102-118.

Well-to-Wheels Energy and Emissions Analysis of a Recycled 1974 VW Super Beetle Converted into a Plug-in Series Hybrid Electric Vehicle

Austin Hausmann, Bryan Strecker, Christopher Depcik

Department of Mechanical Engineering - University of Kansas, Lawrence, Kansas (United States)

Abstract

The low emission and high fuel economy standards set by regulatory agencies are causing an increase in the number of electrified (hybrid, plug-in hybrid, and battery electric) vehicles reaching the marketplace. In order for students to obtain a better understanding of the architecture of these vehicles, a 1974 Volkswagen Super Beetle was converted into a plug-in series hybrid electric vehicle with a generator that runs on used canola oil biodiesel. Moreover, this vehicle is connected to a solar photovoltaic charging station for a comparison of recharging on or off the electrical grid. To analyze this recycling of a vehicle including renewable energy sources requires a life cycle energy and emissions analysis (LCA). To this end, this effort utilizes the Argonne National Laboratory Greenhouse Gases, Regulated Emissions, and Energy Use in Transportation (GREET) model. Moreover, a Matlab-based vehicle dynamics simulation coupled to GREET provides a localized driving cycle examination in the LCA. The resulting outcomes presented include the reduction in energy use and emissions through recycling and component reuse for a vehicle. Moreover, on-road testing with model validation demonstrates fuel savings using a more efficient vehicle over the baseline design. Finally, this effort documents improvements in the sustainability of the vehicle by incorporating solar energy for charging.

Words: 206

Nomenclature

Variable	Description	Units
A_f	Frontal area	[m2]
$C_{20\text{-}hr}$	Typical 20-hour capacity of the battery	[Ah]
C_D	Coefficient of drag	[-]
$CR_{batt}(t)$	Charge removed from the batteries at current time step	[Ah]
$CR_{batt}(t\text{-}1)$	Charge removed from the batteries at the previous time step	[Ah]
C_{total}	Peukert battery capacity	[Ah]
dt	Time difference between steps	[s]
d_{tire}	Tire diameter	[m]
E_N	amount of individual electricity type used in the mix	[kWh]
E_{tot}	Total amount of electricity used in the mix	[kWh]
F_{AD}	Aerodynamic drag force	[N]
$f_{BD,PtW}$	Pump-to-Wheels biodiesel emissions factor	[g/gal]
$f_{BD,WtP}$	Well-to-Pump biodiesel emissions factor	[g/gal]
F_{GR}	Gradation force	[N]
F_{LA}	Linear acceleration force	[N]
F_{RR}	Rolling resistance force	[N]
F_{TE}	Tracrive Force	[N]
g	Gravitational constant	[m/s2]
$G_{BD,PtW}$	Default GREET biodiesel emissions factor for Pump-to-Wheels	[g/mile]
$G_{BD,WtP}$	Default GREET biodiesel emissions factor for Well-to-Pump	[g/mmBtu]
$G_{elec,N}$	Individual default electricity emissions factor	[g/]
G_{final}	Final drive ratio	[-]
$I_{batt}{}^{out}$	Current draw from the batteries	[A]
k	Peukert coefficient	[-]
LHV	Lower heating value	[mmBtu/gal]
m	Mass of the vehicle	[kg]
MPG	Vehicle fuel economy	[mi/gal]
N	number of electricity types in the mix	[-]
N_{gears}	Number of gears in the transmission	[-]
P_{acc}	Accessory power draw	[W]
$P_{motor}{}^{in}$	Power into the motorfrom the battery	[W]
$P_{motor}{}^{out}$	Required output shaft power at the motor	[W]
$P_{batt}{}^{out}$	Battery power out	[W]

$P_{required}$	Power required by the electric motor	[W]
R_{batt}	Battery terminal resistance	[ohm]
SOC	Battery pack state of charge	[-]
t_0	Initial time	[s]
t_1	Final time	[s]
V	Vehicle velocity	[m/s]
$V(t_i)$	Velocity at the current time step	[m/s]
$V(t_{i-1})$	Velocity at the previous time step	[m/s]
V_{batt}	Battery pack voltage	[V]
η_{motor}	Motor efficiency	[-]
$\eta_{transmission}$	Transmission efficiency	[-]
θ	Road angle relative to the horizontal	[deg]
μ_{RR}	Coefficient of rolling resistance friction	[-]
ρ	air density	[kg/m3]
τ_{motor}	motor output torque	[N-m]
Ω	Motor output rotational speed	[rad/s]

1.0: Introduction

Recent legislation by the Environmental Protection Agency (EPA), California Air Resources Board (CARB), and other emission regulatory commissions require that automotive manufacturers must reduce exhaust emissions to miniscule levels [1]. Meeting these requirements is becoming increasingly difficult for traditional internal combustion engine (ICE) technologies. Compounding this problem is the simultaneous requirement of low emissions while maintaining the performance and fuel consumption expectations of consumers and regulatory agencies. In particular, reducing engine out emissions levels from ICEs often results in degradation in performance (e.g., power) through later combustion phasing [2] and additional fuel usage for catalytic exhaust aftertreatment devices (e.g., catalyst or particulate filter regeneration [3-5]).

These pollution concerns coupled with ever-rising oil prices have led many companies to investigate the use of electric drive components in order to increase

efficiency and lessen emissions. Electric drive vehicles are defined as any vehicles that "*use one or more electric motors or traction motors for propulsion*" [6]. For full-scale deployment of electric drive vehicles, many key vehicle logistical parameters require examination including, but not limited to, driving range requirements, charging times[6], and on-road vehicle performance. One of the most common reluctances in purchasing electric vehicles is their limited range. Consumers are often worried about having the range required to complete their daily driving and what they will do if the battery pack starts to run low, often known as range anxiety [7]. Furthermore, although the use of electricity in the vehicle is clean (e.g., zero tailpipe emissions), its production is energy intensive and results in a wide array of emissions. In this area, vehicle life cycle analyses (LCA) examine the emissions produced in powering electrified vehicles (EV), comparing them to conventional internal combustion engine vehicles (ICEV).

In order to quickly train students and increase the pace of understanding regarding EVs while starting a new automotive program from scratch, the simplest approach involves replacing the drive train in an existing vehicle in order to retain the body, chassis, and other particular elements (e.g., transmission) that do not hinder the conversion from an ICEV to an EV. To this end, Das Autohaus of Lawrence, KS generously donated a 1974 Volkswagen (VW) Super Beetle for this effort. Since this vehicle is one of the top selling automobiles in history, it maintains widespread availability of replacement parts, and allows for other institutions to reproduce the results of this paper [8]. Moreover, the construction of a 1.1 kW solar photovoltaic (PV) charging station on campus while adding a removable diesel generator to the vehicle allows for analysis as an EV or plug-in series hybrid electric vehicle (PHEV) including

both conventional and renewable energy sources. This generator operates on biodiesel created from used canola oil from the cafeterias on the authors' campus. Utilizing waste cooking oil diverts waste from landfills, converting it instead to usable fuel, further increasing the sustainability of the vehicle [9]. Biodiesel use also decreases the amount of harmful emissions produced by the vehicle (e.g., carbon monoxide, hydrocarbons, and particulate matter)as compared to ultra low sulfur diesel [10, 11]. Thus, there are a number of fuel sources acting in this system, providing multiple degrees of freedom, allowing for a balanced utilization of multiple sources of conventional and renewable energy in an LCA.

Prior to an estimation of an LCA for the VW, it is pertinent to review the literature regarding the reuse of vehicle components and the benefits of vehicle conversion to a more efficient platform. Later sections document an improvement to current LCA techniques through incorporation of a vehicle dynamics model coupled to a full energy and emissions analysis.

1.1: Reuse of Vehicle Components

Manufacturing vehicle components is a highly energy intensive process, and thus is important to this study when considering the parts reused from the original vehicle. Sullivan, Burnham, and Wang from the Argonne National Laboratory performed an in-depth study of vehicle and component manufacturing in order to improve the Greenhouse Gases, Regulated Emissions, and Energy Use in Transportation (GREET) version 2 model[12]. In particular, this materials recycling work utilizes GREET 2.7 and its Series 1 counterpart: GREET 1.8c. The fuel analysis later in this work utilizes GREET 2011, which boasts updated fuel emissions. Through an extensive literature

review examining material transformation, machining, vehicle painting, HVAC and lighting, material handling, welding, and compressed air use, Sullivan et al. calculate the total energy use per 1532 kg vehicle to be 33.9 GJ, producing 2013 kg of CO_2 in the process [12]. Of these processes, material transformation is the largest contributor at 19.3 GJ and 1065 kg of CO_2 [12]. This total energy use is much lower than the United States Council for the 1998 Automotive Research (USCAR) reports, which states that given a 1530 kg ICEV, approximately 39.9 GJ of energy is required, emitting 2610kg of CO_2 [13]. In comparison, a study conducted by Kobayashi in 1997 reports a total energy consumption of 19.9 GJ and 1.04 kg of CO_2 for a 1270 kg vehicle [12].

Other efforts of Sullivan and Cobas-Flores compare the methodologies of nine different automobile LCAs, separating the vehicle's life into six categories: material production, part and product manufacturing, operation, maintenance, end-of-life disposal, and infrastructure considerations. They then consider the energy requirements and emission burdens of five of these areas (excluding infrastructure considerations due to lack of data). In these, the manufacturing is stated to produce anywhere from 1800 to 7500 kg of CO_2 with 1039 to 2615 kg for assembly, and 39 to 240 kg for end-of-life disposal [14], all depending on the style and size of the vehicles. These studies indicate that the amount of energy used in manufacturing vehicles is variable depending on which processes are included in the LCA.

This energy intensive process of vehicle manufacturing and eventual disposal leads to the potential of component recycling and reuse as a methodology for widespread energy and emissions reductions. This is of interest around the world as indicated by Amelia et al.'s study of automotive component reuse in Malaysia [15],

Chen's discussion of end-of-life vehicle (ELV) recycling in China [16], and Kanari et al.'s study in the European Union [17]. Each of these investigations considers the processes currently utilized in dismantling and recycling ELVs in their respective areas, focusing mainly on the economic benefits and landfill prevention from the automotive industry.

With respect to landfill prevention, Daniels et al. states that 75% of automotive materials are recyclable, resulting in the deposit of 2.7-4.5 million tons per year of material in landfills throughout the United States [18]. Chen discusses multiple forms of component reuse in China, including aftermarket sales, direct reassembly by the manufacturer, debasement (such as tires used to stabilize river banks), and remanufacture, as well as a number of material recycling techniques [16]. Through proposed improvements in the dismantling and reuse facilities via a pilot ELV dismantling plant, Chen boasts an improved reused parts rate from 22.5% to 31.7%, reducing landfill deposits from 10% to 4% of all ELV materials [16].

In this area, Amelia et al. identify component reuse as the most effective method of recycling as it avoids the repair process in remanufacturing and the complete reprocessing of the materials in recycling. The full process in component reuse is disassembly, sorting, cleaning, reassembly, and testing. Thus, it is a relatively low energy intensive process as it does not require raw material extraction, reprocessing, and forming the parts [15]. As a result, the recycling and reuse of vehicle components can lead to significant gains in the areas of energy, emissions, and landfill reduction. However, there are a number of concerns involving reliability and safety of these parts since they were likely developed prior to improved processes [15]. This requires an understanding of the repurposing of a vehicle destined for the junkyard.

1.2: Reuse of More Efficient Vehicle

Sullivan and Cobas-Flores indicate that 60 to 80% of energy use and emission production over the lifetime of the vehicle is due to vehicle operation [14]. This is important when considering the effects of removing inefficient vehicles from the road, often times replacing them with more efficient, newer vehicles (analogous to the authors' efforts of replacing an inefficient drive train with a highly efficient version).

In 2009, the United States passed the Consumer Assistance to Recycle and Save (CARS) Act giving vouchers worth either $3500 or $4500 to citizens trading in old, inefficient vehicles for new fuel-efficient vehicles in an attempt to remove old vehicles from the road. The required fuel economy of the vehicle purchased was required to be at least 22 mpg for passenger cars, 18 mpg for category 1 trucks, and 15 mpg for category 2 trucks [19]. This program issued $2.85 billion, replacing 677,842 cars, light- and heavy-duty trucks, having an average combined fuel efficiency of 24.9 mpg. The vehicles traded in had an average fuel efficiency of 15.8 mpg, improving by 9.2 mpg on average [19]. This program created over 60,000 jobs and raised the national GDP by $3 billion [19].

A number of studies following this program analyzed the energy and emissions savings induced by this program, including Lenski et al.'s LCA approach [20]. This study identifies three main areas that influence the energy and environmental impacts in the LCA: (1) the early retirement of lower efficiency vehicles that are still drivable, (2) the effect of using vehicles that are more efficient as required by the CARS program, and (3) the adverse effect of premature production and disposal of the vehicles in the trade. Calculation of the influence of the first category is straightforward using the

difference in fuel economy, average vehicle miles traveled, and a GREET-calculated emissions coefficient, resulting in a net reduction of 3.7 billion kg of CO_2. The second category investigates the improved fuel economy of CARS-applicable vehicles sold as compared to non-CARS vehicles. In particular, the cars purchased had a 19% greater average level of fuel economy than all new vehicles purchased during this time [21]. This resulted in a total savings of 1.5 billion kg of CO_2. Finally, they calculate emissions estimates for the early production of these new vehicles, and the emissions produced by disposing of the trade-ins earlier than their end-of-life estimated time. This results in a detriment of 800 million kg of CO_2 [20]. Thus, this study calculates a total savings of around 4.4 billion kg of CO_2.

These earlier studies investigate the replacement of the complete vehicle with a more modern design; however, this effort implements a modular approach not a wholesale change. As the prior section discussed, the reuse of vehicle components will have significant energy, emissions, and landfill reduction benefits. Thus, the savings would be greater in comparison to Lenski et al.'s findings by effectively eliminating a significant fraction of the third area. Moreover, it is important to consider a pertinent vehicle platform in order to promote large-scale applications.

In particular, the conversion process of this study is directly applicable to situations similar to the VW Beetle taxi replacements in Mexico City, thus giving this work a widespread consumer base [22]. This work outlines a vehicle renovation usable in this situation, replacing ELVs with modern, efficient versions. This transformation can greatly reduce the magnitude of urban emissions. According to an emissions inventory for the Metropolitan Area of Mexico City, vehicles account for 40% of the total

hydrocarbon (THC) emissions, 98% of the total carbon monoxide (CO) emissions, and 81% of the total nitrogen oxides (NO_x) emissions [23]. As a result, conversion of these vehicles from conventional, inefficient ICEVs will lead to an improvement in the overall air quality in highly populated urban areas.

1.3: Outcomes of Study

This study analyzes the energy and environmental benefits from reusing a majority of the VW parts as part of an LCA incorporating Argonne National Laboratory's GREET Model, specifically GREET2.7 (coupled with the default GREET 1 series 1.8c), released in 2006[24]. The work also examines the energy use and emissions from electricity and biodiesel production utilizing the GREET 1 series, specifically GREET1 2011. In specific, this investigation seeks to provide an understanding of converting an ELV into a more modern vehicle through the following three mechanisms:

- Recycling and component reuse, and the energy use and emissions avoided in this process,
- Fuel savings through the use of more efficient vehicles over their baseline components studied through model validation and testing, and
- The use of renewable energy in improving the fuel sustainability of EVs.

With respect to vehicle operation, the authors drove the Beetle in three different modes: as a hybrid operating in EV mode (i.e., the generator present, but not running), as a series hybrid in extended range mode (i.e., with the generator running), and in EV mode with the generator removed. The use of all three operating modes facilitates analyzing the benefits and drawbacks to each driving style, including showing the balance between the added weight of the generator and the benefit of the extended

range in easing range anxiety. Furthermore, this work studies the energy use and emissions among the three driving styles in improving the vehicle LCA.

2.0: Electrified Vehicle Dynamics Model

In order to understand electric drive vehicle energy usage, this work formulates a model utilizing Newton's Second Law (conservation of momentum) for a constant mass object. The model includes typical physical vehicle parameters and energy flow algorithms in predicting vehicle performance while utilizing relatively simplistic inputs. In particular, the simulation of virtually any conceivable route happens using only vehicle velocity and elevation data. Calibrating the model to the test vehicle allows further efforts implementing a generic drive cycle, such as the EPA's Urban Dynamometer Driving Schedule (UDDS)[25], comparing the fuel economy against the stated EPA efficiency. Furthermore, in the case of the Mexico City taxi replacements, one could create a more representative LCA by allowing the user to analyze the energy usage and resulting emissions of the vehicle simply by inputting a generic Mexico City drive cycle into the model. This provides a better understanding of efficiency losses that facilitate research into making further improvements to the vehicle design. Moreover, this can help reduce range anxiety by using the model to size the vehicle battery pack properly for the demands of the driver.

At each time step in the model, a total tractive force balance is calculated:

$$F_{TE} = F_{GR} + F_{AD} + F_{RR} + F_{LA} \quad (1)$$

where F_{GR} is the gradation force, F_{AD} is the aerodynamic force, F_{RR} is the rolling resistance force, and F_{LA} is the linear acceleration force (all in Newtons). The summation of these forces determines the overall magnitude and direction of the force

required to produce vehicular motion or lack thereof (F_{TE}). Figure 1 shows these forces in a free-body diagram.

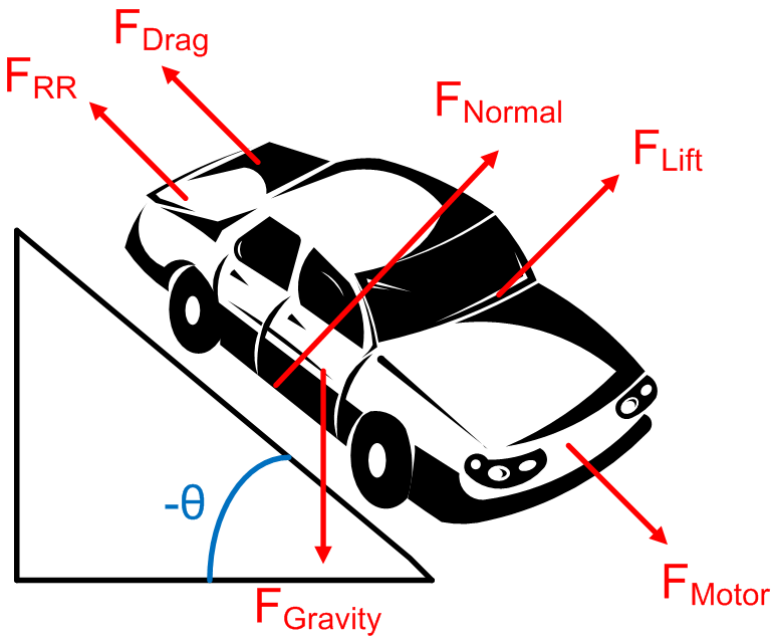

Figure 1: Free body diagram of the forces considered in the dynamics model [26].

Calculation of the gradation force occurs using the total weight of the vehicle and the road angle relative to the horizontal (θ) in order to determine the force required to overcome the vertical change in distance:

$$F_{GR} = mg\sin\theta \tag{2}$$

where m is the vehicle mass and g is the gravitational constant. In this expression, determination of the road angle occurs geometrically:

$$\theta = \tan^{-1}\left\{\frac{\text{elevation}(t_1) - \text{elevation}(t_0)}{0.5\left[\text{velocity}(t_1) + \text{velocity}(t_0)\right](t_1 - t_0)}\right\} \tag{3}$$

where t_0 is the initial time and t_1 is the final time of the time step under investigation. This effect either decelerates the vehicle (positive grade change) or aids in the acceleration of the vehicle (negative grade change).

The aerodynamic force is a function of the air density (ρ), frontal area of the vehicle (A_f), coefficient of drag (C_D), and vehicle velocity (V) [27]:

$$F_D = \frac{1}{2}\rho A_f C_D V^2 \tag{4}$$

The traditional form of the rolling resistance force includes the vehicle weight (mg), rolling resistance coefficient (μ_{RR}), and road angle [28]:

$$F_{RR} = \mu_{RR} mg\cos\theta \tag{5}$$

Note that, the first author has formulated other aerodynamic drag force and rolling resistance models in his master's thesis applicable for this study [29]; however, it is preliminary to include them at this stage. Thus, literature standard models are incorporated.

The final component of the tractive force balance is the linear acceleration force [28]:

$$F_{LA} = m\left[V\left(t_i\right) - V\left(t_{i-1}\right)\right]/dt \tag{6}$$

where $V(t_i)$ is the velocity at the current numerical step and $V(t_{i\text{-}1})$ is the vehicle velocity at the previous numerical step. This linear acceleration force essentially incorporates Newton's Second Law and is a function of the vehicle mass and acceleration required to match the drive cycle recorded velocity profile.

Conversion to the power required by the electric motor at the rear wheels ($P_{required}$) occurs by multiplying the total tractive force by the vehicle velocity:

$$P_{required} = F_{TE} V\left(t\right) \tag{7}$$

This transformation of the force balance into an energy input allows for a more direct calculation of drive train power requirements. Moreover, this energy constraint is not the power output required by the battery pack, but the power applied to the rear wheels

after including all driveline efficiency losses in order to accelerate the vehicle according to the input velocity.

Solving for the battery power requirement systematically happens by moving from the wheels through the driveline to the motor and finally calculating the power draw from the battery pack. First, the use of the transmission efficiency ($\eta_{transmission}$) allows for calculation of the motor output shaft power (P_{motor}^{out}) from the power required at the wheels:

$$P_{motor}^{out} = P_{required}\eta_{transmission} \quad (8)$$

Both automatic and manual transmissions typically use spur and helical gear combinations in order to either reduce or increase the output speed of the motor [30, 31]. Spur and helical gears have a power transmission efficiency of approximately 96-99% per mating pair. The losses are generally a result of fluid drag and friction on the gear contact surfaces [30, 31]. While electrified vehicles do not typically use traditional transmissions [28], correct transmission design optimization could possibly lead to an increase in efficiency and range depending on the vehicle route and application [12-14]. All else being equal, as the number of gears and contact points between the gears increases, the overall efficiency of the transmission decreases.

As a result, estimation of transmission efficiency occurs using the total number of gears as a mathematical power term:

$$\eta_{transmission} = 0.99^{(2+N_{gears})} \quad (9)$$

The value of two in the exponent accounts for the rear differential efficiency and N_{gears} is the number of gear combinations in the transmission. For typical electric vehicle reduction boxes, this value will be one. This method simply assumes a 99% mating efficiency taken to the power of the number of gearing combinations; however, it avoids

obtaining specific information regarding the internals of the vehicle transmission. While this method is elementary, it provides a reasonable method for estimating transmission efficiency while maintaining computational speed. Improving this method further entails utilizing a dynamic transmission efficiency model based on the rotational speed and physical design of each gear [32].

Calculation of the motor torque required (τ_{motor}) then follows using the motor output shaft power divided by the motor speed:

$$\tau_{motor} = P_{motor}^{out} / \Omega \tag{10}$$

where Ω is the rotational speed of the motor in radians per second calculated from the vehicle speed:

$$\Omega = 2\pi G_{final} V(t) / d_{tire} \tag{11}$$

where G_{final} is the final drive ratio of the vehicle and d_{tire} is the diameter of the tire. If the rotational speed of the motor or the requested torque exceeds the limiting values specified by the manufacturer, the values are set to their limits with subsequent recalculation of the force balance.

Determination of motor efficiency (η_{motor}) then occurs by means of a look-up map using the torque and rotational speed of the motor. Details of this process as well as other model implementation features can be found in previous work by the first author [29]. Use of this value in conjunction with the motor output shaft power allows for computation of the incoming motor power requirement:

$$P_{motor}^{in} = P_{motor}^{out} / \eta_{motor} \tag{12}$$

In other words, there is an efficiency loss across the motor that relates the power input to the motor to the actual power delivered by the motor.

Furthermore, the total battery power draw requirement $\left(P_{batt}^{out}\right)$ is now a function of this input motor power requirement and the total power draw of all vehicle accessories (P_{acc}):

$$P_{batt}^{out} = P_{motor}^{in} + P_{acc} \tag{13}$$

The authors present the power draw for these accessories, such as the auxiliary 12-volt system, in Section 4.2.

Determination of the current draw from the battery pack requires knowledge of the battery pack voltage. In order to initialize the simulation, the first numerical time step utilizes the pack voltage at the initial State of Charge (SOC). After computing the voltage and battery power draw, the fundamental power equation allows for determination of the battery current draw. Moreover, in order to provide for a more physical representation of actual battery usage, battery internal resistance effects are integrated [28]:

$$P_{batt}^{out} = V_{batt} I_{batt}^{out} - 2R_{batt}\left(I_{batt}^{out}\right)^2 \tag{14}$$

where V_{batt} is the pack voltage and I_{batt}^{out} is the current draw coming from the batteries. The value of two in the above equation accounts for the resistance (R_{batt}) through each battery terminal (one positive terminal and one negative terminal).

Rearrangement of the terms leads to a quadratic formula representing the current draw of the battery with respect to the battery voltage, internal resistance, and power draw:

$$I_{batt}^{out} = \frac{V_{batt} - \sqrt{\left(V_{batt}\right)^2 - 8\left(R_{batt} P_{batt}^{out}\right)}}{4\left(R_{batt}\right)} \tag{15}$$

This current draw allows for calculation of the voltage drop of the battery pack under load for the next time step.

Electric motor control units often use current and power limiting in order to protect the power source and electric motor from excessive energy draws [28, 33, 34]. In order to account for this, the motor controller often includes an adjustable constant current limit (e.g., maximum current allowed). Hence, the model incorporates a user defined current limit that checks against the current calculated in Eqn. (15). If the calculated current is greater than the defined current limit, the current draw at the time step under calculation in the simulation is then set to the limit value.

It is important to note that since calculation of the motor power occurs from the specified acceleration in an input file, it may require a current draw beyond the current limit. Hence, this necessitates a recalculation of the motor power and vehicle acceleration in order to account for the implemented current draw limit. This is done using an iterative loop that reduces the velocity of the vehicle in small steps (0.1 m/s increments) until the current requirement that is needed to match this velocity is equal to the current draw limit. Furthermore, calculation of a new force balance happens at each step of the iterative loop using this new velocity estimate. Hence, it is possible that the electrified drive train cannot match the intended driving profile (e.g., in the case of a theoretical drive cycle).

Due to the desire to keep the design as simple and inexpensive as possible, the VW implements a brushed DC motor that is incapable of regenerative braking. Thus, in order to retain transferability to other vehicles in the future, the model includes a

regenerative braking scheme; however, it is not included in this work and instead is described in the first author's thesis [29].

Determination of the final current draw allows for calculation of the charge removed (CR) from the battery pack. The charge removed is a function of the current draw, the Peukert coefficient (k), and the time duration of the current draw:

$$CR_{batt}(t) = CR_{batt}(t-1) + \left[\frac{I_{ref}\left(I_{batt}^{out}/I_{ref}\right)^{k}}{\left(3600/dt\right)} \right] \tag{16}$$

where 3600 is used to convert the discharge capacity from amp-seconds to amp-hours and dt is the time step of the model in seconds. This is similar to Coulomb counting with the addition of the Peukert constant (k) to account for the intrinsic cell losses [35].

Then, tracking the charge removed over the course of the simulation allows for determination of the SOC of the battery pack at each time step:

$$\mathrm{SOC}(t) = 1 - \frac{CR_{batt}(t)}{C_{total}} \tag{17}$$

Note the capacity is the Peukert capacity:

$$C_{total} = \left[\left(C_{20-hr} \Big/ 20 \right)^{k} \right] 20 \tag{18}$$

where $C_{20\text{-}hr}$ is the typical 20-hour capacity specified by the battery manufacturer. This 20-hour capacity is the capacity of the battery related to a constant discharge of one amp for 20 hours. Effectively, the use of Eqn. (18) normalizes the battery capacity based on Peukert's coefficient.

3.0: Solar PV Vehicle Charging Station

This effort implements a solar photovoltaic electricity charging station in order to study the effects of renewable energy on the life cycle emissions of the vehicle. The

solar array utilized in the fueling station consists of six solar panels: two Schuco S SPU-4 series 180 W monocrystalline panels, and four Kyocera KD-185GX-LPU 185 W monocrystalline panels, for a total of 1.1 kW. The array consists of pairs of panels in series, the three pairs wired in parallel to bring the total current up to 23 A at 24 VDC given ideal conditions. The combined surface area of these panels is 8.06 m^2, which is important when calculating the available energy of the array. The system implements a Unirac roof mounting system for safety and stability of the array. In addition, this apparatus allows for an adjustable vertical tilt from 27 to 52 degrees above the horizontal (given the -10 degree incline of the roof), facilitating by-month solar tracking based on the latitude of Lawrence, KS.

The system implements a Xantrex XW device controlling the charge of an intermediate storage battery pack. This controller was chosen for its power capabilities since it is able to handle up to 60VDC with 140 A input current. This leaves ample room for increasing the solar array in future efforts. This unit also includes built-in ground fault protection in the event of a short circuit. A standard breaker box provides further protection, facilitating a manual shutdown if the need arises, as well as offering additional over-current protection. The intermediate battery pack includes four Intimidator AGM 8A31DTM lead acid batteries that are similar in chemistry and capacity to the batteries utilized in the high voltage pack in the Beetle, thus serving as a comparable auxiliary storage unit. The final 12VDC system consists of four batteries wired in parallel for 5.0 kWh of energy storage. Finally, an AIMS 5000 W pure sine wave inverter converts the stored DC power to the 120VAC power required by the Beetle's on-board charger.

3.1: Solar Data Logger

The system implements a Micro Circuit Labs SDL-1 Solar Data Logger, measuring and recording the available solar irradiance at the site. Data collected over the course of one-year yields a balanced estimate of the average solar irradiance. This unit uses a PIC16F88 microcontroller, a 10-bit A/D converter, and a BPW34 silicon photodiode to measure the intensity of the incident solar radiation normal to the position of the data logger. With 32 Kbytes of EEPROM, the logger is able to store up to 16,320 readings, transferrable via USB for post-processing in Excel.

Figure 2 shows the average daily solar irradiance based on the collection date. Furthermore, Figure 3 illustrates a sample of the data collected. Within this plot, one can see the variations throughout each day and across several days. The data logger takes samples every 150 seconds in order to allow for a longer sampling period. Over the course of this study, the average solar irradiance per day was 4.44 kWh/(m^2·day). This is close to the yearly average of 4.07 kWh/(m^2·day) for nearby Topeka, KS (approximately 28 miles) as reported by the Kansas Corporation Commission (KCC) Energy Programs' Photovoltaic Electrical Energy Production for 2005[36]. The numbers given in the KCC report are averages over 15 years, thus yearly variations in weather patterns account for this difference.

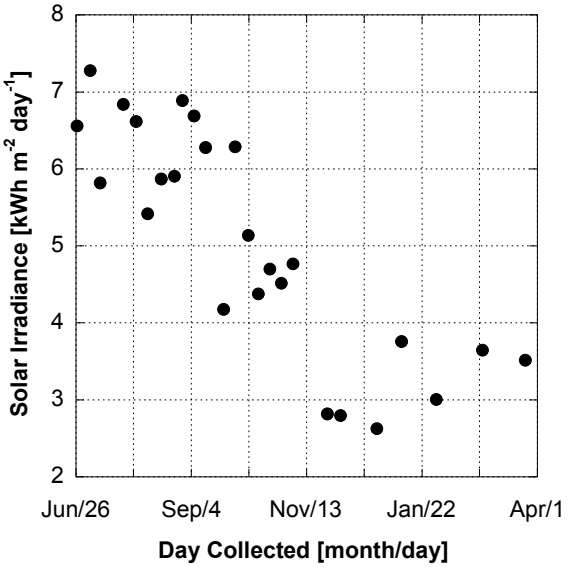

Figure 2: Solar irradiance as a function of the time of year at the charging location of the VW employed in this study.

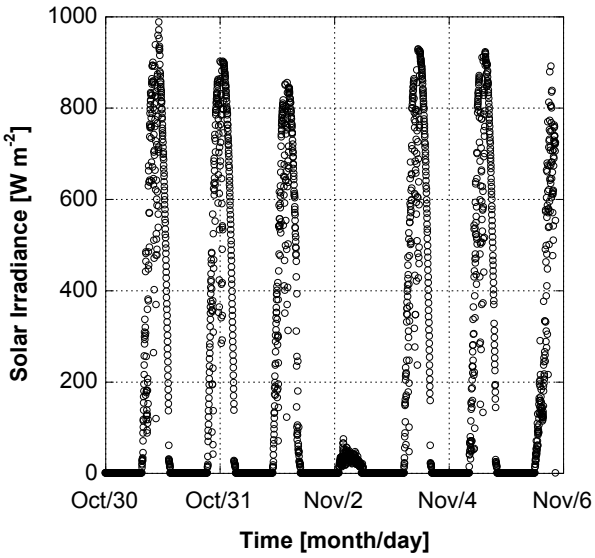

Figure 3: Daily solar irradiance during a few days at the charging location of the VW employed in this study.

4.0: Analysis and Discussion of the Three Analysis Mechanisms

Equipped with a better understanding of the energy usage requirements and solar energy availability, this work can now analyze the system according to the three mechanisms indicated in the introduction. Section 4.1 outlines the component recycling and reuse analysis for the VW. Section 4.2 describes the vehicle model validation and testing processes in calculating the vehicle driving energy use. Section 4.3 gives the total energy and emissions analysis.

4.1: GREET 2.7 Recycling and Reuse Energy and Emissions Analysis

This work seeks to explore the energy use and environmental effects of recycling VW parts, first performing a full energy and emissions analysis on the conversion process. The calculation of energy use and emissions avoided in reusing stock parts of the VW utilizes many of the default assumptions in GREET, retaining a generalized analysis. In particular, GREET 2.7 determines the amount of different materials utilized in the production of the vehicle on a by-weight ratio of the overall vehicle weight. Thus, this study utilizes a modified inventory list retaining the individual part default compositions. The total vehicle emissions generated in the production process, which includes manufacturing the components, assembly, disassembly, and recycling the parts, accurately represents the savings through reuse. Table1shows the parts retained in the GREET default analysis separated by vehicle systems with their assumed weights and weight ratios.

Table 1: Retained component and system masses and by-weight ratios.

Component/System	Component/ System Mass [kg]	By-Weight Ratio [%]
Body	*260.6*	*58.86*
Body-in-white	140.9	31.82
Body panels	48.5	10.96
Body hardware	6.1	1.37
Welds and blank fasteners	18.2	4.11
Glass	24.3	5.48
Exterior trim	6.1	1.37
Sealers and deadeners	1.1	0.25
Door modules	15.2	4.11
Powertrain	*6.1*	*1.37*
Weld blanks and fasteners	6.1	1.37
Transmission	*68.5*	*15.46*
Transmission	53.2	12.02
Differential	15.2	3.42
Chassis	*107.7*	*24.31*
Cradle	18.2	4.11
Driveshaft/axle	44.9	10.15
Corner suspension	24.8	5.60
Steering system	13.5	3.05
Weld blanks and fasteners	6.1	1.37
Total	*442.9*	*100%*

This work utilizes the default material constituents of the components as depicted in Burnham, Wang, and Wu's development report [37]. The production stages required in the creation of the materials and components include mining of the ores and minerals, processing these materials, and creating the final product. For example, steel production includes the following: taconite mining, ore pelletizing and sintering, coke production, utilizing a blast furnace and arc furnace, O_2 processing, sheet production and rolling, and finally stamping. Table 2 contains the full list of materials required for the aforementioned components, along with their respective total weights. One should note the lack of recently developed lightweight materials. The theoretical components modeled in this work represent a standard ICEV as this design closely mimics the stock

Beetle parts. This short list of basic materials is largely different from the analyses in Lenski et al.'s LCA of the US CARS program, which considers a broad spectrum of vehicles and newly developed materials and components [20].

Table 2: Materials included in the vehicle production analysis.

Material	Mass [kg]
Steel	341.78
Average Plastic	32.82
Rubber	3.57
Copper	0.12
Glass	24.37
Organic	4.95
Cast Iron	15.98
Wrought Aluminum	18.01
Total	**441.6**

The GREET 2 series analyzes the processes for creating these materials and components, calculating the energy use and total emissions produced therein. The calculation of transportation and distribution energy requirements uses the GREET 1 series; specifically, the authors utilized the coupled version to GREET2.7, GREET1.8c, for this task [37]. Table 3 contains these results for this study, specifically for the processes relevant to this study: manufacturing the components, and assembly, disposal, and recycling (ADR).

GREET 1.8c analyzes a number of pollutants, including carbon monoxide (CO), carbon dioxide (CO_2), volatile organic compounds (VOC), oxides of nitrogen (NO_X), particulate matter smaller than 10 microns (PM_{10}) and smaller than 2.5 microns ($PM_{2.5}$), oxides of sulfur (SO_X), and methane (CH_4). Additionally, GREET 1.8c calculates the total greenhouse gases (GHG) as a CO_2 equivalent. One should note the high amount of CO_2 emissions relative to the literature when considering the lack of components to

make a complete vehicle. This difference is due to the included transportation and distribution processes, as well as the disposal processes for the original ICEV Beetle. Both of these are significantly energy intensive, causing a large increase in total emissions produced [24]. Finally, GREET calculates the total energy used in component creation, separated by energy type (fossil fuel, coal, natural gas, and petroleum).

Table 3: Calculated emissions and energy use avoided in the reuse of Beetle stock components.

	mmBtu or g per vehicle lifetime		
	Components	ADR	Total
Energy Use [mmBtu]			
Total energy	18.1	12.8	30.9
Fossil fuels	16.7	11.6	28.4
Coal	6.9	5.9	12.8
Natural gas	8.2	5.5	13.8
Petroleum	1.6	0.2	1.8
Emissions [g]			
CO_2	1425601.0	986942.6	2412543.5
CO_2 (VOC, CO, CO_2)	1441250.6	987284.1	2428534.7
CH_4	2550.1	1708.8	4258.9
N_2O	15.5	14.0	29.6
GHGs	1509633.1	1034181.4	2543814.5
VOC: Total	187.7	93.4	281.2
CO: Total	13808.5	301.3	14109.9
NO_x: Total	1509.8	1106.0	2615.8
PM_{10}: Total	2874.9	1089.0	3963.9
$PM_{2.5}$: Total	1164.5	304.2	1468.7
SO_x: Total	1941.7	1783.7	3725.4

4.2: Experimentation and Model Validation

In order to investigate model accuracy, the 1974 VW (Table 4) provided the platform for collecting various performance data. The VW utilizes both 120 VAC and 230 VAC on-board battery chargers that integrate with the vehicle generator and

encompass a variety of charging options. This includes conventional grid electricity from a 120VAC or 230VAC outlet, charging via the biodiesel generator at 230VAC, or charging via the solar PV station at 120VAC. These options facilitate a balanced availability of renewable energy, adding a degree of freedom and versatility to the work. Furthermore, a combined route consisting of both urban and highway driving around Lawrence, Kansas (Figure 4) offered a standard, relatively repeatable driving cycle for comparison within the model.

Table 4: 1974 Volkswagen Super Beetle series hybrid specifications.

Transmission	Original Four Speed w/ Reverse
Drive motor	NetGain Warp 9, 120 VDC Brushed Series Wound
Motor controller	NetGain Controls Classic DC Speed Controller
Battery pack	Discover Energy EV31A-A 10S1P 120 VDC, 115 Ah
DC-DC converter	ElCon TDC-400-120, 400 W
Generator	Yanmar L100V 5.5 kW operating on 100% biodiesel
120 VAC Charger	ElCon PFC 2500, 1.5 kW
230 VAC Charger	Zivan NG3 F7-PH, 3 kW
Tire Size	185/75R16
Weight with generator	2747 lbs
Weight without generator	2534 lbs

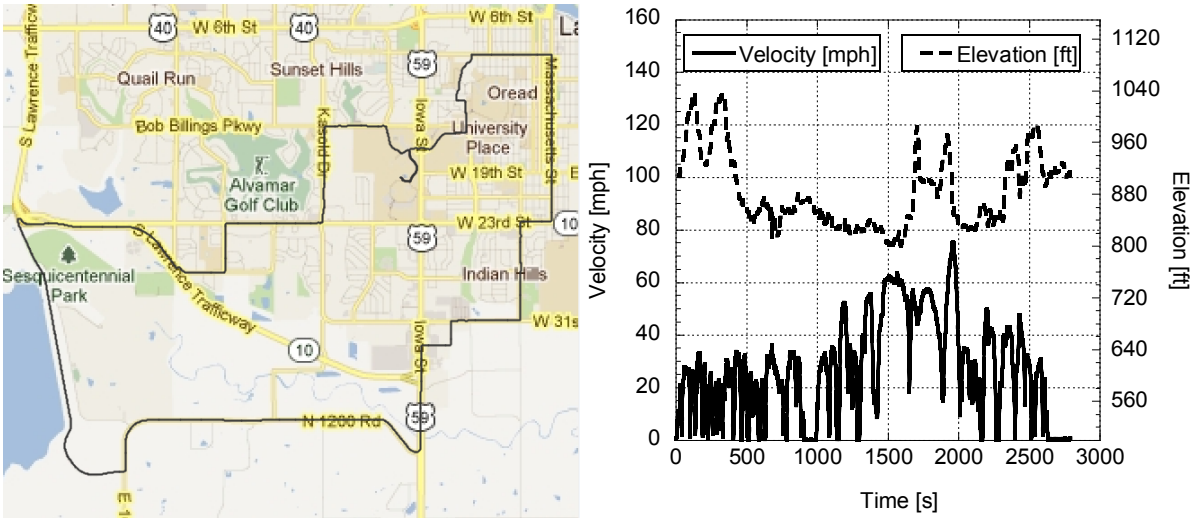

Figure 4: Map (left) along with velocity and elevation profile (right) for Lawrence, Kansas combined usage test route.

The route covers over 21.2 miles with an average velocity of 25.3 mph, top speed of 75 mph, and 2370feet of cumulative elevation change. The authors implement seven route traces with a focus on maintaining the posted speed limit as much as possible to aid in route consistency. Three runs feature the biodiesel powered generator in the vehicle but not in operation (hybrid operating in EV mode), one test features the generator running and charging the batteries (hybrid mode), and three tests feature the generator removed from the car in battery electric vehicle (BEV) mode. This combination allows the authors to model the effects of operating in hybrid mode, as well as the effects of the generator weight on vehicle performance.

Recording of battery and motor performance data uses the interface module provided with the NetGain Classic Motor Controller. This interface module communicates with the vehicle controller via a Controller Area Network (CAN) bus in order to monitor vehicle performance information. Data is stored at a 5Hz rate on a micro standard digital memory card in comma-separated values (CSV) format.

A Race Technology DL1 GPS based data logger collects test data on a compact flash card while measuring speed, acceleration, and elevation data. It records at a 20Hz rate using a combination of GPS signals and an on-board six-axis accelerometer. An external battery pack powers the DL1, thus eliminating outside effects on the vehicle battery pack. The data logging process for the motor controller and GPS data loggers starts and ends simultaneously in order to ease in the alignment of time stamps during post-processing. Race Technology provides analysis software named RT Analysis with which one can convert data from the route into numerous formats for subsequent examination. For the work described herein, this conversion into .mat matrices at a 5Hz rate (to coincide with the powertrain performance data) allows for easy use in MATLAB. It is important to note that MATLAB provides the platform for both model generation and data analysis in this effort. Finally, before each test route, the authors measured the vehicle weight using a set of Longacre AccuSet 72701 four-wheel scales. The use of the four-wheel scales allows for completely isolating the vehicle while taking measurements of all wheel loads independently. The scales chosen offer a 0.5 pound per pad accuracy for a total of two pounds per 6000-pound (capacity) accuracy.

Operating the vehicle in hybrid mode requires forethought in order to ensure that the vehicle charger becomes active. When first connecting the charger to the supply power, it initializes a routine to determine if battery charging is necessary. If the charger determines that the battery pack is at an acceptable SOC, the charger will power down and not check the pack again for an extended period. Consequentially, starting the generator as soon as the test run begins will not charge the battery pack at any point

during the 50-minute test. Therefore, starting the generator roughly four miles into the test run ensures that the battery pack has reached less than a 90% SOC.

Table 5: Route statistics from three driving modes

	Test Time	Energy Used	Efficiency		Final Voltage	Average Current
	[s]	[kWh]	[kWh/mi]	[mpg_e]	[VDC]	[A]
Hybrid in EV Mode (1)	3145	7.23	0.335	100.6	117	75.6
Hybrid in EV Mode (2)	3256	7.33	0.341	99.0	118	73.0
Hybrid in EV Mode (3)	3020	7.52	0.351	95.9	119	80.1
Series Hybrid Mode	2866	7.20	0.335	100.6	122	79.1
BEV Mode (1)	2788	6.84	0.318	106.0	120	74.2
BEV Mode (2)	2963	6.85	0.319	105.5	121	73.8
BEV Mode (3)	3002	6.82	0.318	106.1	120	72.5

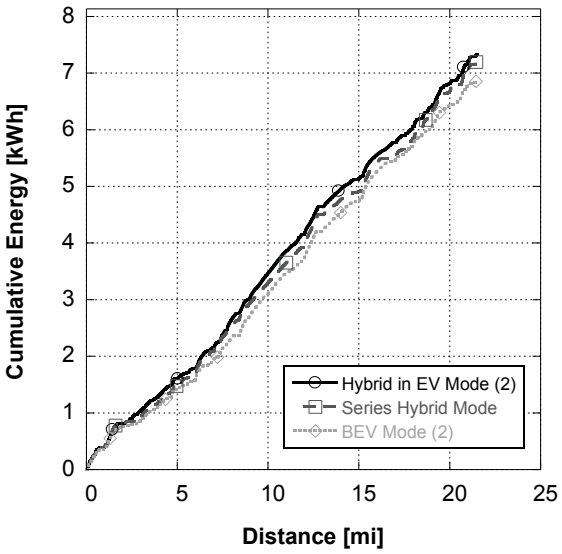

Figure 5: Volkswagen energy profiles based on operational mode.

Table 5 provides the test run statistics of the three previously mentioned operating modes. Figure 5 demonstrates the weight and energy usage effects between the three operating modes with the energy profiles for the median test run of each mode indicated. Both sets of data for the hybrid configuration result in roughly 7.25 kWh of energy usage with the primary difference being that the vehicle regains about 1.75 kWh

of this energy if the generator is in operation during the test run. Because of the weight savings due to removing the generator (~100 kg), the BEV configuration demonstrates less total energy usage (6.85 kWh). The EPA calculates the fuel economy of EVs utilizing a gasoline equivalency factor of 33.7 kWh per gallon of gasoline [38]; thus, the Beetle achieves an average of 98.5 mpge as a series hybrid operating in EV mode, 100.6 mpge as a series hybrid, and 106.1 mpge in full EV mode. Figure 6 presents the voltage and current profiles using the median energy usage trial for each mode. Because of the dynamic variability associated with monitoring the electric power system, this figure presents these profiles using one-minute rolling averages.

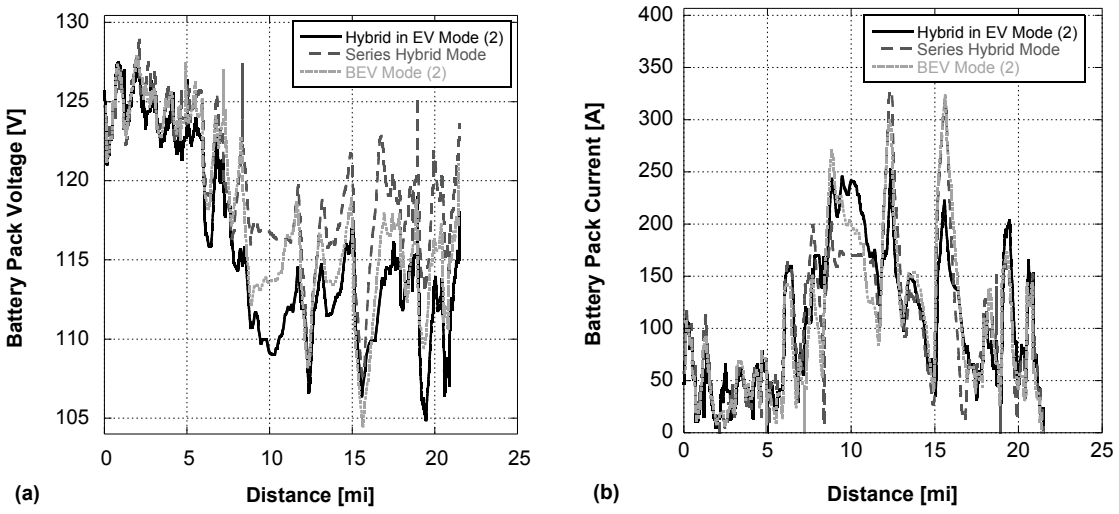

Figure 6: Battery a) voltage and b) current for the three operational modes.

The series hybrid mode has a higher battery pack voltage since the generator is constantly charging the battery pack during the route. In addition, this results in lower current draws because higher pack voltages require less current needed in order to deliver the same amount of power. In BEV mode, the voltage and current are typically between the values of either hybrid mode. This relates directly to the weight savings by

removing the generator; e.g., better than the hybrid with generator off, but not as good when the generator is on.

After the vehicle returns from the test run, the batteries are given time overnight to recover (both chemistry and temperature) before being placed on charge. The Energy Detective 5000 (TED) hardware provides monitoring of this charging process from the conventional grid. The TED hardware is a power line communication system integrated into the electrical system of the building in which the vehicle is stored. The system uses voltage sensing modules and hall-effect current clamps placed in the building's electrical panel. This system continuously measures the supply voltage and current through the charging circuits while storing to a memory module on a per-minute basis. This allows for measurement of vehicle charging curves in order to investigate the energy usage profiles of the vehicle. The curves are stored in a CSV format and are retrievable through connection to a personal computer. Figure 7plots the battery pack charging data from the electrical grid using the test cases with and without generator operation. When comparing a test run with the generator in operation to a test run without this added power, it appears that the generator is able to recharge about 1.5 to 1.8 kWh during the test. This matches expectations as the charger was inputting roughly 2.75 kW (Figure 6) over roughly 40 minutes (2.75 kW × 40 minutes = 1.8 kWh). Less power is required in order to return the battery pack to full charge conditions regardless of the drive cycle that is considered (generator on/off), when using the 230 VAC charger. This is likely an indication of charger efficiency when converting VAC power (supply) to VDC power (battery pack).

Figures 8a and 8b plot the battery pack charging data using the solar PV charging station on two separate days via charging rates of 1700 W and 1100 W, respectively (note that the 120 VAC charger in the vehicle allows different charging profiles to be stored). Data collection for these plots utilized a Watts Up? Pro data logger in order to track the power use through the AIMS Inverter's 120 VAC output. The resolution of this logger is +/- 1.5%, providing ample accuracy for this application. The total energy used in the first charging cycle is 7.45 kWh over the course of 5.25 hours, while the second charge cycle utilized 4.98 kWh over the course of 11 hours. Both charging cycles vary greatly due to a low voltage cutout in the intermediate battery pack. In particular, when the input voltage is lower than 10 VDC, this causes the inverter to stop working until the voltage in the batteries rise to a safe level. This results in the charging power fluctuations because there was insufficient available solar energy to recharge the intermediate battery pack fast enough to account for the draw on the pack from the vehicle. Figures 9a and 9b plot the available solar irradiance throughout each of these specific charging days. The authors took the first charge cycle in early September, while the second is from early November. This difference in time of year shows the effect on the available solar energy, as is described in Section 3.1. This supports the idea that full utilization of solar energy requires a significant amount of energy storage, as suggested by Carrasco et al. in their study of renewable energy grid integration [39]. Furthermore, a larger solar array would collect enough energy at a fast enough rate to keep up with the demand of the battery charger, although this would result in inefficient use throughout low utilization periods and a higher required capital investment.

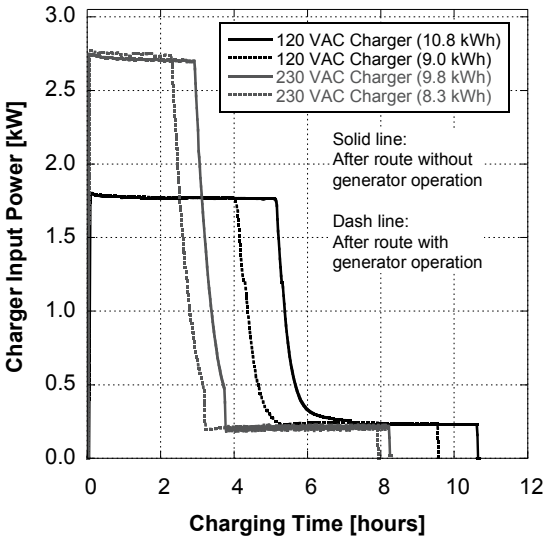

Figure 7: Charging curves from the electrical grid for the vehicle employed in this study.

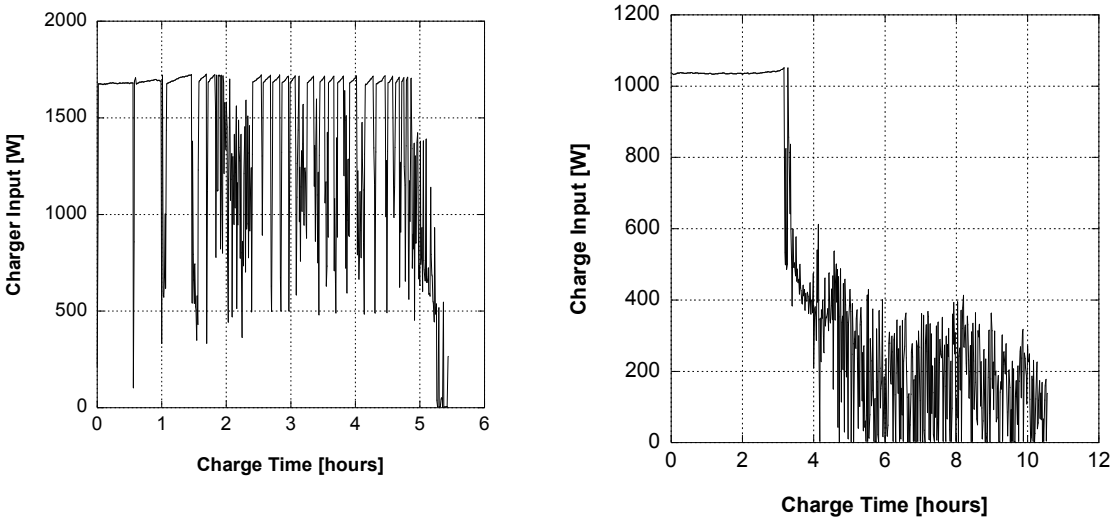

Figure 8: Solar PV charging curve for the vehicle in early September (left) and early November (right).

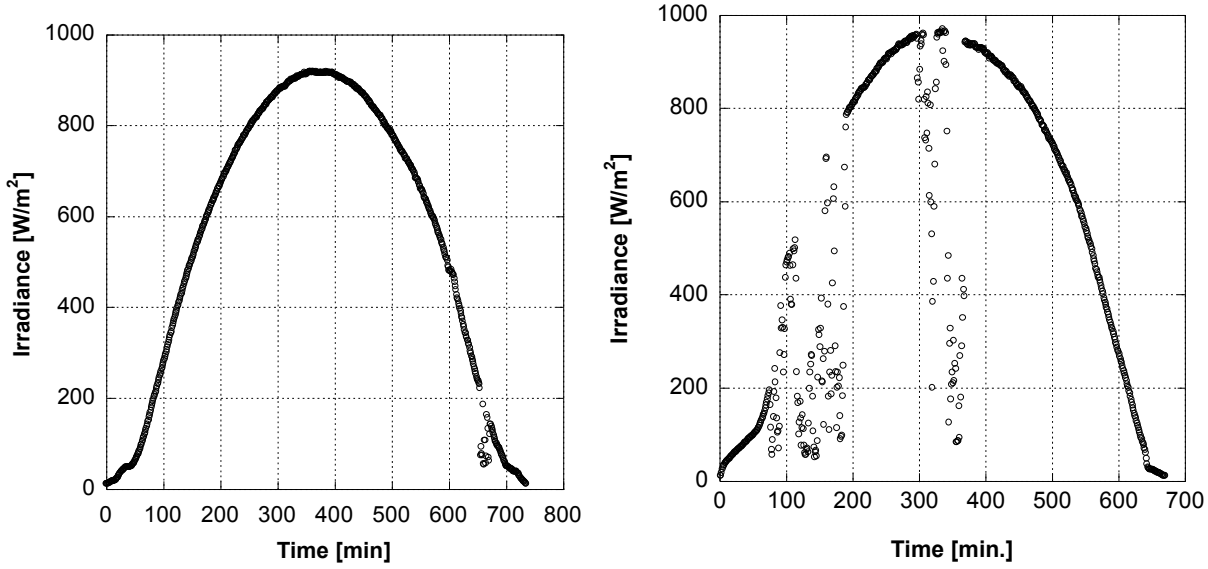

Figure 9: The available solar irradiance throughout the September (left) and November (right) solar PV charge cycles.

According to the irradiance data collected, during the months of December and January the average available energy is only 2.75 to 3.00 kWh/(m^2·day). This means it would take anywhere from 1.9 to 2.3 days to attain a full charge depending on the driving style. Likewise, driving at the end of the day forces one to wait a full day before the vehicle is ready to drive the anticipated range. In this situation, one must use a conventional electricity source to obtain a single-day charge time. Alternately, the months of July and August average between 6.5 and 7 kWh/(m^2·day). Thus, the emissions produced would vary between zero emissions from solar to standard emissions from the grid. This type of situation models the real world and emphasizes the need for bulk electricity storage, as discussed in Barton and Infield's study on the economic benefits of intermittent renewable energy storage [40]. In this area, a number of studies investigate EVs as a source of energy storage in vehicle-to-grid technology; however, this is out of the scope of this study and left to future work [41-43].

Table 6: 1974 Volkswagen Super Beetle series hybrid model parameters.

Vehicle Geometry	
Wheelbase [m]	2.42
GVWR [kg]	1290
Unloaded Mass [kg]	907
Frontal Height [m]	1.07
Frontal Width [m]	1.55
Coefficient of Drag [-]	0.48
Coefficient of Rolling Resistance [-]	0.01
Transmission and Tire Parameters	
Transmission Gear Ratio [-]	2.06 (2^{nd} gear)
Rear Differential Gear Ratio [-]	4.125
Tire Size Specification	195/65R15
Motor	
Model	NetGain Warp 9
Current Draw Limit [A]	400
Regenerative Braking Ratio [-]	-
Battery	
Model	Discover Energy EV31A-A
Series Strings	10
Parallel Strings	1
Nominal Cell Voltage [V]	12
Cell Capacity [Ah]	115
Cell Impedance [ohms]	0.1
Pack Configuration	10S1P
Pack Energy [kWh]	14
Battery Weight [kg]	354
Auxiliary Draw [watts]	135

At this point, enough information exists in order to compare and contrast a VW simulation with the real world test data. Table 6 provides the full specifications required in modeling the VW. In order to simulate the generator effect on battery pack energy, the model adds the bulk charge power (2.75 kW) from the 230 VAC charger to the overall energy balance as a positive power draw beginning at the time in which the generator is started.

Table 7: Model simulation results in comparison to test data.

	Energy Used [kWh]		Efficiency [kWh/mi]		Final Voltage [V]		Average Current [A]	
	Test Data	Model	Test Data	Model	Test Data	Model	Test Data	Model
Hybrid in EV Mode (1)	7.23	7.36	0.335	0.347	117	118.0	75.6	80.5
Hybrid in EV Mode (2)	7.33	7.55	0.341	0.356	118	117.9	73.0	78.3
Hybrid in EV Mode (3)	7.52	8.12	0.351	0.383	119	117.4	80.1	87.4
Series Hybrid Mode	7.20	7.65	0.335	0.361	122	120.6	79.1	88.4
BEV Mode (1)	6.84	7.21	0.318	0.340	120	118.6	74.2	86.0
BEV Mode (2)	6.85	7.23	0.319	0.341	121	118.7	73.8	79.7
BEV Mode (3)	6.82	7.17	0.318	0.338	120	118.8	72.5	78.2

Table 8: Relative error comparison between test data and model.

	Total Energy Usage[kWh]		Final Voltage [V]		Average Current [A]	
	Test Data	Relative Error	Test Data	Relative Error	Test Data	Relative Error
Hybrid in EV Mode (1)	7.23	1.80%	117	0.85%	75.6	6.48%
Hybrid in EV Mode (2)	7.33	3.00%	118	0.08%	73.0	7.26%
Hybrid in EV Mode (3)	7.52	7.98%	119	1.34%	80.1	9.11%
Series Hybrid Mode	7.20	6.25%	122	1.15%	79.1	11.76%
BEV Mode (1)	6.84	5.41%	120	1.17%	74.2	15.90%
BEV Mode (2)	6.85	5.55%	121	1.90%	73.8	7.99%
BEV Mode (3)	6.82	5.13%	120	0.10%	72.5	7.86%

This comparison between the experimental data and the model begins by comparing the measured energy usage to the modeled energy usage. Table 8 presents this assessment in terms of relative model error. Overall, the associated error is likely due to the numerous assumptions made in the model, as well as the accuracy associated with creating input files from data logged vehicle tests.

The authors utilize this model in order to calculate the energy used in driving this vehicle for an improved energy and emissions LCA. Of importance, this validated model now allows for a transferrable calculation of the energy required in other drive cycles. For example, utilizing a drive cycle typical of Mexico City allows one to study the effects of electrifying the ICEV taxi fleet currently being phased out of use [22]. This

will improve the LCA for this particular application and can aid in the economic decision regarding the decommissioned vehicles. Moreover, this methodology can be repeated for any vehicle or location and illustrates an enhancement to LCA.

4.3: GREET Electricity and Biodiesel Energy and Emissions Analysis

In order to study the inherent energy use and emissions produced in electricity generation, this work utilizes GREET1 2011 to analyze the electricity and biodiesel used in vehicle operation. Although using electricity does not produce emissions, the processes involved in extracting the fuel, refining, transportation and distribution, as well as burning the fuel are energy intensive. The vehicle in this study utilizes a combination of solar energy, standard grid energy, and biodiesel produced from used canola oil.

Solar energy is inherently clean aside from the production of the panels. However, the production of the silicon panels is out of the scope of this study as it involves the creation of the power plant (i.e., the panel). Including this analysis requires a similar analysis on building the facilities to produce electricity and biodiesel in order to retain a consistent LCA. However, as found the limitations of the solar array do not allow for a complete charge at the full capabilities of the on-board charger.. Thus, the authors developed an electricity emissions weighted average based on the United States Energy Information Administration's Monthly Energy Review released in 2011, specifically the United States 2010 Electricity Generation profile for all sectors [44]. In the case of a theoretical Mexico City application, a consumption mix relevant to that area would be required to obtain a representative emissions profile.

Table 9 presents the emissions factors developed in GREET 1 for this consumption mix, solar energy, and rapeseed oil biodiesel. One should note that the

authors utilized GREET's rapeseed oil option since it does not contain a complete analysis for used canola oil. As rapeseed is a widely utilized option in the production of canola oil, it offers a viable substitute [45]. It is important to distinguish between the different production mechanisms of emissions: either in the creation of the fuels, commonly denoted as the "Well-to-Pump (WtP)" phase, or in driving the vehicle, referred to as "Pump-to-Wheels (PtW)". Thus, electricity does not have any PtW emissions, which is why the EPA denotes battery electric vehicles as zero emissions vehicles [1]. Biodiesel, on the other hand, has both WtP and PtW emissions and energy usage. Performing a consistent analysis on biodiesel (BD) usage requires the creation emission and energy factors for the PtW component (denoted $f_{BD,PtW}$) using:

$$f_{BD,PtW} = G_{BD,PtW} * MPG \quad (19)$$

where $G_{BD,PtW}$ is the default driving emission factor in [g/mile], and MPG is the default fuel economy of a biodiesel vehicle in GREET. Furthermore, the WtP calculation includes both emissions and energy factors:

$$f_{BD,WtP} = G_{BD,WtP} * LHV \quad (20)$$

where $G_{BD,WtP}$ is the default emission/energy factor in GREET, and LHV is the lower heating value of biodiesel in [mmBtu/gal]. Finally, this requires calculation of the emissions and energy factors for the US 2010 Consumption Mix:

$$f_{elec,tot} = \frac{\sum_1^N E_N * G_{elec,N}}{E_{tot}} \quad (21)$$

where $G_{elec,N}$ is the individual default electricity emissions factors for the various electricity sources, E_N is the amount of this type of electricity over the course of 2010 in [kWh], E_{tot} is the total amount of electricity used in 2010, and N is the number of electricity sources widely utilized in the US. The electricity sources considered in Table

9 include coal, natural gas, petroleum, nuclear, hydroelectric, geothermal, solar photovoltaic, wind, and biomass-fired power plants [44]. Furthermore, the authors developed a second electricity generation mix based on the available solar usage, consisting of 70% solar, 30% coal-fired electricity, representing the solar PV array and the North Lawrence Power Plant. This 70/30 mix sources in the early November solar charge and the average energy use of the three driving styles.

Table 9: Emissions factors developed in GREET1 2011.

	US 2010 Electricity Generation Mix	Solar Photovoltaic/ Coal Mix	Rapeseed BD WtP	Rapeseed BD PtW
	[g/kWh]	[g/kWh]	[g/kWh]	[g/kWh]
VOC	0.062	0.029	0.431	0.084
CO	0.589	0.337	0.118	0.265
NO_x	0.826	0.388	0.319	0.187
PM_{10}	0.913	0.603	0.037	0.009
$PM_{2.5}$	0.246	0.159	0.022	0.008
SO_x	1.2456	0.773	0.187	0.000
CH_4	1.828	0.490	0.411	0.002
N_2O	0.011	0.004	0.187	0.008
CO_2	693.478	360.339	67.115	283.831
CO_2 (w/ C in VOC & CO)	694.598	360.959	68.642	284.508
GHGs	743.423	374.278	134.780	286.853

In order to obtain a consistent comparison, the authors utilized the gasoline-biodiesel equivalency ratio according to the California Energy Commission (0.96 gallons of gasoline per gallon biodiesel) [46], as well as the gasoline-electricity equivalency factor (33.7 kWh per gallon of gasoline), bringing all units to the standard [g/kWh]. With this comparison, one can see reduced emissions from biodiesel in PM_{10}, $PM_{2.5}$, SO_x, CH_4, and CO_2. However, the style in which the fuel is used is the best comparison for

different fuels, in the same units as the EPA regulations on vehicle emissions, [g/mile]. Thus, in a comparative analysis between the three vehicle styles, the authors calculated the emissions produced based on the amount of electricity used during each drive cycle, as well as the amount of biodiesel used while operating as a series hybrid. Through utilizing the same drive cycle for each of these driving styles, the authors validate the vehicle model driving under a variety of conditions, causing the study to be more transferrable to other applications such as the Mexico City taxi replacement scenario. Table 10 contains the results of these analyses, where Table 10a considers the United States electricity consumption mix, and Table 10b considers only using the solar PV/coal mix.

Table 10a: Emissions results for US 2010 electricity consumption mix (USCM).

	USCM Hybrid in EV Mode	USCM Hybrid Mode	USCM EV Mode
	[g/mile]	[g/mile]	[g/mile]
VOC	0.022	0.225	0.020
CO	0.205	0.307	0.190
NO_x	0.287	0.418	0.266
PM_{10}	0.317	0.253	0.294
$PM_{2.5}$	0.085	0.076	0.079
SO_x	0.432	0.396	0.402
CH_4	0.635	0.637	0.589
N_2O	0.004	0.082	0.003
CO_2	240.755	320.706	233.636
CO_2 (with C in VOC & CO)	241.143	321.889	223.997
GHGs	258.094	362.235	239.742

Table 10b: Emissions results for solar photovoltaic electricity.

	Solar Hybrid in EV Mode	Solar Hybrid Mode	Solar EV Mode
	[g/mile]	[g/mile]	[g/mile]
VOC	0.010	0.216	0.009
CO	0.117	0.242	0.109
NO_x	0.135	0.305	0.125
PM_{10}	0.209	0.173	0.194
$PM_{2.5}$	0.055	0.053	0.051
SO_x	0.268	0.275	0.249
CH_4	0.170	0.294	0.158
N_2O	0.001	0.080	0.001
CO_2	125.099	235.064	116.204
CO_2 (with C in VOC & CO)	125.314	236.118	116.403
GHGs	129.938	267.336	120.699

These results show that although the emissions per mile are slightly higher when in series hybrid mode due to fuel use, some emissions are slightly lower, including PM_{10} and $PM_{2.5,}$ as well as SO_x when considering the US consumption mix. The reason for this is the low sulfur and particulate content in biodiesel when compared to coal-fired electricity. The carbon and nitrogen-based emission rates are still higher when using biodiesel, except when utilizing purely solar energy as the electricity source. Thus, depending on the availability of solar energy, one can have a varying range of emission rates for an EV and series hybrid. As stated previously, this availability is one of the major drawbacks to solar and other forms of renewable energy as electricity from a coal-fired or nuclear power plant is far more reliable and consistently available, emphasizing the need for bulk utility renewable energy storage.

Finally, Table 11 contains the energy use in producing the electricity and biodiesel for each of the driving styles, allocated in units of [g/mile], as calculated using the GREET1 2011 default energy factors [24].

Table 11: Well-to-Wheel energy usage.

	USCM Hybrid in EV Mode	USCM Series Hybrid Mode	USCM EV Mode
	[Btu/mile]	[Btu/mile]	[Btu/mile]
Total energy	2935.879	2613.179	2727.123
Fossil fuels	2625.409	2446.297	2438.729
Coal	1711.350	1303.014	1589.664
Natural gas	849.537	962.670	789.130
Petroleum	64.523	180.613	59.935
	Solar Hybrid in EV Mode	**Solar Series Hybrid Mode**	**Solar EV Mode**
	[Btu/mile]	[Btu/mile]	[Btu/mile]
Total energy	1161.782	1299.480	1079.173
Fossil fuels	1161.099	1361.991	1078.539
Coal	1142.365	881.687	1061.137
Natural gas	3.009	335.826	2.795
Petroleum	15.724	144.478	14.606

These results show the large amount of energy required in producing the electricity used in the drive cycles, as the series hybrid driving style has the lowest total energy use. Furthermore, operating as a series hybrid relieves some of the range anxiety in EV use, making it more approachable to the public. Solar energy is once again the best energy source studied here, though it does suffer from the previously stated availability issues.

5.0: Conclusion

This work outlines a Well-to-Wheel energy and emissions analysis of a plug-in series hybrid conversion from a 1974 Volkswagen Super Beetle using the GREET energy and emissions model and a computer vehicle model. The authors performed a materials life cycle energy and emissions analysis using GREET2.7 on parts reused in the conversion to an EV, showing over 2,400 kg of CO_2 emissions and 30 MMBtu of

energy use avoided due to the processes required in remanufacturing or recycling the old parts and manufacturing new components.

The authors implemented a vehicle model based on Newton's Second Law, studying vehicle energy use, validating this model using data collected on a combination city/highway drive cycle with significant elevation change. The results from these drive cycles show the effects of running a series hybrid in three different scenarios; (1) hybrid operating in EV mode, (2) hybrid mode, and (3) BEV mode. Furthermore, this data provided input for an emissions and inherent energy use analysis in a WtW fuel study using GREET1 2011. The results show that, when utilizing rapeseed oil biodiesel and the 2010 US average electricity consumption mix, the emissions range from 240 to 320 g of CO_2 per mile. However, the implementation of a 1.1 kW solar photovoltaic fueling station facilitates the vast improvement to 235 g of CO_2 per mile.

One issue with utilizing solar energy is in its availability. This study shows the ability of this PV system to charge the VW in a single day during the summer. However, during the winter months, multiple days of optimal irradiance are required in order to charge the VW back to full capacity. Furthermore, an average solar irradiance of 4.44 kWh/(m^2·day) requires a photovoltaic array larger than what is utilized in this build to be able to charge at the optimal speed. As a result, fully utilizing renewable energy requires energy storage, and although this design implements an intermediate battery pack, it provides only 40% of the Beetle's requirements. This is enough for short-term, low capacity storage for emergencies, but it does not suffice for multiple-day requirements.

6.0: References

1. United States Environmental Protection Agency. *Summary of Current and Historical Light-Duty Vehicle Emission Standards*. 2010 3/7/2012; 6/21/2012; Available from: http://www.epa.gov/greenvehicles/detailedchart.pdf.
2. Heywood, J.B., *Internal combustion engine fundamentals, 1988*, 2002, McGraw-Hill, New York.
3. Nam, G.W.; Park, J.W.; Lee, J.H.; Yeo, G.K.; *The effect of an external fuel injection on the control of LNT system; the diesel NOx reduction system.* SAE technical paper, 2007: pp. 01-1241.
4. Webb, C.C., P.A. Weber, and M. Thornton, *Achieving Tier 2 Bin 5 Emission Levels with a Medium Duty Diesel Pick-Up and a NOX Adsorber, Diesel Particulate Filter Emissions System-Exhaust Gas Temperature Management*, 2004, SAE International.
5. Whitacre, S.D.; Adelman, B.J.; May, M.P.; McManus, J.G.; *Systems Approach to Meeting EPA 2010 Heavy-Duty Emission Standards Using a NOx Adsorber Catalyst and Diesel Particle Filter on a 15L Engine*, 2004, SAE International.
6. Faiz, A., C.S. Weaver, and M.P. Walsh, *Air pollution from motor vehicles: standards and technologies for controlling emissions* 1996: World Bank Publications.
7. Pearre, N.S.; Kempton, W.; Guensler, R.L.; Elango, V.V.; *Electric vehicles: How much range is required for a day's driving?* Transportation Research Part C: Emerging Technologies, 2011.
8. McIntyre, D.A. *The Best-Selling Cars of All Time*. The 24/7 Wall St., 2012.
9. Sheehan, J.; Comobreco, V.; Duffield, J.; Graboski, M.; Shapouri, H.; *Life cycle inventory of biodiesel and petroleum diesel for use in an urban bus. Final report*, 1998, National Renewable Energy Lab., Golden, CO (US).
10. United States Environmental Protection Agency, *A Comprehensive Analysis of Biodiesel Impacts on Exhaust Emissions: Draft Technical Report*, 2002, Office of Transportation and Air Quality.
11. E. Cecrle; C. Depcik; A. Duncan; J. Guo; M. Mangus; E. Peltier; S. Stagg-Williams; Y. Zhong; *An Investigation of the Effects of Biodiesel Feedstock on the Performance and Emissions of a Single-Cylinder Diesel Engine.* Energy & Fuels, 2012. **26**(4): pp. 2331 - 2341.
12. Sullivan, J., A. Burnham, and M. Wang, *Energy-consumption and carbon-emission analysis of vehicle and component manufacturing*, 2010, Argonne National Laboratory (ANL).
13. Sullivan, J.L.; Williams, R.L.; Yester, S.; Cobas-Flores, E.; Chubbs, S.T.; Hentges, S.G.; Pomper, S.D.; *Life Cycle Inventory of a Generic U.S. Family Sedan Overview of Results USCAR AMP Project*, 1998, SAE International.
14. Sullivan, J. and E. Cobas-Flores. *Full vehicle LCAs: a review*. 2001.
15. Amelia, L.; Wahab, D.A.; Che Haron, C.H.; Muhamad, N.; Azhari, C.H.; *Initiating automotive component reuse in Malaysia.* Journal of Cleaner Production, 2009. **17**(17): pp. 1572-1579.
16. Chen, M., *End-of-life vehicle recycling in China: Now and the future.* JOM Journal of the Minerals, Metals and Materials Society, 2005. **57**(10): pp. 20-26.

17. Kanari, N., J.L. Pineau, and S. Shallari, *End-of-life vehicle recycling in the European Union.* JOM Journal of the Minerals, Metals and Materials Society, 2003. **55**(8): pp. 15-19.
18. Daniels, E.J.; Carpenter, J.A.; Duranceau, C.; Fisher, M.; Wheeler, C.; Winslow, G.; *Sustainable end-of-life vehicle recycling: R&D collaboration between industry and the US DOE.* JOM Journal of the Minerals, Metals and Materials Society, 2004. **56**(8): pp. 28-32.
19. U.S. Department of Transportation: National Highway Traffic Safety Administration, *Consumer Assistance to Recycle and Save Act of 2009*, 2009.
20. Lenski, S.M., G.A. Keoleian, and K.M. Bolon, *The impact of 'Cash for Clunkers' on greenhouse gas emissions: a life cycle perspective.* Environmental Research Letters, 2010. **5**: p. 044003.
21. Eric Bolton, U.S.D.o.T. *Cash for Clunkers Wraps up with Nearly 700,000 car sales and increased fuel efficiency, U.S. Transportation Secretary LaHood declares program "wildly successful"*. [Web Page] 2009 August 26, 2009 [cited 2012 July 6, 2012]; August 26, 2009; Available from: http://www.dot.gov/affairs/2009/dot13309.htm.
22. Stevenson, M. *Mexico City phases out iconic VW Beetle taxis*. USA Today: Travel, 2012.
23. Schifter, I.; Diaz, L.; Mugica, V.; Lopez-Salinas, E.; *Fuel-based motor vehicle emission inventory for the metropolitan area of Mexico city.* Atmospheric Environment, 2005. **39**(5): pp. 931-940.
24. Wang, M., *Argonne National Lab's Greenhouse Gases, Regulated Emissions, and Energy Use in Transportation Model.* Center for Transportation Research, Energy Systems Division, Argonne National Laboratory, Iowa, 2011.
25. EPA Office of Transportation and Air Quality (OTAQ). *EPA Urban Dynamometer Driving Schedule (UDDS)*. 2012 July 5, 2012]; Available from: http://www.epa.gov/otaq/standards/light-duty/udds.htm.
26. Dowling, A. *Electric Vehicle Cruise Control*. 2009; Available from: https://controls.engin.umich.edu/wiki/index.php/ElectricVehicleCruiseControl.
27. Fox, R.W., A.T. McDonald, and P.J. Pritchard, *Introduction to fluid mechanics*. Vol. 7. 1985: John Wiley & Sons New York.
28. Larminie, J., J. Lowry, and I. NetLibrary, *Electric vehicle technology explained* 2003: Wiley Online Library.
29. Hausmann, A., *Advances in Electric Drive Vehicle Modeling with Subsequent Experimentation and Analysis*, in *Department of Mechanical Engineering*2012, University of Kansas. p. 171.
30. Bosch, R., *Bosch Automotive Handbook* 8th ed 2011: SAE International.
31. Donley, M.G., T.C. Lim, and G.C. Steyer, *Dynamic analysis of automotive gearing systems*, 1992, Society of Automotive Engineers, 400 Commonwealth Dr, Warrendale, PA, 15096, USA.
32. Genta, G., *Motor vehicle dynamics: modeling and simulation*. Vol. 43. 1997: World Scientific Publishing Company Incorporated.
33. Powell, B., K. Bailey, and S. Cikanek, *Dynamic modeling and control of hybrid electric vehicle powertrain systems.* Control Systems Magazine, IEEE, 1998. **18**(5): p. 17-33.

34. Hori, Y., Y. Toyoda, and Y. Tsuruoka, *Traction control of electric vehicle: Basic experimental results using the test EV "UOT Electric March".* Industry Applications, IEEE Transactions on, 1998. **34**(5): pp. 1131-1138.
35. Ng, K.S.; Moo, C.S.; Chen, Y.P.; Hsieh, Y.C.; , *Enhanced coulomb counting method for estimating state-of-charge and state-of-health of lithium-ion batteries.* Applied Energy, 2009. **86**(9): pp. 1506-1511.
36. Kansas Corporation Commission Energy Programs, *Kansas Solar Resource Map*, 2005. p. 3.
37. Burnham, A., M.Q. Wang, and Y. Wu, *Development and applications of GREET 2.7 -- The Transportation Vehicle-CycleModel*, 2006. p. Medium: ED.
38. U. S. Environmental Protection Agency, *Fact Sheet: New Fuel Economy and Environment Labels for a New Generation of Vehicles.* 2011.
39. Carrasco, J.M., Franquelo, L.G.; Bialasiewicz, J.T.; Galvan, E.; Guisado, R.C.P.; Prats, Ma A. M.; Leon, J.I.; Moreno-Alfonso, N.; *Power-Electronic Systems for the Grid Integration of Renewable Energy Sources: A Survey.* Industrial Electronics, IEEE Transactions on, 2006. **53**(4): pp. 1002-1016.
40. Barton, J.P. and D.G. Infield, *Energy storage and its use with intermittent renewable energy.* Energy Conversion, IEEE Transactions on, 2004. **19**(2): pp. 441-448.
41. Kempton, W. and J. Tomić, *Vehicle-to-grid power implementation: From stabilizing the grid to supporting large-scale renewable energy.* Journal of Power Sources, 2005. **144**(1): pp. 280-294.
42. Peterson, S.B., J. Apt, and J.F. Whitacre, *Lithium-ion battery cell degradation resulting from realistic vehicle and vehicle-to-grid utilization.* Journal of Power Sources, 2010. **195**(8): pp. 2385-2392.
43. Sioshansi, R. and P. Denholm, *Emissions Impacts and Benefits of Plug-In Hybrid Electric Vehicles and Vehicle-to-Grid Services.* Environmental Science & Technology, 2009. **43**(4): pp. 1199-1204.
44. U.S. Energy Information Administration, *Table C9. Electric Power Sector Consumption Estimates, 2010*, 2011.
45. Shahidi, F., *Canola and rapeseed: production, chemistry, nutrition, and processing technology*1990: Springer.
46. Commission, T.C.E., *Gasoline Gallon Equivalents (GGE) for Alternative Fuels Fuel British Thermal Unit (Btu) Estimates for Transportation Vehicles (Lower Heating Values).* 2012.

Well-to-Wheels Emissions and Cost Analysis of a Conventional and Electrified Vehicle Fleet

Bryan Strecker and Christopher Depcik

Department of Mechanical Engineering - University of Kansas, Lawrence, Kansas (United States)

Abstract

The number of electrified vehicles on the road increases daily, and as such, the requirements for EPA vehicle emissions regulations may change in order to reflect their influence in the marketplace. Furthermore, according to the EPA, a vehicle fleet must meet an overall average emissions level. The EPA considers battery electric vehicles, such as the Nissan LEAF, to be zero tailpipe emissions vehicles. However, the production of electricity to charge this vehicle is anything but a zero emissions process. As a result, this study performs a Well-to-Wheels emissions and cost analysis investigating a fleet of 800+ vehicles utilizing Argonne National Lab's Greenhouse Gases, Regulated Emissions, and Energy Use in Transportation (GREET) Model, as well as the EPA's Motor Vehicle Emissions Simulation (MOVES) package. In particular, this study incorporates ten vehicle models formulated from Newton's Second Law of Motion along with a number of vehicle specific efficiency maps in order to calculate the influence of the electrification of a fleet. For purposes of this report and confidentiality of the sponsor, the detailed information involving this fleet of vehicles has been omitted from this report. Moreover, the sponsors have reviewed this chapter and agreed to its contents.

Words: 195

Nomenclature

Variable	Description	Units
a, b, c	BSFC map optimization factors	[-]
A_f	Vehicle frontal area	[m2]
$bmep$	Brake mean effective pressure	[Pa]
$bsfc$	Brake specific fuel consumption	[g/kWh]
C_d	Aerodynamic coefficient of drag	[-]
C_f	Cost factor	[$/gal]
$C_{f,elec}$	Electricity cost factor	[$/kWh]
C_l	Aerodynamic coefficient of lift	[-]
C_{mile}	Cost of driving one mile	[$/mile]
$C_{mile,1,2}$	Cost of driving per mile of vehicles 1 and 2	[$/mile]
$C_{mile,elec}$	Electricity cost per mile	[$/mile]
$C_{P1,2}$	Principal cost of vehicles 1 and 2	[$]
CR_i	Cumulative battery pack charge removed	[Ah]
CR_{i-1}	Cumulative battery pack charge removed at previous time step	[Ah]
C_{tot}	Total cost of driving	[$]
$C_{tot,elec}$	Total electricity cost	[$]
C_{year}	Fuel cost of driving the vehicle per year	[$/year]
d	Distance between two points given elevation change	[m]
$d_{break\text{-}even}$	Cost break-even point as a function of distance	[miles]
d_{diff}	Horizontal distance between two points	[m]
dt	Time duration of time step	[s]
d_{tot}	Total length of a drive cycle	[miles]
d_{year}	Total yearly distance driven	[miles/year]
E_i	Electricity used in the current time step	[kWh]
$Elev_k$	Elevation at current time step	[m]
$Elev_{k-1}$	Elevation at previous time step	[m]
EM	Emissions rate	[g/mile]
E_{tot}	Battery pack discharge capacity	[W]
$E_{tot,i}$	Total electricity used	[kWh]
$E_{tot,i-1}$	Total electricity used up to the previous time step	[kWh]
f_{CH4}	Emission factor for methane	[g/gfuel]
f_{CO2}	Emission factor for carbon dioxide	[g/gfuel]
$f_{em,elec}$	Electricity emissions factor	[g/kWh]
$f_{emission}$	Emission factor	[g/gfuel]
$f_{emission,E85}$	E85 emission factor	[g/gfuel]
$f_{emission,PtW}$	Pump-to-Wheels emission factor	[g/gfuel]
$f_{emission,WtP}$	Well-to-Pump emission factor	[g/gfuel]
f_{GHG}	Emission factor for greenhouse gases	[g/gfuel]
f_{GREET}	Emission factor produced by GREET	[g/mile]

f_{N2O}	Emission factor for nitrous oxide	[g/gfuel]
F_{TE}	Tractive force required	[N]
G_0	Final drive gear ratio	[-]
$G_{0\text{-}6}$	Transmission gear ratios	[-]
G_i	Current transmission gear ratio	[-]
h	Vehicle height	[m]
I_0	Normalized current draw	[A]
i_g	Number of the transmission gear in use	[-]
I_i	Current draw	[A]
$imep$	Indicated mean effective pressure	[Pa]
$imep_0$	Normalized indicated mean effective pressure	[Pa]
$isfc$	Indicated specific fuel consumption	[g/kWh]
$isfc_0$	Normalized indicated specific fuel consumption	[g/kWh]
k	Peukert coefficient	[-]
Lat_k	Latitude of current time step	[deg]
$Lat_{k\text{-}1}$	Latitude of previous time step	[deg]
LHV	Lower heating value of a fuel	[mmBtu/gal]
Lon_k	Longitude of current time step	[deg]
$Lon_{k\text{-}1}$	Longitude of previous time step	[deg]
$\dot{m}_{fuel}$	Fuel flow rate	[kg/s]
$m_{em,E85}$	Mass of emissions	[g]
$m_{em,elec,i}$	Instantaneous electricity emissions	[g]
$m_{em,elec,tot,i}$	Cumulative electricity emissions at current time step	[g]
$m_{em,elec,tot,i\text{-}1}$	Cumulative electricity emissions at previous time step	[g]
$m_{em,tot}$	Cumulative total emissions produced	[g]
$m_{em,tot,PtW}$	Total mass of Pump-to-Wheels emissions at current time step	[g]
$m_{em,tot,WtP}$	Total mass of Well-to-Pump emissions at current time step	[g]
$m_{em,year}$	Total yearly emissions	[g/year]
$m_{emission,PtW}$	Instantaneous Pump-to-Wheels emissions mass	[g]
$m_{emission,WtP}$	Instantaneous Well-to-Pump emissions mass	[g]
$m_{fuel,i}$	Instantaneous liquid fuel used	[g]
$m_{fuel,tot}$	Total fuel used in the current time step	[g]
$m_{vehicle}$	Gross vehicle weight	[kg]
MPG	Vehicle fuel economy	[miles/gal]
$MPGe$	Electric vehicle fuel efficiency (miles per gallon equivalent)	[miles/galeq]
MPG_{E85}	E85 miles per gallon	[miles/gal]
MPG_{GREET}	GREET-stated fuel economy of a vehicle	[miles/gal]
N	number of fleet vehicles	[-]
n_c	Torque converter input to output speed ratio	[-]
n_g	Number of gears in the transmission	[-]

n_R	Number of rotations per engine cycle	[-]
P_{acc}	Vehicle accessory power draw	[W]
P_b	Brake power	[W]
P_{batt}	Battery power draw	[W]
P_{ICE}	Internal combustion engine power in a parallel hybrid	[W]
$P_{ICE,0}$	Normalized internal combustion engine power	[W]
$P_{ICE,max}$	Maximum internal combustion engine output power	[W]
$P_{motor,max}$	Maximum electric motor power output	[W]
$P_{motor,out}$	Output motor power	[W]
P_{regen}	Regenerative braking power required	[W]
r_{tire}	Tire radius	[m]
SOC_0	Initial battery pack state of charge	[-]
SOC_i	Current battery pack state of charge	[-]
$t_{break\text{-}even}$	Time cost break-even point	[years]
V	Velocity	[m/s]
v	Volumetric electricity/gasoline equivalent	[gal]
V_0	Normalized velocity factor	[m/s]
V_d	Internal combustion engine displacement volume	[m3]
$Vdc_{i\text{-}1}$	Battery voltage at previous time step	[V]
w	Vehicle width	[m]
$\eta_{EV,correct}$	Optimized electric drive train efficiency	[-]
$\eta_{final\ drive}$	Final drive efficiency	[-]
$\eta_{ICE,mechanical}$	Internal combustion engine mechanical efficiency	[-]
$\eta_{ICE,th}$	Internal combustion engine thermal efficiency	[-]
η_{mg}	Efficiency of a motor acting as a generator	[-]
η_{motor}	Electric motor efficiency	[-]
η_{regen}	Regenerative braking efficiency	[-]
η_t	Standard transmission efficiency	[-]
η_{tc}	Torque converter efficiency	[-]
$\eta_{t,ECVT}$	Electronic continuously variable transmission efficiency	[-]
$\mu_{rolling}$	Rolling friction coefficient	[-]
ρ_{fuel}	Density of a fuel	[g/gal]
τ_0	Normalized torque factor	[N-m]
τ_{axle}	Axle torque	[N-m]
$\tau_{axle,max}$	Maximum allowable axle torque	[-]
τ_b	Brake torque	[N-m]
τ_p	Torque converter pump torque	[N-m]
τ_t	Torque converter turbine torque	[N-m]
ω_{em}	Electric motor rotational speed	[rot/min]
ω_{ICE}	Internal combustion engine rotational speed	[rot/s]
$\omega_{ICE,0}$	Normalized internal combustion engine rotational speed	[rot/s]

ω_p	Torque converter pump rotational speed	[rot/s]

1.0: Introduction

The recent influx of electrified vehicles in the US market necessitates research and development into the energy use, emissions produced, and cost of these vehicles as compared to a conventional vehicle fleet [1]. Furthermore, the recent push towards renewable energy supports the need for research into renewable energy storage and, in general, more efficient use of this energy platform.

Recent studies involving greenhouse gas (GHG) and toxic emissions have shown the detrimental effects of vehicle emissions. In particular, sulfur oxides (SO_x) cause breathing problems in children and the elderly with short time exposure leading to wheezing, chest tightness, and shortness of breath [2]. Furthermore, the combination of SO_x and particulate matter (PM) leads to respiratory illness while aggravating existing cardiovascular disease [2]. The environmental effects of SO_x and nitrous oxides (NO_x) lead to increased acid rain, poisoning lakes and other bodies of water, as well as causing damage to buildings and monuments [2]. Moreover, NO_x can irritate the lungs and lower the body's resistance to sickness. Also, NO_x has an adverse effect on both terrestrial and aquatic ecosystems [3].

Hydrocarbon emissions, specifically volatile organic compounds (VOC), cause a loss of coordination, damage to the liver, kidneys, and central nervous system, among other detrimental health effects [4]. Methane gas (CH_4) detrimentally affects the ozone layer more so than carbon dioxide (CO_2) [5]. Likewise, nitrous oxide (N_2O) has a global warming potential even higher, estimated at 298 times the influence of carbon dioxide

(CO_2) [6]. Thus, it is of vital importance that the emission levels produced by a vehicle fleet be reduced since transportation accounts for 28% of the US total energy use [7].

This study implements a Well-to-Wheels (WtW) fuel emissions and cost analysis, supported by Argonne National Lab's Greenhouse Gases, Regulated Emissions, and Energy Use in Transportation Model (GREET), version GREET2012. Furthermore, this effort incorporates the US Environmental Protection Agency's Motor Vehicle Emissions Simulator (MOVES), version MOVES2010b, for the most up-to-date emissions use profiles in the Pump-to-Wheels (PtW) segment of the analysis (i.e., fuel use in vehicles). Of importance, Chapter 2 of this thesis describes the work performed with MOVES.

GREET separates the WtW analysis into two main areas: Well-to-Pump (WtP), which consists of fuel feedstock extraction, refining, fuel creation, and transportation, and the fuel use in the vehicles, or the PtW analysis. As mentioned in the Abstract, it is important to calculate the full WtW analysis since the EPA views battery electric vehicles (BEV) as zero tailpipe emissions vehicles [8]. However, electricity production creates a number of harmful emissions, as documented through electrified vehicle life cycle analyses (LCA) [6, 9, 10].

In order to improve the transferability of this analysis, the study includes a number of vehicle dynamics models, created in the Matlab programming language. These models are important in order to study the effects of various drive cycles and driving styles. In particular, the fuel economy of vehicles changes drastically because of city or highway driving. Furthermore, the inclusion of these models improves the accuracy of the energy use and emissions profiles of the specific vehicles in the study. The basis for the models is Newton's Second Law of Motion, utilizing a number of power

draw (i.e., energy usage) algorithms in order to simulate the fuel use in the various types of vehicles studied.

The vehicles in this study include a 2011 Chevrolet Impala, 2005 Chevrolet Silverado 1500HD (1/2-Ton), 2009 Chevrolet Silverado 2500HD (3/4-Ton), 2011 Chevrolet Uplander, 2011 Chevrolet Volt, 2011 Nissan LEAF, 2012 Ford Fusion Hybrid, 2011 Chevrolet Silverado Hybrid, 2011 Ford Transit Connect, and 2006 Toyota Prius. Each of these vehicles has a separate model corresponding to its specific powertrain. The basic powertrain designs include a conventional vehicle equipped with a gasoline internal combustion engine (ICE: Silverado 1500, Silverado 2500, Impala, and Uplander), a series hybrid (Volt), two BEV (LEAF and Transit), and three parallel hybrids (Prius, Silverado Hybrid, and Fusion Hybrid). Figure 1 provides a basic layout structure and connectivity for these different powertrains.

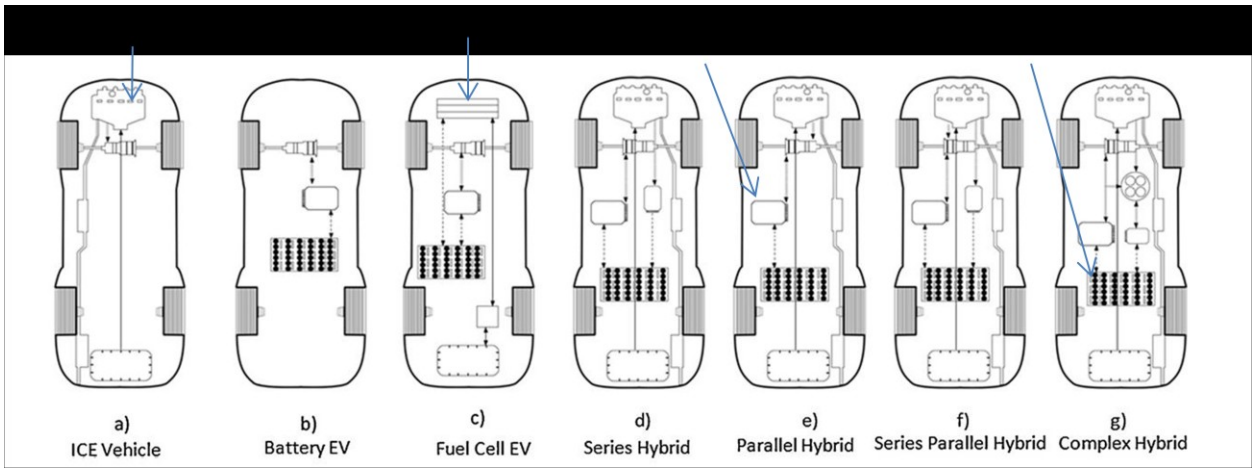

Figure 1: A number of different vehicle powertrains indicating the location of battery pack, motor, and ICE [11].

The conventional vehicle powertrain consists of an ICE and a basic four to six gear transmission, with the ICE acting as the sole provider of vehicle tractive force (Figure 1a). The series hybrid (Figure 1d) consists of one or two electric motors with a

small ICE used as a generator for the high voltage (HV) battery pack in order to help extend the range, reducing range anxiety common with BEVs [12]. Range anxiety is the fear that the limited range of a BEV will restrict the distance capabilities of the average driver. The generator active in series hybrids acts to re-charge the HV battery pack, extending the vehicle's range; e.g., from the 100 miles stated range of the LEAF to the 300 mile declared extent of the Volt [13, 14]. The powertrain of a parallel hybrid (Figure 1e) consists of one or two electric motors and an ICE engine with all three capable of adding (individual or simultaneously) to the tractive force of the vehicle. Finally, the BEV powertrain (Figure 1b) is the simplest of these, consisting of only one electric motor and a single-gear transmission. The ability of an electric motor to reach high rotational speed without losing efficiency allows the transmission to be simple, consisting generally of only one reduction gear.

Parallel hybrids are the most difficult to model since the transmission is generally an electronic Continuously Variable Transmission (CVT). Without the exact control algorithm of each vehicle, determining which motor or ICE is adding traction is all but impossible. A study performed by Arata et al. developed a complex theoretical algorithm mimicking the Toyota Prius powertrain [15]. However, due to limitations on time and data logging capabilities (discussed later in this chapter), this effort employs simple models including the optimization of control algorithm and efficiencies. By employing parameter optimization for each of the vehicle models through modifying theoretical assumptions allows the simulations to closely mimic actual vehicle performance.

In specific, the conventional vehicles optimize the theoretical brake specific fuel consumption (bsfc) maps created using an ICE thermodynamic cycle simulation program employed in the course ME636 at the University of Kansas. This simulation calculates fuel usage based on basic engine parameters. Furthermore, optimization of the BEV models occurred by adjusting the efficiency of the powertrain and electric motor. A similar optimization procedure was followed for the series hybrid model. Sections 3.1 through 3.6 explain the application of these model optimizations in more detail. Finally, modeling these vehicles required data collection implementing a number of vehicle data loggers. The following section describes these data loggers and the other equipment required in order to accomplish this task.

2.0: Data Logging and Drive Cycle Determination

This work utilized three data loggers in measuring actual drive cycles with recorded fuel use data. The conventional vehicles use the Auterra DashDyno, which reads signals through the vehicles' on-board diagnostics (OBDII) port [16]. This data logger, shown in Figure 2, incorporates a Garmin 18x GPS device (also shown in Figure 2) [17] connected to the DashDyno when recording the GPS coordinates of the vehicle throughout the drive cycle. The combination of these devices allows the recording of a number of useful parameters including, but not limited to, time, ICE rotational speed, vehicle velocity, fuel flow rates, and GPS coordinates in degree-decimal format. The author used the GPS coordinates, along with an online elevation lookup tool by GPSVisualizer in order to create a comma-separated value file in Microsoft Excel containing six parameters: time [s], ICE rotational speed [rot/min], vehicle velocity [m/s], elevation [m], fuel flow rate [g/s], and cumulative fuel used [g] [18].

Figure 2: Garmin GPS 18x OEM (left) and Auterra DashDyno (right) [17, 19].

In the case of the Nissan LEAF, data recording occurred with a data logger created by Gary Giddings, an entrepreneur located in California [20]. This LEAF Logging System (LLS) measures the instantaneous State of Charge (SOC) of the HV battery pack, among other useful parameters, through the vehicle's Controller Area Network (CAN). It incorporates three Olimex AVR-CAN development boards in order to follow three of the four LEAF CAN strings employed by the LEAF vehicle control unit. Finally, Gary's own program, CAN-do, reads the translated messages through an RS232-USB hub that is connected to a personal computer (PC) [20]. The combination of this system and the Garmin 18x GPS allowed for the collection of the time, SOC, velocity, and elevation profiles of the drive cycle, in a similar fashion as the DashDyno. However, differences arose when utilizing the Garmin GPS 18x with the LLS in comparison to the DashDyno.

Specifically, the DashDyno takes the readings from the GPS 18x and converts them to a degree-decimal format prior to saving to an output file that is immediately ready for upload in GPSVisualizer. For the LLS system, when employing the GPS 18x with a PC, the author used two programs to read and log the GPS data, as well as two created Matlab programs (MP#1 and MP#2) that convert the output into parameters usable by the vehicle models. The LLS system employs a Franson GpsGate Client in

order to create a virtual communications port that reads the Garmin GPS 18x signal in National Marine Electronics Association (NMEA) format [21]. The subsequent incorporation of a RS232 Data Logger by Eltima Software allows for logging of the GPS signal data via the virtual communications port created by the GpsGate Client [22]. This program simply records the data, saving it to a text file in comma-separated format that is readable by Microsoft (MS) Excel. Ensuing input of this text file into a Matlab-based conversion program (MP#1) translates the NMEA formatting to degree-decimal format, like the DashDyno output, usable in calculations and by GPSVisualizer.

In specific, this conversion program first calculates a whole number degree by dividing the NMEA format by 100, rounding down this new value to the nearest whole number. Then, the program computes the latitude and longitude minutes by dividing the remaining values by sixty. Finally, the program adds the degree whole number to the "minutes" decimal, obtaining the final latitude and longitude in degree-decimal format. The program ends by saving these values to a comma-separated value MS Excel file. Subsequent uploading of this file into GPSVisualizer results in the values for the elevation profile for each time step.

Inputting this resultant file into a second Matlab program (MP#2)results in the distance and velocity at each time step based on GPS coordinates and the elevation profile. This velocity and distance calculation is a multi-step process, with the first step involving the total planar distance between time steps:

$$d_{diff} = \cos^{-1}\{(\sin Lat_{k-1} * \sin Lat_k) + [\cos Lat_{k-1} * \cos Lat_k * \cos(|Lon_{k-1} - Lon_k|)]\} * 111230 \quad (1)$$

where d_{diff} is the distance between the two points [m], Lat_{k-1} is the latitude of the previous time step [deg], Lat_k is the latitude of the current time step [deg], Lon_{k-1} is the longitude of the previous time step [deg], Lon_k is the longitude of the current time step [deg], and the conversion number indicates the change from global latitude degrees to meters [m deg^{-1}]. The program then finds the total distance taking into consideration the elevation difference between the two points:

$$d = \sqrt{d_{diff}^2 + (Elev_{k-1} - Elev_k)^2} \quad (2)$$

where d is the total distance between the two points [m], $Elev_{k-1}$ is the elevation at the previous time step [m], and $Elev_k$ is the elevation at the current time step [m]. Furthermore, the program evaluates the velocity at each time step (V [m/s]):

$$V = {}^{d} / {}_{dt} \quad (3)$$

where dt is the time between steps [s]. Using these, the author creates a final parameter file containing the time [s], elevation [m], velocity [m/s], and HV battery pack SOC [-] for use in the vehicle models.

Finally, for the remaining hybrids, this effort employed an AutoEnginuity ScanTool data logger in combination with the Garmin GPS 18x and a PC to capture fuel usage [23]. For these hybrids, the velocity and elevation profiles utilize the same algorithm with the GPS 18x as the LEAF. However, issues arose with this data logger regarding its ability to stay connected to the vehicle via the OBDII port. Moreover, there were limitations of the PC in creating the drive cycle profiles, and the inability to record both ICE and motor rotational speeds simultaneously with the fuel use data led to the necessity of creating a number of simplified hybrid models [24]. Future work will

mitigate these issues through the creation of a number of additional drive cycles, each recording various parameters allowing for continued investigation into the power use algorithms of the individual vehicles.

To recap, after in-vehicle data collection and analysis, a single file for each vehicle and drive cycle contained the time, elevation, vehicle velocity, HV battery pack SOC (for EVs), cumulative fuel use, and ICE rotational speed (for conventional vehicles) for the specific test accomplished. This file feeds into the models via a lookup table and provides the input for running the specific vehicle models. Embedded within these models are the emissions profiles of each vehicle via a series of emissions factors. The following section describes the steps taken in creating these factors.

2.1: Liquid Fuel and Electricity Emissions Factors

The programs utilized in creating the liquid fuel and electricity emissions factors employed in the vehicle dynamics model and the fleet analysis include Argonne's GREET model, as well as the EPA's MOVES package. For enhanced predictions, EPA MOVES analysis replaced the standard GREET PtW fuel analysis of the gasoline-powered passenger cars and passenger trucks studied. The author created tables for diesel-powered passenger cars and passenger trucks; however, due to issues with the MOVES statistical database, this work does not incorporate these tables. Chapter 2 of this thesis contains more information on these issues. This chapter focuses on the use of GREET in creating final emissions factors for the various fuels, as Chapter 2 of this thesis contains the full MOVES investigation.

There are two main areas of study in the GREET liquid fuel analysis, the first of which is the WtP segment that includes the feedstock acquisition, refining, fuel creation,

and final transportation to the end user. The second area of study is the PtW analysis, which consists of burning the fuel by the end user in the vehicle powertrain. The electricity WtW analysis consists of these two main areas as well, although the PtW segment produces zero emissions since electricity use is inherently clean in the vehicle. However, the WtP segment is broken down into two main areas: feedstock acquisition and refining, and the use of this fuel in the power plant for electricity production. Sections 2.2.1 through 2.2.3 describe each of these areas in some detail based on the fuel type, as well as the conversion to emissions factors for use in the vehicle dynamics models.

2.1.1: Liquid Fuel WtP

The liquid fuel WtP analysis performed in GREET consists of the feedstock recovery, feedstock transportation, feedstock storage, feedstock refining/fuel production, fuel transportation, and fuel storage. In the case of petroleum-based fuels, crude oil extraction considers drilling, both on-shore and offshore, oil sands recovery through surface mining and in-situ production, and the processes involved in each of these. Once recovered, the oil sands are refined through bitumen extraction and upgrading in order to recover the maximum amount of oil. Ocean tankers, barges, and heavy-duty trucks transport this crude oil to the refinery storage. This analysis utilizes default fuel shares for each of these processes, as well as for the refining processes into gasoline and diesel. Transportation and distribution mediums of the refined gasoline and diesel include ocean tanker, barge, pipeline, rail, and truck.

In the case of ethanol-based fuels, GREET analyzes the energy and fuel use in fertilizer and pesticide production, the corn and other feedstock extraction via farm

equipment, and transportation to ethanol production plants. GREET considers both dry- and wet-milling ethanol plants in the ethanol production analysis. Furthermore, recent updates to the GREET program contain the inclusion of carbon sequestration in farming the plant matter used in ethanol production, lowering the WtW CO_2 emissions.

Finally, GREET considers the production of fuel additives, including Methyl Tertiary Butyl Ether (MTBE), Tertiary Amyl Methyl Ether (TAME), and Ethyl Tertiary Butyl Ether (ETBE). These additives are required in order to meet the gasoline oxygen requirements for reformulated gasoline. The production processes include production, transportation, and storage [6].

GREET produces emissions profiles for these fuels in units of grams of emissions per mmBtu of fuel produced. Calculation of the specific profiles of each fuel requires computation of emissions profiles in units of grams of emissions per gram of fuel incorporating the lower heating value and density of each fuel:

$$f_{emission} = \frac{f_{GREET} * LHV}{\rho_{fuel}} \quad (4)$$

where $f_{emission}$ is the fuel emission factor used in this analysis [g/g_{fuel}], f_{GREET} is the emission factor produced by GREET [g/mmBtu], LHV is the lower heating value of the fuel [mmBtu/gal], and ρ_{fuel} is the density of the fuel [g/gal]. One should note that the emissions factors for GHG are calculated using default GREET values for CO_2 equivalents of N_2O and CH_4 [6]:

$$f_{GHG} = f_{\mathrm{CO_2}} + 25 * f_{\mathrm{CH_4}} + 298 * f_{\mathrm{N_2O}} \quad (5)$$

where $f_{\mathrm{CH_4}}$ is the fuel emission factor for CH_4 [g/g_{fuel}], $f_{\mathrm{CO_2}}$ is the fuel emission factor for CO_2 [g/g_{fuel}], $f_{\mathrm{N_2O}}$ is the fuel emission factor for N_2O [g/g_{fuel}], and f_{GHG} is the resultant GHG emission factor [g/g_{fuel}].

Table 1 provides the emissions profiles for the WtP segment of the liquid fuel use analysis. The specific nomenclature in the table refers to Ultra-Low Sulfur Diesel (ULSD), Conventional Gasoline (CG), 85%/15% ethanol/gasoline mix (E85), wherein ethanol utilizes a 50%/50% dry and wet milling mixture during processing (50/50 Mix). One should note that this analysis utilizes the default values for the ratios of production methods and transportation emissions, thus representing a national average for these processes. Future work may improve upon this methodology by incorporating data specific to certain areas of the country.

Table 1: WtP liquid fuel emissions profiles.

[g_{em}/g_{fuel}]	ULSD	CG	E85 - Dry Mill	E85 - Wet Mill	E85 - 50/50 Mix
VOC	0.00033	0.00112	0.00135	0.00141	0.00138
CO	0.00048	0.00051	0.00077	0.00103	0.00090
NO_x	0.00185	0.00194	0.00246	0.00296	0.00271
PM_{10}	0.00027	0.00030	0.00075	0.00140	0.00108
$PM_{2.5}$	0.00015	0.00016	0.00026	0.00050	0.00038
SO_x	0.00097	0.00103	0.00152	0.00182	0.00167
CH_4	0.00519	0.00539	0.00568	0.00742	0.00655
N_2O	0.00001	0.00005	0.00090	0.00085	0.00088
CO_2	0.67617	0.71958	1.25814	1.69273	1.47543
GHG	0.81026	0.87220	1.67469	2.13753	1.90611

2.1.2: Liquid Fuel PtW

GREET examines the PtW liquid fuel analysis using a series of time-sheet emissions tables, altering these values according to the vehicle type in consideration. These time-sheet tables contain emissions profiles in units of [g/mile] according to statistical analyses performed in the EPA's MOBILE6.2 package [25]. However, the EPA's MOVES series including an updated statistical analysis has recently replaced MOBILE6.2. Thus, the author developed a series of new time-sheet tables using MOVES. Chapter 2 of this thesis describes the steps taken in this process. Of importance for this chapter, GREET contains three separate time-sheet tables, corresponding to light-duty vehicles (LDV), light-duty trucks lower than 3750 gross vehicle weight (LDT1), and light-duty trucks higher than 3750 gross vehicle weight (LDT2). However, MOVES lumps these vehicles together into passenger cars (LDV) and passenger trucks (LDT1 and LDT2). This is because MOVES creates the emissions profiles based on driving style as opposed to vehicle weight. This is consistent with EPA Tier 2 vehicle emissions regulations, which holds the same requirements for all vehicles, regardless of type or weight class. Thus, the author created two time-sheet tables corresponding to gasoline passenger cars and gasoline passenger trucks. Tables 2 and 3 contain these tables, with units of [g/mile].

Table 2: Gasoline passenger car time-sheet table developed using MOVES2010b.

Year	Model Year	MPG	VOC	CO	NO_x	PM_{10}	$PM_{2.5}$	CH_4	N_2O
2000	**1995**	24.6	0.4393	7.8388	1.3458	0.0124	0.0115	0.0378	0.0290
2005	**2000**	24.5	0.2384	5.1617	0.7981	0.0087	0.0080	0.0184	0.0158
2010	**2005**	24.2	0.1472	4.2301	0.1640	0.0066	0.0061	0.0175	0.0062
2015	**2010**	24.6	0.0788	3.0730	0.0992	0.0066	0.0060	0.0100	0.0063
2020	**2015**	29.2	0.0681	3.0850	0.0994	0.0064	0.0059	0.0111	0.0042
2025	**2020**	31.0	0.0669	3.0529	0.0987	0.0064	0.0059	0.0109	0.0041
2030	**2025**	31.0	0.0664	3.0227	0.0979	0.0064	0.0059	0.0100	0.0041
2035	**2030**	31.1	0.0634	2.9526	0.0960	0.0063	0.0058	0.0097	0.0039
2040	**2035**	31.1	0.0608	2.8964	0.0945	0.0063	0.0058	0.0094	0.0038

Table 3: Gasoline passenger truck time-sheet table developed using MOVES2010b.

Year	Model Year	MPG	VOC	CO	NO_x	PM_{10}	$PM_{2.5}$	CH_4	N_2O
2000	**1995**	18.6	0.8669	15.6572	2.6979	0.0231	0.0213	0.0701	0.0684
2005	**2000**	17.4	0.4596	8.0914	1.3592	0.0167	0.0154	0.0406	0.0531
2010	**2005**	16.8	0.1998	6.2928	0.4137	0.0125	0.0115	0.0393	0.0128
2015	**2010**	18.6	0.0971	4.5696	0.2502	0.0123	0.0113	0.0223	0.0124
2020	**2015**	23.0	0.0824	4.5149	0.2489	0.0119	0.0110	0.0233	0.0070
2025	**2020**	24.3	0.0810	4.4566	0.2478	0.0118	0.0109	0.0228	0.0069
2030	**2025**	24.3	0.0818	4.4389	0.2474	0.0118	0.0109	0.0214	0.0069
2035	**2030**	24.3	0.0795	4.3555	0.2455	0.0117	0.0108	0.0207	0.0067
2040	**2035**	24.4	0.0772	4.2734	0.2436	0.0117	0.0107	0.0200	0.0064

These time sheet tables contain the emissions profiles for VOC, CO, NO_x, PM_{10}, $PM_{2.5}$, CH_4, and N_2O. GREET calculates the remaining emissions (i.e., SO_x and CO_2) based on the specific fuel's carbon and sulfur ratios by weight. Thus, the final GREET PtW emissions tables contain all ten of the emissions mentioned. However, as stated, the emissions are in units of [g/mile]. Increasing the accuracy of the emissions produced by each individual vehicle requires computation of an emissions profile based on the time-sheet fuel efficiency and the fuel density:

$$f_{emission} = \frac{f_{GREET} MPG_{GREET}}{\rho_{fuel}} \quad (6)$$

where MPG_{GREET} is the GREET-stated fuel economy of the vehicle [miles/gal]. Table 4 contains the final emissions factors for gasoline and diesel passenger cars and passenger trucks.

Table 4: Final emissions profiles ($f_{emission}$) for gasoline cars and trucks, diesel trucks, and E85 cars and trucks.

[g_{em}/g_{fuel}]	Gasoline Car	Gasoline Truck	Diesel Truck	E85 Car	E85 Truck
VOC	0.001264	0.001191	0.000843	0.000966	0.000843
CO	0.036324	0.037502	0.002673	0.029640	0.022914
NO_x	0.001408	0.002465	0.001888	0.001116	0.001340
PM_{10}	0.000057	0.000075	0.000090	0.000064	0.000071
$PM_{2.5}$	0.000052	0.000069	0.000084	0.000059	0.000066
SO_x	0.000061	0.000061	0.000020	0.000014	0.000014
CH_4	0.000151	0.000234	0.000019	0.000116	0.000093
N_2O	0.000054	0.000076	0.000078	0.000095	0.000070
CO_2	3.244741	3.244737	2.831113	2.878471	2.889632
GHG	3.270174	2.269549	2.854784	2.909662	2.912883

2.1.3: Electricity WtW Emissions Factors

BEVs are commonly referred to as zero emission vehicles, but this study shows that this is not necessarily the case when considering the production of electricity. The US currently utilizes a number of electricity sources, including coal, oil, natural gas (NG), and biomass-fired power plants along with multiple types of nuclear power, and a number of renewable sources, including hydroelectric, wind, solar thermal, solar photovoltaic (PV), and geothermal power plants. The most prominent of these are coal, natural gas, nuclear, and wind [26]. However, the US utilizes all of these at some level. Thus, GREET includes the processes involved in each of these production sources.

Many of these electricity sources incur inherent energy use during the extraction, refining, transportation, and combustion processes. As a result, GREET analyzes the

energy use and emissions produced in each of these processes in the creation of final emissions factors. For example, the processes for coal include mining, cleaning, transportation to the power plants, and finally combustion of the fuel. Within each of these processes, the analysis is broken down even further. For example, 31% of coal mines are underground, while the remaining 69% involves surface mining that produces large amounts of particulate matter and dust. Moreover, the methods of transportation for coal include barge, rail, and truck. Likewise, the mining of uranium for use in nuclear power plants produces particulate matter, and transportation requires great care [25]. Although there are inherent emissions in wind, solar PV, hydroelectric, and geothermal power plants, the source of these emissions involve the creation of the power plants, which is not included in GREET. Thus, this effort considers these renewable sources to be 100% emission-free. Table 5 contains the final emissions factors for each of the emissions sources in units of grams of emissions per kWh electricity produced. Note that the category "Renewables" includes wind, solar PV, hydroelectric, and geothermal.

Table 5: Electricity emissions factors for various sources of electricity ($f_{em,elec}$).

[g/kWh]	Coal	Natural Gas	Oil	Nuclear	Renewables	Biomass
VOC	0.0953	0.0707	0.0824	0.0021	0	0.0812
CO	1.1176	0.2793	0.3142	0.0163	0	0.9729
NO_x	1.2868	0.8347	2.2980	0.0291	0	1.4519
PM_{10}	1.9968	0.0333	0.0763	0.0178	0	0.1627
$PM_{2.5}$	0.5253	0.0303	0.0497	0.0051	0	0.0867
SO_x	2.5629	0.1073	6.3507	0.0233	0	0.3641
CH_4	1.6242	4.4754	1.1287	0.0466	0	0.1021
N_2O	0.0119	0.0139	0.0053	0.0002	0	0.1278
CO_2	1194.1229	597.2161	1013.1828	14.9107	0	43.8769
GHG	1240.3148	713.8894	1043.7310	16.1707	0	84.7195

Finally, this study utilizes a custom electricity mix: the 2010 US electricity generation mix [27]. The calculation of this emissions profile involves a weighted average developed using the total amounts of electricity used from each of these sources. Table 6 contains these percentage constituents and Table 7 contains the emissions results for this mix.

Table 6: Constituents of the US electricity generation mix [27].

Source	2010 US Electricity Generation Mix
Coal	44.98%
Natural Gas	24.05%
Oil	0.90%
Nuclear	19.65%
Hydroelectric	6.34%
Geothermal	0.37%
Solar PV	0.03%
Wind	2.31%
Biomass	1.37%

Table 7: Emissions profile of the US electricity mix ($f_{em,elec,}$ [g/kWh]).

Emission	2010 US Electricity Generation Mix
VOC	0.0621
CO	0.5892
NO_x	0.8259
PM_{10}	0.9127
$PM_{2.5}$	0.2462
SO_x	1.2456
CH_4	1.8278
N_2O	0.0105
CO_2	693.4784
CO_2 (w/C in VOC & CO)	694.5980
GHGs	743.4231

One should note the high levels of CO_2, GHG, SO_x, PM_{10}, $PM_{2.5}$, and CO from the production mix. This is due to the relatively high amount of coal-fired electricity consumed and low relative amount renewable sources of energy in the US. One should note that new technologies including biomass-assisted coal combustion improvements to emissions reduction in coal-fired power plants are decreasing the overall coal emissions profile, thus, these emissions will reduce with subsequent updates to GREET illustrating this change. Section 4 contains more information on these technologies and their recent advancements. This supports the idea that further research is necessary in the area of renewable energy storage, such as vehicle-to-grid technology (V2G). Chapter 5 of this thesis contains more information on V2G technology.

The emissions factors created here are useful in determining the emissions produced per unit of energy expended. The next sections describe the vehicle dynamics models utilized in determining the fuel use of each vehicle over the recorded drive cycles.

3.0: Vehicle Dynamics Models

This work employs ten separate vehicle models, representing the ten vehicles in the study. Each of these models follows Newton's 2nd Law of Motion, as presented in Chapter 3; e.g., Equation1 through Equation7 in that specific chapter. However, differences arise in calculating the power required by the engine or motor. The vehicles labeled as Baseline Vehicles (BV) evaluate the power draw and fuel use in a similar manner to a conventional vehicle; whereas, each of the Electrified Vehicles (EV) employs a separate power draw scheme based on the individual vehicle powertrain. Sections 3.2 through 3.6 describe these power draw and fuel use algorithms. However,

of importance are the input specifications for each of the vehicles. General specifications such as frontal area, coefficient of drag, and gross weight are important to correctly calculate the force balance utilized in these models. Section 3.1 describes a number of these specifications and some of the assumptions made due to lack of information in the literature about these vehicles.

3.1: Vehicle Model Inputs

The vehicle specifications required of the force algorithms include the frontal area (A_f), the tire radius (r_{tire}), the coefficient of drag (C_d), the coefficient of lift (C_l), the rolling resistance friction coefficient ($\mu_{rolling}$), the total mass of the vehicle including passenger mass ($m_{vehicle}$), the internal combustion engine volume (V_d), and the transmission gear ratios ($G_{0\text{-}6}$). Table 8 contains the specifications for each of the four conventional vehicles.

The frontal area is a specification often omitted from vehicle specification lists, and, thus, is calculated for each of the vehicles as a function of the width and height, with a generalized correction factor of 85% [28]:

$$A_f = 0.85hw. \tag{7}$$

where h is the vehicle height [m] and w is the vehicle width [m]. One can measure the frontal area using a graphical program and scaled pictures of the front of the vehicle; however, this was not accomplished for this study for simplicity. An investigation by Hausmann et al. contains more information on this process [11].

Table 8: Conventional vehicle input specifications [29-37].

Variable	Units	Chevrolet Impala	Chevrolet Silverado1/2-Ton	Chevrolet Silverado 3/4-Ton	Chevrolet Uplander
A_f	[m^2]	2.347	3.065	3.360	2.843
r_{tire}	[m]	0.340	0.387	0.340	0.351
C_d	[-]	0.33	0.43	0.45	0.34
C_l	[-]	0.25	0.4	0.4	0.4
$\mu_{rolling}$	[-]	0.01	0.01	0.01	0.01
$m_{vehicle}$	[kg]	1776	2258	2875	2083
V_d	[m^3]	0.00351	0.00429	0.00599	0.0039
G_1	[-]	2.921	3.06	4.03	2.92
G_2	[-]	1.568	1.62	2.36	1.56
G_3	[-]	1	1	1.53	1
G_4	[-]	0.705	0.7	1.15	0.7
G_5	[-]	-	-	0.85	-
G_6	[-]	-	-	0.67	-
G_0	[-]	2.86	3.73	3.73	3.29

The electrified vehicles require similar inputs, although the transmission is often an electronic continuously variable transmission (ECVT); thus, it does not include any specific gear ratios. Furthermore, in a BEV, the absence of an ICE relieves the requirement for the engine volume. Table 9 provides the specifications required for the hybrid electric vehicles, while Table 10 indicates the specifications for the Nissan LEAF and the Ford Transit EV.

Table 9: Parallel and series hybrid vehicle specifications [38-47].

Variable	Units	Chevrolet Volt	Ford Fusion Hybrid	Chevrolet Silverado Hybrid	Toyota Prius
A_f	[m^2]	2.185	2.220	3.200	2.230
r_{tire}	[m]	0.334	0.328	0.387	0.310
C_d	[-]	0.28	0.33	0.41	0.26
C_l	[-]	0.25	0.25	0.40	0.25
$\mu_{rolling}$	[-]	0.01	0.01	0.01	0.01
$m_{vehicle}$	[kg]	1788	1687	2528	1330
V_d	[m^3]	0.00140	0.00250	0.00597	0.00150
G_0	[-]	-	2.57	3.08	3.93
HV Nominal Voltage	[VDC]	330	275	320	201.6
HV Pack Capacity	[Wh]	16000	1370	2100	1310
Max Current	[A]	336	95	188	104

Table 10: BEV vehicle specifications [48-52].

Specification	Units	Nissan LEAF	Ford Transit EV
A_f	[m^2]	2.270	3.610
r_{tire}	[m]	0.316	0.324
C_d	[-]	0.29	0.4
C_l	[-]	0.25	0.25
$\mu_{rolling}$	[-]	0.01	0.01
$m_{vehicle}$	[kg]	1690	1960
G_0	[-]	7.94	8.28
HV Nominal Voltage	[VDC]	403	320
HV Pack Capacity	[Wh]	24000	28000
Max Current	[A]	199	328

The models utilize these technical specifications, as well as various efficiency maps, battery discharge curves, and engine brake specific fuel consumption maps. The following sections describe in better detail these efficiency and discharge maps and the steps involved in accessing this information.

3.2: Conventional Vehicle Power Draw and Fuel Use

Each of the conventional ICE vehicles applies the same power draw scheme based on the vehicle's tractive force (F_{TE} [N]), and ICE rotational speed (ω_{ICE} [rot/s]), as measured by the in-vehicle data logger. However, prior to calculating the power draw and fuel use, the model estimates the transmission gear in use at each time step based on an algorithm that checks the ratio of torque converter pump and turbine speeds given the available gear ratios. In conventional vehicles, a torque converter de-couples the automatic transmission from the engine, allowing the engine to idle at low speeds

without causing the vehicle to move. This is important to keep the engine running while the vehicle is at a stop. This algorithm uses the fact that the ratio of the output to the input speed of the torque converter must be less than one:

$$n_c = \frac{V G_0 G_i}{2\pi \omega_{ICE} r_{tire}} < 1 \tag{8}$$

where n_c is the ratio of input speed to output speed of the torque converter [-], G_i is the current transmission gear ratio [-], V is the vehicle's velocity at the current time step [m/s], G_0 is the final drive gear ratio, and r_{tire} is the radius of the tire [m]. From this algorithm, the model finds the gear ratio (thus the transmission gear in use) and ratio of output to input speed of the torque converter. These are both necessary in calculating the efficiency of the transmission and the torque converter.

Applying the now known transmission gear in use, the model calculates the efficiency of a standard conventional vehicle transmission, η_t [53]:

$$\begin{aligned} \eta_t = \Bigg\{ & \left[0.96 - \left(7.07 * 10^{-4} \left[\frac{s}{m} \right] \right) V - \left(2.9 * 10^{-5} \left[\frac{s^2}{m^2} \right] \right) V^2 \right] \\ & * \left[0.998 \left(1 - 0.007 \left(n_g - i_g \right) \right) \right. \\ & \left. - \left(1.965 * 10^{-4} \left[\frac{s}{m} \right] * V * 2.08^{n_g - i_g} \right) \right] \Bigg\} \end{aligned} \tag{9}$$

where n_g is the number of gears in the transmission [-] and i_g is the number of the gear in use [-]. Furthermore, the model utilizes the rotational speed ratio of the torque converter in calculating the torque converter efficiency. However, first the model computes the torque of each of the torque converter pump and turbine normalized by the rotation speed of the pump:

$$\frac{\tau_p}{\omega_p^2} = 1.564 * 10^{-3} + 1.0892 * 10^{-3} n_c - 2.2777 * 10^{-3} n_c^2 \quad (10)$$

$$\frac{\tau_t}{\omega_p^2} = 3.1530 * 10^{-3} + 1.1030 * 10^{-5} n_c - 3.0648 * 10^{-3} n_c^2 \quad (11)$$

where τ_p is the torque of the torque converter pump [N-m], τ_t is the torque of the torque converter turbine [N-m], and ω_p is the torque converter pump rotation speed [rot/s] which need not be evaluated as the desired value is the ratio of the pump and turbine torques (see equation 12). These torques are estimated based on a least-squared curve-fit optimization as performed by Kotwicki in his torque converter dynamics model [54].

Finally, the model calculates the torque converter efficiency:

$$\eta_{tc} = {}^{\tau_p}/_{\tau_t} \quad (12)$$

Using the tractive force required (F_{TE} [N]), the vehicle's velocity, and the efficiencies of the transmission and torque converter, the model determines the brake power (P_b [W]):

$$P_b = \frac{F_{TE} V}{\eta_t \eta_{tc}} \quad (13)$$

As the first step in calculating the engine's current fuel consumption rate, the model formulates the engine's brake mean effective pressure ($bmep$ [Pa]):

$$bmep = \frac{P_b n_R}{\omega_{ICE} V_d} \quad (14)$$

where n_R is the number of rotations per engine cycle [rot], or two in the case of these vehicles, ω_{ICE} is the ICE rotation speed [rot/s], and V_d is the engine displacement volume [m^3]. An engine's $bmep$ is a measure of the pressure inside the cylinder, normalized to the volume of the engine. This parameter is useful in comparing the power of engines independent of their size [55]. From this value, the model finds the indicated mean effective pressure ($imep$ [bar]), which is independent of frictional losses in the engine:

$$imep = \frac{bmep}{\eta_{ICE,mech} * 100000} \tag{15}$$

where $\eta_{ICE,mech}$ is the mechanical efficiency of the engine [-], assumed to be 0.90, and the value of 100000 indicates the conversion of Pa to bar [Pa/bar]. This conversion factor is necessary for use in determining the fuel consumption via the method described later in this section. The next step involves calculating the engine's brake specific fuel consumption, or $bsfc$. The $bsfc$ is a measure of the fuel consumption rate normalized by the power produced [55]:

$$bsfc = \frac{\dot{m}_{fuel}}{P_b} \tag{16}$$

where $\dot{m}_{fuel}$ is the fuel flow rate in [kg/s].

Due to a lack of information regarding each individual engine's $bsfc$ characteristics (not published in the literature because of proprietary reasons), this effort employs an approximation developed using Dr. Christopher Depcik's *Cycles* program [56]. This program models an ICE thermodynamic cycle based on a constant volume combustion assumption. The process involves creating a best-fit curve for indicated

specific fuel consumption (*isfc* [kg/s]) calculations as a function of *imep*. Specific *imep* values are created by lowering the intake pressure, simulating an increasingly throttled gasoline engine. Important inputs include the fuel type (C_7H_{17}), equivalence ratio (1.0), engine compression ratio, reference ambient temperature and pressure (300 K, 1 bar, respectively), and the volume of one cylinder in the engine studied. This process produces a quadratic best-fit curve on a logarithmic scale:

$$isfc = e^{\left[a*\ln\left(\frac{imep}{imep_0}\right)^2 + b*\ln\left(\frac{imep}{imep_0}\right)+c\right]} * isfc_0. \quad (17)$$

where $imep_0$ is a factor normalizing the *imep* to balanced units [bar], and $isfc_0$ is used to give the proper units for *isfc,* equal to 1 [kg/s]. The factors a, b, and c are dimensionless factors determined by the best-fit curve developed in *Cycles*, and are optimized based on a least-squared curve fit routine described in Section 3.9. One should note that the Ford Fusion Hybrid's 1.8L Duratec engine runs on an Atkinson combustion cycle. Hence, the *Cycles* program is only able to estimate roughly the output of this particular novel thermodynamic cycle (i.e., larger expansion ratio than compression ratio). As a result, the estimate in this effort includes the simulation of a larger geometric compression ratio than what is reported in the literature for the engine.

The *Cycles* program does not take into account the thermal inefficiency, which includes heat transfer to the engine coolant and walls, imperfect combustion, and fuel conversion efficiency. Thus, the models utilize a generalized efficiency of 35% due to a lack of information about the specific engines at hand, correcting the *Cycles* estimations, with any inaccuracies corrected via the optimization routine. As a result, the modle computes the *bsfc* in units of [g/kWh]:

$$bsfc = \frac{isfc}{\eta_{ICE,th}} \tag{18}$$

where $\eta_{ICE,th}$ is this estimated fuel conversion, heat transfer, and combustion thermal efficiency. Finally, the model determines the fuel flow rate ($\dot{m}_{fuel}$) for the current time step in [g/s]:

$$\dot{m}_{fuel} = \frac{bsfc_i * P_b}{1000 * 3600} \tag{19}$$

where 1000 is a conversion factor in [W/kW] and 3600 is a time conversion factor in [s/hr].

In the case that the tractive force required is negative, the model assumes the vehicle is slowing down with the brakes engaged or coasting. In the conventional vehicle routine, the approach is simple, assuming an idle power draw measured by an On-Board Diagnostics 2.0 (OBDII) data logger, described in Section 2.1. This value changes depending on a number of factors, including engine temperature, intake pressure, engine size, and the current engine rotational speed, and thus the models assume a fuel flow rate of 0.60 grams of fuel per second, which is a rough average of these values. Calibration of the *bsfc* equation acts to mitigate any error in the assumptions presented in this section. Section 3.9 describes this optimization routine.

3.3: Electrified Vehicle Fuel and Electricity Consumption Algorithms

Given the varied powertrains of the six electrified vehicles studied, this effort employs a number of different power and fuel consumption algorithms ranging in complexity based on the information available to the public. For example, the model for the Nissan LEAF consumption algorithm includes a motor efficiency map, a generalized

lithium-manganese battery discharge curve, and specific data available through the LEAF-specific CAN string data logging mentioned prior. Alternatively, the Ford Transit EV, due to a lack of public information on the vehicle and a malfunctioning AutoEnginuity data logger, uses a simplistic model similar to the Volkswagen Beetle PHEV model described in Chapter 3 of this thesis. Sections 3.4 through 3.6 describe each of these power and fuel use algorithms in detail.

3.4: Nissan LEAF Electricity Consumption

The Nissan LEAF algorithm is the most accurate of the BEV models utilized in this fleet analysis because of a vast amount of information available on the electric motor and battery technology incorporated in this vehicle design. Furthermore, the implementation of a single reduction gear transmission and the absence of a torque converter in this BEV allows for direct calculation of the required motor power, torque, and rotational speed. Finally, a simplistic model of the vehicle's regenerative braking capabilities provides for an uncomplicated model with high accuracy.

The power use algorithm first determines the brake power (P_b) required by the motor according to Equation 7 in Chapter 3 of this thesis. Next, the model computes the electric motor instantaneous efficiency via an interpolation lookup map created from the Nissan LEAF efficiency map shown in Figure 3 [57]. Utilizing this map required the application of a figure digitization program, TechDig 2.0 [58]. This program takes in digital readings based on user-set axes values, saving the data in tab-delimited format. A Matlab cubic-spline interpolation routine increases the resolution of the data to ten revolutions per minute (rpm) and one Newton-meter (N-m) motor torque, saving the final efficiency map as a comma-separated value MS Excel spreadsheet.

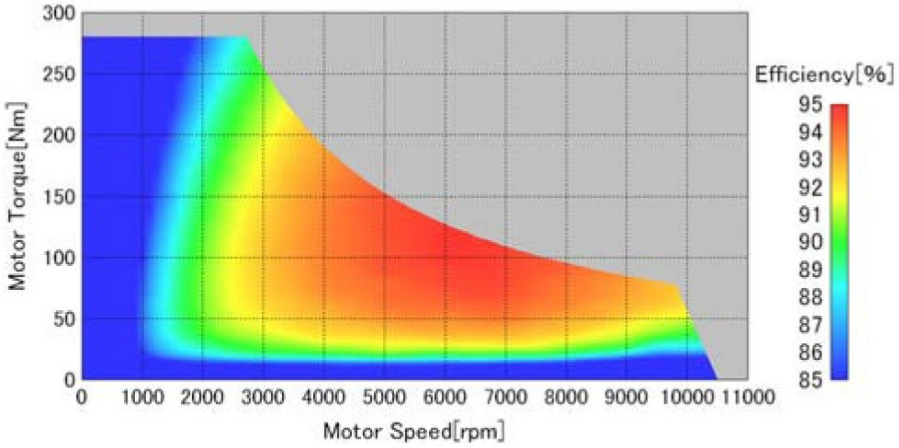

Figure 3: LEAF electric motor efficiency map [57].

In order to access this lookup map properly, the model first calculates the motor rotational speed, ω_{em}, in rotations per minute as a function of the vehicle velocity, the tire radius, and the final gear ratio of the combined transmission and final drive, G_0:

$$\omega_{em} = \frac{VG_0 * 60}{2\pi r_{tire}} \tag{20}$$

where 60 is a time conversion factor [s/min].

Subsequently, the required motor brake torque (τ_b [N-m]) is found as a function of the brake power and motor speed in radians per second [55]:

$$\tau_b = \frac{P_b * 60}{2\pi\omega_{em}} \tag{21}$$

where 60 is again the time conversion factor applied prior [s/min].

Given the two variables of motor speed and brake torque, the model calls the efficiency lookup map, finding the motor efficiency (η_{motor} [-]). Finally, the model assesses the total battery draw (P_{batt} [W]) and the resultant current draw (I_i [Ampere]):

$$P_{batt} = \frac{P_b}{\eta_{motor}} + P_{acc} \quad (22)$$

$$I_i = \frac{P_{batt}}{Vdc_{i-1}} \quad (23)$$

where P_{acc} is the accessory draw of auxiliary systems in the vehicle [W], and Vdc_{i-1} is the high voltage battery pack DC voltage at the previous time step [VDC].

The reason for applying the voltage at the previous time step is because the model utilizes the current draw to find the voltage via a lookup table created in a similar manner to the motor efficiency map. This map is based on the vehicle specific battery chemistry's typical discharge characteristics and current draw. Figure 4 shows a $LiMn_2O_4$ discharge curve, the same battery chemistry in the LEAF. Although this is not the exact LEAF battery discharge curve, it provides for a good estimate of the discharge characteristics in absence of exact knowledge. Similarly to the motor map, this effort usesTechDig2.0 and a cubic-spline interpolation routine in the creation of a voltage lookup map. This map is a function of the SOC of the vehicle's high voltage pack at the previous time step with a resolution of 0.01% SOC (calculated as 100% minus capacity in Figure 4). Moreover, the map includes the discharge C-rating with a resolution of 0.1 C. Of importance, the C-rating is a measure of the battery's discharge rate normalized to the pack capacity. For example, the LEAF battery pack has a capacity of 24 kWh and a nominal voltage of 403.2 Vdc, resulting in a final capacity of 59.5 Ah. Thus, if the motor draws 59.5 amps, the motor will fully discharge the battery pack in one hour resulting in a C-rating of 1C. Likewise, a C-rating of 0.5C corresponds to a discharge rate of 29.8 A, and a C-rating of 5C corresponds to a discharge rate of 297.6 A. This C-

rating is important in determining the pack voltage since a higher discharge rate results in a lower instantaneous voltage, as well as a lowered available capacity.

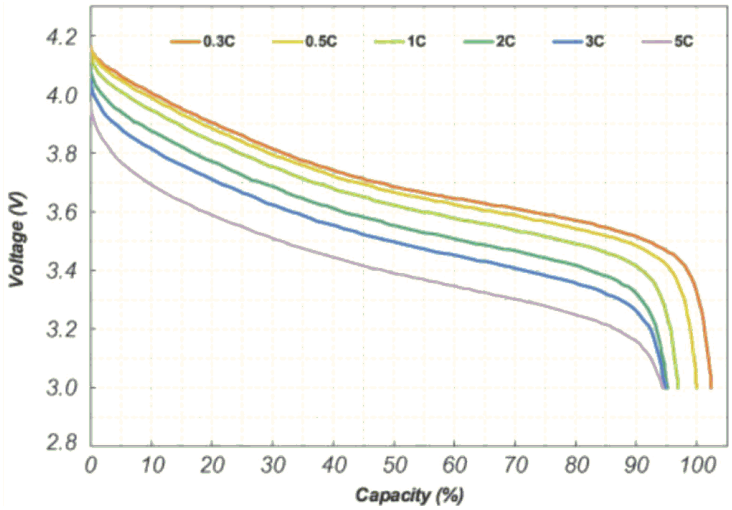

Figure 4: $LiMn_2O_4$ discharge curve as a function of different C-ratings [59].

Therefore, the model calculates the C-rating as a function of the discharge current (I_i [Ampere]), the pack discharge capacity (E_{tot}[W]), and the voltage at the previous time step, Vdc_{i-1}:

$$C_i = \frac{I_i Vdc_{i-1}}{E_{tot}} \tag{24}$$

The model then implements the LEAF voltage lookup map, finding the current HV battery pack voltage according to the C-rating and the previous time step's HV battery pack SOC. Finally, the model determines the capacity removed from the battery pack according to Peukert's Law:

$$CR_i = CR_{i-1} + \frac{I_0 \left(\frac{I_i}{I_0}\right)^k * dt}{3600} \tag{25}$$

where CR_{i-1} is the cumulative capacity removed from the high voltage battery pack up until the previous time step [Ah], I_i is the discharge current for the current time step

[Ampere], I_0 is a current normalization factor in 1 [Ampere], dt is the duration of the current time step [s], 3600 is a time conversion factor [s/hr], and k is the Peukert coefficient, a dimensionless constant calibrated to the specific battery type.

Employing the Peukert coefficient is a widely utilized method in order to account for the particular phenomena in batteries in which a higher discharge current results in lowered usable pack capacity [29, 60, 61]. A number of alternate methods are available that improve upon this simplistic approach, including Hausmann and Depcik's inclusion of a temperature dependency [11]. However, due to a lack of information available on the Nissan LEAF HV pack, this simplistic expression assumes the Peukert coefficient to be equal to unity. Further testing on specific Nissan LEAF batteries may lead to an improved estimate for this coefficient.

The model finishes the Nissan LEAF electricity consumption routine by calculating the State of Charge of the battery pack:

$$SOC_i = SOC_0 - \frac{CR_i V dc_i}{E_{tot}\eta_{EV,correct}} \tag{26}$$

where SOC_i is the state of charge of the HV battery pack at the current time step [-], SOC_0 is the initial SOC at the start of the drive cycle [-], and $\eta_{EV,correct}$ is the optimized efficiency of the electric drive train [-] including motor controller, transmission, and other power losses in the system. Optimization of this dimensionless constant follows similarly to the optimization routine for the determination of individual $bsfc$ map calculations in Section 3.2. This resulted in an efficiency value of 70%.

In the case that the tractive force required is negative, the model assumes the vehicle is slowing down via available regenerative braking power. Electrified vehicles

perform regenerative braking by switching the polarity of the electric motor, thus acting as a generator in order to recharge the HV battery pack. However, in general motors are limited in their ability to recover this power for two reasons: the electric motors act inefficiently since this is not their main intended operation, and often times friction braking systems are utilized in the case of high deceleration for safety[62, 63].

As a result, the model first obtains the regenerative braking power required (P_{regen} [W]):

$$P_{regen} = F_{TE} V \eta_{regen} \tag{27}$$

where η_{regen} is an estimated regenerative braking efficiency of 30%, accounting for the inefficiency of the generator, motor controller, and electric transmission. This is a simplistic approach because of the lack of information regarding the Nissan LEAF regenerative braking system. The model estimates this value based on rough average motor (η_{motor}) and electric transmission efficiencies ($\eta_{EV,correct}$) (85% and 70%, respectively), along with a 50% reduction to account for the inefficiency of the motor acting as a generator:

$$\eta_{regen} = \eta_{mg} \eta_{motor} \eta_{EV,correct} \tag{28}$$

where η_{mg} is this 50% efficiency reduction. The model then finds the regenerative braking current input:

$$I_i = \frac{P_{regen}}{V dc_{i-1}} \tag{29}$$

Finally, the model calculates the C-rating, battery draw, and charge removed via Equations 24, 22, and 25, respectively. One should note that since the tractive force is

negative, the battery draw and charge removed are also negative, resulting in power added to the HV battery pack.

A number of the hybrid vehicles modeled in this study implement a combination of the two power-use routines described (i.e., *bsfc* and motor/voltage maps). However, because of the lack of information available in the literature on a number of the vehicles, some of the models are far more simplistic than the conventional vehicle and Nissan LEAF models described. Sections 3.5 and 3.6 describe the different methods used.

3.5: 2011 Chevrolet Volt Power Draw Algorithm

The Chevrolet Volt utilizes a series hybrid power train, acting as an Extended Range Electric Vehicle (EREV)that employs a gasoline generator for charging in the event of a low HV battery pack SOC. Thus, the power draw algorithm for the Chevrolet Volt consists of a logic switch statement based on three variables: the vehicle velocity, the tractive force required, and the HV battery SOC at the previous time step. A study on the GM "Voltec" multi-mode electric transaxle described by Miller et al. illustrates the functionality of the Chevrolet Volt [64]. This algorithm functions as indicated in Figure 5: if the SOC is above 30%, the vehicle acts in BEV mode; whereas, if the SOC is lower than 30%, the vehicle acts in EREV mode.

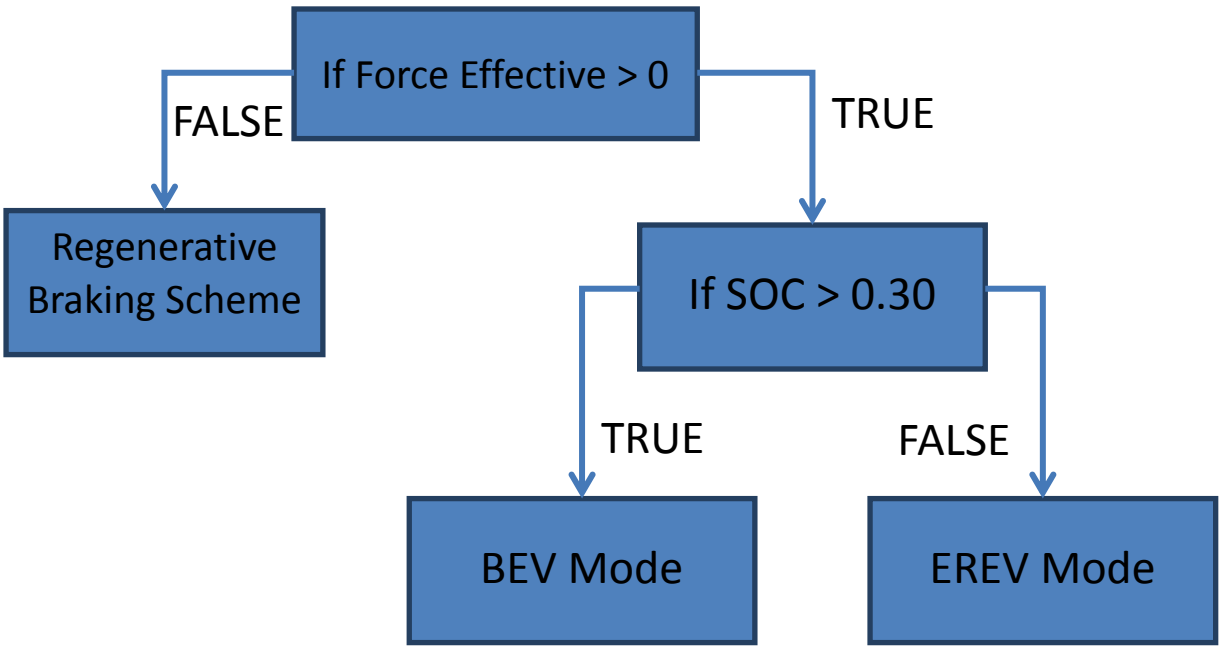

Figure 5: Chevrolet Volt power use algorithm.

3.5.1: Volt BEV Mode Operation

The Volt operates as a BEV when the tractive force required and the vehicle's velocity are both positive. In this operational mode, the model first determines the axle torque limit ($\tau_{axle,max}$ [N-m]) as a function of the vehicle's velocity, based on the motor's efficiency map as shown in Figure 6 [64]. Similar to before, TechDig 2.0 allows for digitalization of the torque limit from this map (top line that decreases with vehicle speed beyond approximately 50 kph) followed by subsequent creation of torque limit equations using least-square curve fits. In the event that the vehicle velocity is lower than 50 kph, the model utilizes Equation 30; whereas, the model employs Equation 31 for higher velocities where $V_0$is a velocity normalization factor of 1 [m/s] and τ_0 is a torque conversion factor of 1 [N-m].

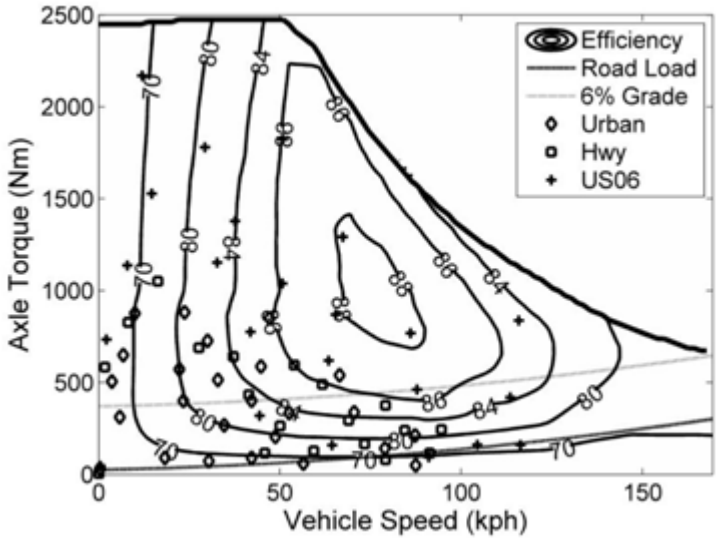

Figure 6: The Chevrolet Volt electric motor efficiency map when operating in BEV mode[64].

$$\tau_{axle\,,max} = \tau_0 * \left(2.3301\frac{V}{V_0} + 2448.4\right) \tag{30}$$

$$\tau_{axle\,,max} = \tau_0 * \left[-0.0252 * \left(\frac{V}{V_0}\right)^3 + 3.8562\left(\frac{V}{V_0}\right)^2 - 216.91\frac{V}{V_0} + 4945.1\right] \tag{31}$$

The model then computes the combined motor efficiency in the same manner as the Nissan LEAF based on the efficiency map in Figure 5. However, this time it uses the vehicle velocity with a resolution of 1 km/hr, and the calculated axle torque with a resolution of 10 N-m:

$$\tau_{axle} = F_{TE} * r_{tire}\,. \tag{32}$$

The model checks this torque against the maximum torque, setting it equal to the maximum if exceeding. Future iterations of this work include recalculating the force algorithm similar to the methodology used by Hausmann in his thesis efforts [11].

Next, the model determines the battery power draw as a function of the motor efficiency (η_{motor}) and an efficiency correction dimensionless constant ($\eta_{EV,correct}$) optimized according to the previously described methods in Sections 3.2 and 3.4:

$$P_{batt} = \frac{F_{TE} V}{\eta_{motor}\, \eta_{EV,correct}} \tag{33}$$

Note that the optimization returned a value equal to 1.11 for the efficiency correction parameter. Obviously, this is physically impossible for efficiency. However, this is a result of the inaccuracies in calculating the motor efficiency via lookup map, primarily due to issues with extraction resolution.

The model computes the charge removed from the HV battery pack as a function of the battery power draw, the length of the current time step, and the HV battery pack's nominal voltage. Note that this effort employs the nominal voltage of the pack due to the lack of publicly available discharge characteristics; hence, this further accounts for some of the error in the efficiency correction parameter. Finally, the model analyzes the HV battery pack's SOC at the current time step according to Equation 26.

3.5.2: Volt EREV Mode Operation

The powertrain of the Chevrolet Volt operates in EREV mode when the SOC is lower than or equal to 30%. The use of one of the motors as a generator leaves one motor available for producing the required tractive force. In this driving style, the algorithm assumes the power required of the battery pack to come directly from the ICE, thus producing a net zero draw from the pack. Figure 7 provides the efficiency map for this mode of operation [64].

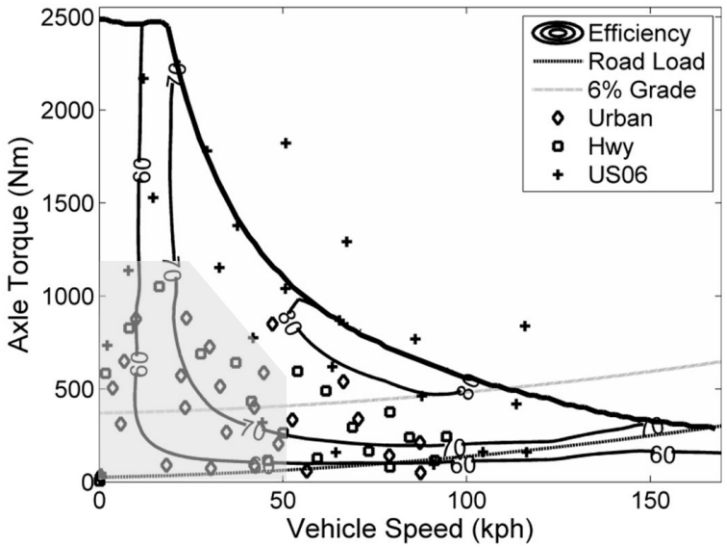

Figure 7: The Chevrolet Volt electric motor efficiency map when operating in EREV mode [64].

As before, employing TechDig 2.0 allows determination of axle torque curve equations and efficiency lookup maps. In particular, when the vehicle is travelling slower than 18 kph, the maximum axle torque is simply 2500 N-m. Otherwise, the analysis finds the axle torque via a least-square curve fit as a function of vehicle velocity:

$$\tau_{axle,max} = \tau_0 \left[12591 \left(\frac{V}{V_0} \right)^{-0.942} \right] \tag{34}$$

Then, the model obtains the axle torque required via Equation 32 that is compared and set to the maximum in the event it is higher than allowed. Next, the model finds the motor efficiency via the lookup map, finally determining the required power draw of the HV battery pack, again utilizing the nominal voltage. The model assumes that the power required from the motor comes from the gasoline generator, resulting in a net zero power draw from the HV battery pack.

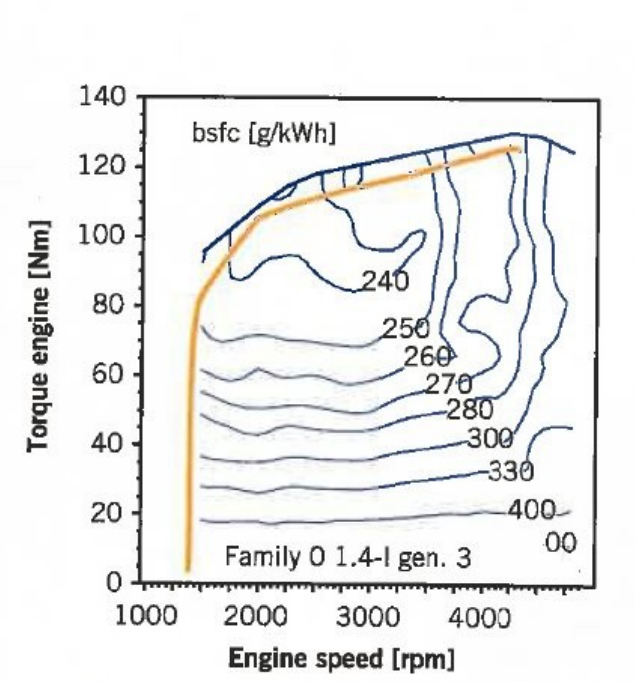

Figure 8: Volt ICE *bsfc* map [65].

For the engine, a search through the literature allowed for discovery of the $bsfc$ map for the GM 1.4L I4 gasoline engine in the Chevrolet Volt, as shown in Figure 8. Using the optimal operation curve in this map (orange) captured through TechDig 2.0, results in the creation of a curve-fit equation for the engine $bsfc$ as a function of required battery power, a normalized battery power ($P_{batt,0}$ [W]), and a normalized brake specific fuel consumption equal to 1 ($bsfc_0$ [g/kWh]):

$$bsfc = bsfc_0 \left[6.478 * 10^{-25} \left(\frac{P_{batt}}{P_{batt,0}} \right)^6 - 1.261 * 10^{-19} \left(\frac{P_{batt}}{P_{batt,0}} \right)^5 + 9.710 \right.$$
$$* 10^{-15} \left(\frac{P_{batt}}{P_{batt,0}} \right)^4 - 3.759 * 10^{-10} \left(\frac{P_{batt}}{P_{batt,0}} \right)^3 - 7.704 \qquad (35)$$
$$\left. * 10^{-6} \left(\frac{P_{batt}}{P_{batt,0}} \right)^2 - 0.07963 \left(\frac{P_{batt}}{P_{batt,0}} \right) + 569.6 \right].$$

From this, the model determines the fuel flow rate at the current time step, setting the overall charge removed to the previous time step with the proper conversion factors:

$$\dot{m}_{fuel} = \frac{P_{batt} * bsfc_i}{1000 * 3600} \quad (36)$$

3.5.3: Volt Regenerative Braking Mode Operation

In the case of the last operational mode involving regenerative braking, the Volt model simply applies the same assumptions and algorithm employed for the Nissan LEAF in Section 3.4. Likewise, if the vehicle is at a stop, the model assumes the vehicle does not use any electricity or gasoline. This is not the case for the real vehicle, although it is a reasonable assumption for short stops. In reality, when in EREV mode, the Volt continues to run the gasoline generator, recharging the HV battery pack, albeit rather slowly [64]. This is also the same reason the Volt does not contain a torque converter, as the proprietary planetary gear train transmission allows the engine to spin while at a complete stop, charging the HV battery pack through one of the two motors.

The final step in the Volt power draw algorithm involves calculating the SOC of the HV battery pack according to Equation 26 with an assumed electric powertrain efficiency, $\eta_{EV,correct}$, equal to one. This is because optimization happens via the aforementioned efficiency constants in the calculation of the battery draw (i.e., Equation 33).

3.5.4: Chevrolet Silverado Hybrid, Toyota Prius, and Ford Fusion Hybrid Power Draw Algorithms

The models for the Chevrolet Silverado Hybrid, Toyota Prius, and Ford Fusion Hybrid all operate via a similar methodology since they utilize a parallel hybrid powertrain implementing a gasoline internal combustion engine and one or two electric

motors, all capable of adding to vehicle traction. However, due to a lack of detailed information in the literature about the specific operational algorithms used, this effort includes three simplistic models based on a straightforward approach. Furthermore, each of these vehicles implements an ECVT, thus making it all but impossible to ascertain the rotational speeds of the motors and internal combustion engines. Likewise, the data logger tracking the fuel efficiency of these vehicles is the AutoEnginuity ScanTool, which is not capable of tracking fuel use and engine/motor speeds simultaneously [24].

As illustrated by Figure 9, when the vehicle's HV battery pack SOC is higher than 60%, the model assumes that the vehicle operates using the electric motor first, and depending on the power required, may operate solely in BEV mode. When the SOC drops below 60%, the vehicle operates in parallel hybrid mode, applying the gasoline engine first and only using the electric motor when the required power and torque are larger than the engine's capabilities. The algorithm assumes the 60% SOC as this is a general average SOC observed across all drive cycles with these vehicles. As a result, the five operational modes for these three vehicles include BEV mode, parallel hybrid motor-first mode, conventional ICE, parallel hybrid ICE-first mode, and a basic regenerative braking scheme. The largest difference between the three is in the calculation of the ICE $bsfc$. In the case of the Toyota Prius, the $bsfc$ map and the optimal operation curve are available in the literature. Therefore, the model utilizes these parameters in order to estimate the $bsfc$ as accurately as possible [47].

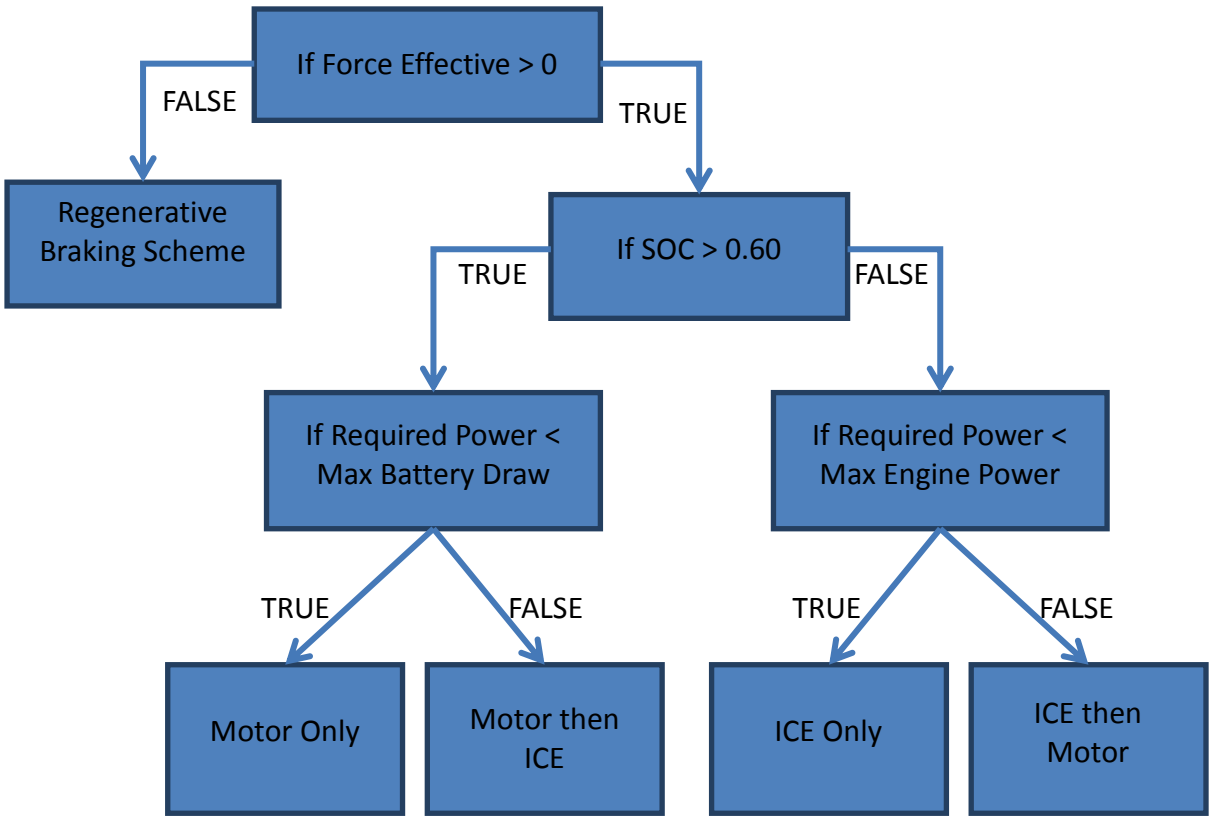

Figure 9: Parallel hybrid power use algorithm.

As stated, the models assume that when the HV battery pack is above 60% SOC, the vehicle operates using the electric motor first, and when the motors cannot supply enough power to the wheels, the ICE makes up the difference. Likewise, when the HV battery pack is below 60% SOC, the vehicle operates by utilizing the ICE first, letting the electric motor supply the remaining power if necessary. Thus, the models first determine the required output power according to Equation 13 with initial efficiencies equal to one as the model will take into consideration the true efficiencies in a later calculation. The model then enters a multiple-variable logic switch on the SOC, required output power, and vehicle velocity. When the SOC is above 60% and the required power is lower than the maximum output motor power, the model implements a simple BEV power draw algorithm, calculating the battery output power:

$$P_{batt} = \frac{P_{motor,out}}{\eta_{finaldrive}\ \eta_{t,ECVT}\eta_{motor}} \tag{37}$$

where $P_{motor,out}$ is the output motor power [W], $\eta_{final\ drive}$ is the final drive efficiency, $\eta_{t,ECVT}$ is the dimensionless transmission efficiency, and η_{motor} is the dimensionless combined motor efficiency. These three efficiencies are assumed equal to 0.95, 0.98, and 0.85, respectively. Future work includes employing motor efficiency maps, as well as calculating and/or looking up transmission efficiencies in a manner similar to that of the LEAF and conventional vehicles. The next steps in BEV mode include finding the battery output current, C-rating, and charge removed according to Equations 23, 24, and 25, respectively.

In the event that the motors cannot supply the necessary power, the model computes the engine output power (P_{ICE} [W]):

$$P_{ICE} = P_b - P_{motor,max} \tag{38}$$

where $P_{motor,max}$ is the maximum output motor power [W]. In the case of the Prius, Figure 10 along with TechDig 2.0 allows for calculation of a $bsfc$ curve-fit:

$$\begin{aligned} bsfc_i &= bsfc_0 \\ &* e^{\left\{ \begin{array}{c} 6.91291*10^{-3} ln\left(\frac{P_{ICE}}{P_{ICE,0}}\right)^6 - 0.375027\, ln\left(\frac{P_{ICE}}{P_{ICE,0}}\right)^5 + 8.45049\, ln\left(\frac{P_{ICE}}{P_{ICE,0}}\right)^4 - 101.257\, ln\left(\frac{P_{ICE}}{P_{ICE,0}}\right)^3 \\ + 680.773\, ln\left(\frac{P_{ICE}}{P_{ICE,0}}\right)^2 - 2436.7\, ln\left(\frac{P_{ICE}}{P_{ICE,0}}\right) + 3637.21 \end{array} \right\}} \end{aligned} \tag{39}$$

where $P_{ICE,0}$ is the normalized ICE output power equal to 1 [W].

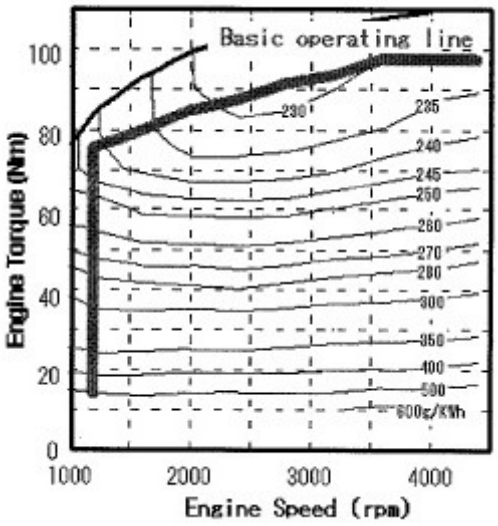

Figure 10: Toyota Prius brake specific fuel consumption map with a dark line indicating the optimal pathway for maximum fuel economy [47].

In the case of the Fusion, Figure 11along with TechDig 2.0 provides for the calculation of the engine speed as a function of power output:

$$\omega_{ICE} = \omega_{ICE,0}\left[6.456532 * 10^{-11}\left(\frac{P_{ICE}}{P_{ICE,0}}\right)^3 - 2.068801 * 10^{-6}\left(\frac{P_{ICE}}{P_{ICE,0}}\right)^2 + 5.22733 * 10^{-2}\left(\frac{P_{ICE}}{P_{ICE,0}}\right) + 896.5454\right] \quad (40)$$

where $\omega_{ICE,0}$ is a normalized ICE rotation speed equal to 1 [rot/s].

Likewise, using Figure 12 results in the creation of a similar equation for the Silverado Hybrid:

$$\omega_{ICE} = \omega_{ICE,0}\left(0.018257\frac{P_{ICE}}{P_{ICE,0}} + 318.559792\right) \quad (41)$$

The Fusion and Silverado Hybrid $bsfc$ map estimations are products of the ICE *Cycles* program similar to the process described in Section 3.2. Optimization occurred with

these maps so that the final fuel economy of the Fusion was equal to 39 mpg, and the final fuel economy of the Silverado was 21 mpg, which are the EPA-stated combined city/highway fuel economies of these vehicles [66]. A lack of time available with the Ford Fusion Hybrid and faulty data logging with the AutoEnginuity ScanTool led to incomplete data sets, leading to erroneous fuel consumption calculations. This can be mitigated in future efforts by performing a number of additional drive cycles while making hardware improvements to the ScanTool.

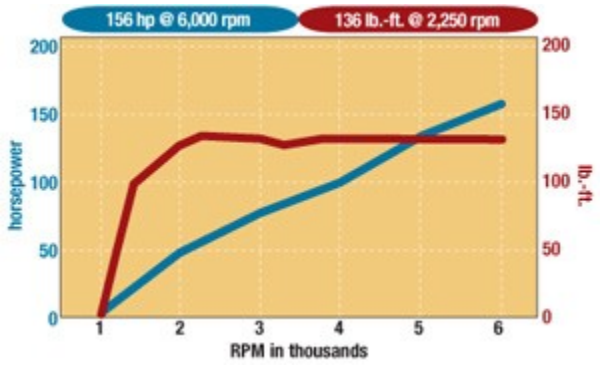

Figure 11: Fusion optimum performance power and torque curve [67].

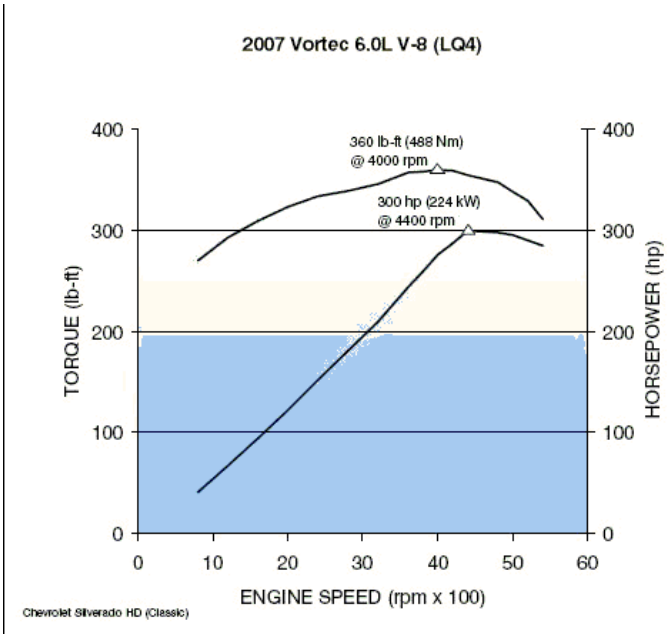

Figure 12: Silverado Hybrid optimum performance power and torque curve [68].

In the case when the HV battery SOC is below 60%, the model assumes the required brake power as coming from the ICE, following the algorithms listed in the conventional vehicle analysis. Furthermore, when the required power is higher than is available from the ICE, the remaining power required by the motors is calculated:

$$P_{motor} = P_b - P_{ICE,max} \quad (42)$$

where $P_{ICE,max}$ is the maximum output ICE power. The motors provide the remaining power according to the LEAF algorithm, utilizing the nominal voltage due to a lack of information on the specific battery packs used by the three vehicles. Proposed future work includes implementing similar battery chemistry discharge curves optimized by a dimensionless efficiency in order to improve this estimate.

Finally, the models calculate the regenerative braking schemes for these vehicles according to Equations 27 through 29, assuming the same 30% power capture efficiency due to a lack of information and efficiency maps in the literature.

3.6: Ford Transit Connect EV Power Draw Algorithm

The Ford Transit EV model applies a relatively simple algorithm, similar to the BEV procedures of the Fusion Hybrid, Silverado Hybrid, and the Toyota Prius. Specifically, Equation 7 in Chapter 3 of this thesis determines the power required of the vehicle. Moreover, the model calculates the power required of the HV battery pack as a function of the motor efficiency (assumed equal to 85%) according to Equation 37. Once again, calculation of the current draw implements the HV battery pack nominal voltage assumption according to Equation 29. The model finds the C-rating and charge removed according to Equations 24 and 25, respectively. Finally, the regenerative braking scheme is similar to that of the previous electrified vehicles, utilizing the same

30% power capture efficiency. The author optimized this model using the overall electric powertrain efficiency when calculating the charge removed at each time step, resulting in a final EV correction ($\eta_{EV,correct}$) efficiency of 70%.

The inclusion in future work of a motor efficiency map lookup table would increase the accuracy of the motor efficiency. However, inadequate data in the literature prevents its incorporation at this time. Furthermore, the introduction of a discharge curve lookup table similar to that of the LEAF in future work would improve this calculation, and subsequently the C-rating and charge removed calculations.

3.7: Total Fuel Use and Emissions Analysis

The final step in calculating the electricity and liquid fuel usage involves computing the fuel use at each time step followed by a subsequent calculation of the cumulative total. In the case of liquid fuel, each of the power use algorithms described in Sections 3.2 through 3.6 results in a fuel flow rate in units of [g/s]. Thus, the model calculates the instantaneous liquid fuel used, $m_{fuel,i}$ [g]:

$$m_{fuel,i} = \dot{m}_{fuel} * dt \tag{43}$$

where dt is the length of the current time step. Likewise, the mode figures the amount of electricity used in each time step, E_i [kWh]:

$$E_i = \frac{CR_i * Vdc_i}{1000 * 3600} \tag{44}$$

Utilizing each of these fuel and electricity amounts, the model sums the total amounts of energy used as follows:

$$m_{fuel,tot,i} = m_{fuel,tot,i-1} + m_{fuel,i} \tag{45}$$

$$E_{tot,i} = E_{tot,i-1} + E_i \quad (46)$$

Instantaneous and cumulative emission determination incorporates the liquid fuel and electricity used along with the emission factors developed in GREET as described in Section 2.2. In the case of liquid fuel, the model employs two sets of emissions, representing WtP and PtW. For electricity, there are no PtW emissions since the use of electricity does not produce any tailpipe emissions. The model first finds the instantaneous liquid fuel use emissions produced in the WtP processes, and the PtW processes:

$$m_{emission,WtP,i} = f_{emission,WtP} * m_{fuel,i} \quad (47)$$

$$m_{emission,PtW,i} = f_{emission,PtW} * m_{fuel,i} \quad (48)$$

where $m_{emission,WtP,i}$ is the WtP instantaneous emissions mass [g], and $f_{emission,WtP}$ is the fuel emission factor for the WtP processes [g/g_{fuel}]. Likewise, $m_{emission,PtW,i}$ is the PtW instantaneous emission mass [g], and $f_{emission,PtW}$ is the fuel emission factor for the PtW fuel burn [g/g_{fuel}]. Subsequently, the model determines the cumulative total emissions ($m_{em,tot,WtP,i}$ and $m_{em,tot,PtW,i}$) for each process [g]:

$$m_{em,tot,WtP,i} = m_{em,tot,WtP,i-1} + m_{emission,WtP,i} \quad (49)$$

$$m_{em,tot,PtW,i} = m_{em,tot,PtW,i-1} + m_{emission,PtW,i} \quad (50)$$

Likewise, the instantaneous emissions ($m_{em,elec,i}$ [g]) and cumulative emissions ($m_{em,elec,tot,i}$ [g]) are a function of electricity production at each time step:

$$m_{em,elec,i} = f_{em,elec} * E_i \quad (51)$$

$$m_{em,elec,tot,i} = m_{em,elec,tot,i-1} + m_{em,elec,i} \quad (52)$$

Finally, development of emission profiles in units of grams of emissions per mile driven is of use to consumers and for a fleet report. Thus, the model evaluates the individual emission rates for liquid fuel WtP, PtW, and WtW use, as well as for electricity use:

$$EM = \frac{m_{em,tot}}{d_{tot}} \quad (53)$$

where EM is the emission rate in units of grams per mile driven [g/mile], $m_{em,tot}$ is the cumulative total emissions produced throughout the drive cycle [g], and d_{tot} is the length of the drive cycle [miles].

3.8: Additional Useful Metrics

The model calculates a number of other useful metrics in order to compare the vehicles against one another in addition to the emissions profiles. These include the vehicle fuel economy in miles per gallon, the miles per gallon equivalent for electrified vehicles ($MPGe$), and the cost of driving the vehicles based on the fuel used, both as a cumulative total, and on a per-mile basis.

The simplest of these metrics is the miles per gallon (MPG) fuel economy:

$$MPG = \frac{d_{tot} * \rho_{fuel}}{m_{fuel,tot,i}} \quad (54)$$

The EV-equivalent metric is the mile-per-gallon equivalent developed by the EPA, which incorporates a value for energy available in one gallon of gasoline. In particular, the EPA documents that one gallon of gasoline is equivalent to 33.7 kWh of electricity [69]. Thus, the model evaluates a volumetric equivalent for the electricity used (v [gal]):

$$v = \frac{E_{tot}}{33.7} \tag{55}$$

where 33.7 is this gasoline-electricity equivalency [kWh/gal]. The model uses this volumetric equivalent (in gallons) in order to find the MPGe of the EV at hand [miles/gal$_{eq}$]:

$$MPGe = \frac{d_{tot}}{\frac{m_{fuel,tot,i}}{\rho_{fuel}} + v} \tag{56}$$

Finally, the US Department of Energy's Clean Cities Alternative Fuel Price Report provides the cost of liquid fuel used presented in Table 11, whether it is gasoline, diesel, or E85 (in the case of the Chevrolet Impala and the 1/2-Ton Chevrolet Silverado) [70].

Table 11: The cost of liquid fuel per gallon as reported by the DoE's Clean Cities Alternative Fuel Price Report [70].

Fuel Type	Fuel Cost [$/gal]
Gasoline	3.86
ULSD	4.06
E85	3.45

Thus, the model calculates the total cost and the cost per mile driven:

$$C_{tot} = \frac{d_{tot} * C_f}{MPG} \tag{57}$$

$$C_{mile} = \frac{C_{tot}}{d_{tot}} \tag{58}$$

where C_{tot} is the total cost [$], C_f is the fuel cost factor [$/gal], and C_{mile} is the cost per mile [$/mi] driven. In the case of electricity use, total and per-mile cost are a function of the electric energy use:

$$C_{tot,elec} = E_{tot} C_{f,elec} \tag{59}$$

$$C_{mile,elec} = \frac{C_{tot,elec}}{d_{tot}} \tag{60}$$

where $C_{tot,elec}$ is the total electricity cost [$], $C_{f,elec}$ is the electricity cost per kWh [$/kWh], and $C_{mile,elec}$ is the cost per mile driven [$/mi]. This work utilizes the electricity cost factors from the US Energy Information Administration's data for the average electricity cost for NE Kansas as of August, 2012: $0.0955 per kWh [71].

3.9: Optimization Routine

Each of the described models inherently suffers some error for various reasons. For this reason, this work implements an optimization routine based in Matlab, entitled "FMINCON", which seeks a constrained minimum of a user-created function. This work implements a root-mean-squared (RMS) difference between two parameters. For example, optimization of the $bsfc$ map for the 2011 Chevrolet Impala begins with an initial guess, estimated by the *Cycles* program, and normalized to a number between 0 and ten in order to apply equal importance to each value (7.46, 4.21, and 5.7591 for a, b, and c in equation 17, respectively). The user sets an allowed range for each variable optimized, and given the accuracy of the initial guess, the routine allows for a smaller range. The given ranges for the Impala are 5 - 8, 3 - 8, and 3 - 8 for a, b, and c, respectively. Next, the user sets the tolerance level on the variables and RMS results (10^{-5} in this case). Finally, the optimization routine determines the results of the model

a number of times (the maximum number set to 10^6 in this case), seeking the best-fit curve based on slightly altering the optimized variables, seeking to reduce this RMS factor. The routine finishes when it finds the best values for all of the given variables, returning the final values. In the case of the 2011 Chevrolet Impala, the parameters utilized in the RMS function are the model-calculated and the recorded cumulative fuel use throughout the given drive cycle. The optimized results are 5.67412, 7.78329, and 5.99133, respectively. Figure 13 shows the initial and final results of this optimization for the Impala.

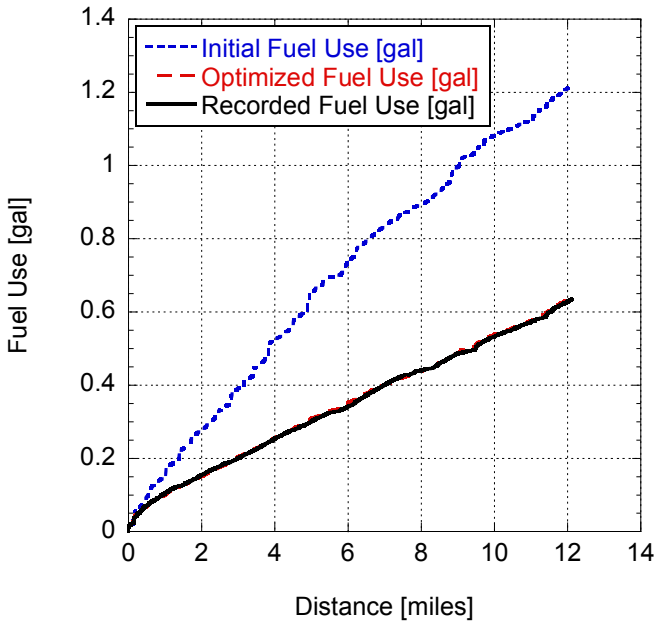

Figure 13: Initial and optimized cumulative fuel use compared the drive cycle recorded fuel use.

This work implements similar routines for the EV models, typically based on either the continuous battery SOC (LEAF), or the final fuel economy (parallel hybrids). In the case of the Chevrolet Volt, the work employed a dual optimization, first on the continuous SOC, then on the cumulative fuel consumption. The use of these

optimization routines act to drastically reduce error in the algorithm and parameter assumptions, such as the thermal efficiency of conventional vehicles, and the EV powertrain efficiencies, giving the most accurate results based on the recorded drive cycles.

4.0: Results and Fleet Analysis

An Excel spreadsheet organizes the results into four main worksheets, titled "Baseline Vehicles (WtW)," "New Vehicle Fleet (WtW)," "Differences," and "Cost Analysis." Each of these worksheets provides useful data separated into tables found through the models described and an analysis based on fleet-reported statistics, including average yearly miles traveled, the total number of vehicles, and average yearly fuel use (a number of statistics are omitted here for confidentiality purposes). The following sections describe each of these worksheets in detail.

4.1: Baseline Vehicles (WtW)

The baseline vehicles worksheet contains information on the Chevrolet Impala, the 1/2- and 3/4-ton Silverados, the Chevrolet Uplander, and nearly 400 diesel line trucks (which includes 396 Class 2, 3, and 4 diesel powered line trucks, bucket trucks, diggers/derricks, among other specialty line trucks). A computer model has not been developed for the line trucks due to a lack of data logging capabilities, but can be included in future work.

Three main tables divide this worksheet, each separated into three segments corresponding to the WtW, WtP, and PtW analyses. Table 12 provides a basic parameter table depicting the vehicle name, model years, fuel type, number of vehicles in the fleet, average yearly fuel consumption, and average yearly miles driven. The

second table, indicated here as Table 13, included in the Baseline Vehicles worksheet includes information on the fuel economy (MPG), fuel type, and per-mile emissions profiles for the various fuels and fuel economies.

Table 12: Basic parameters for baseline vehicles

Vehicle Type	Model Year(s)	Total Fuel Used	Fuel Type	Yearly Miles Traveled	Number of Vehicles
Chevrolet Impala	2007 - 2011	807	Unleaded / E85	21000	40
Chevrolet Silverado 1/2-Ton	2004 - 2011	1226	Unleaded / E85	18400	270
Chevrolet Silverado 3/4-Ton	2005 - 2011	2041	Unleaded	24500	100
Chevrolet Uplander	2011	1486	Unleaded	27500	60
Line Truck	2003 - 2012	2166	Diesel	13000	396

Table 13: WtW emissions profiles of the four conventional vehicles.

			Emissions [g/mile]									
Vehicle	**MPG**	**Fuel**	**VOC**	**CO**	**NO_x**	**PM_{10}**	**$PM_{2.5}$**	**SO_x**	**CH_4**	**N_2O**	**CO_2**	**GHG**
Chevy Impala	26.02	CG	0.258	3.990	0.363	0.039	0.023	0.119	0.601	0.011	430	448
	19.01	CG	0.353	5.462	0.497	0.054	0.032	0.162	0.823	0.015	588	613
	19.23	E85	0.347	3.681	0.663	0.228	0.087	0.284	1.158	0.143	706	777
	14.05	E85	0.474	5.039	0.908	0.312	0.120	0.388	1.585	0.195	966	1064
Chevrolet Silverado 1/2-Ton	15.01	CG	0.434	7.140	0.828	0.071	0.043	0.206	1.058	0.023	745	778
	18.71	CG	0.348	5.728	0.664	0.057	0.035	0.165	0.849	0.018	598	624
	11.48	E85	0.581	6.170	1.112	0.383	0.146	0.475	1.941	0.239	1183	1303
	14.31	E85	0.466	4.949	0.892	0.307	0.117	0.381	1.557	0.192	949	1045
Chevrolet Silverado 3/4-Ton	12.00	CG	0.543	8.927	1.035	0.089	0.054	0.257	1.323	0.029	931	973
	10.49	CG	0.621	10.22	1.185	0.102	0.062	0.294	1.514	0.033	1066	1113
Chevrolet Uplander	18.51	CG	0.352	5.791	0.672	0.058	0.035	0.167	0.858	0.019	604	631
	15.81	CG	0.412	6.777	0.786	0.068	0.041	0.195	1.004	0.022	707	739
Line Truck	6.99	ULSD	0.537	1.447	1.712	0.167	0.107	0.453	2.386	0.040	1608	1679

One should note the different values for the fuel economy for each of the vehicles in Table 13. The first row contains the emissions profile based on the fuel economy calculated from the fleet-reported distance and fuel use data, while the second entry corresponds to the model-calculated fuel economy. Both are included in order to provide perspective into the differences between the drive cycle driven and logged and the typical driving style utilized by each of the vehicles. For example, the Chevrolet Impala boasts a significantly higher fuel economy based on the fleet-reported data. This is likely due to a higher amount of highway driving, leading to a better overall fuel

economy for this vehicle. This trend also corresponds to the fuel economy differences of the Chevrolet Uplander and the Chevrolet Silverado 3/4-Ton.Conversely, the lower fuel economy of the Chevrolet Silverado 1/2-Ton is likely due to extended idling times experienced by these vehicles. Both of the fuel economies and their respective emissions profiles are within reason, as studied by the DoE-stated range of fuel economies [66].

Furthermore, Table 13 provides the fuel economy for E85-fueled vehicles based on the flex fuel economy as stated by the US DoE (17 and 13 for the Impala and Silverado, respectively).The absence of drive cycles fueled by E85 prohibited the modeling of this fuel, although it is still of interest. The analysis implements a ratio of the fuel economies (E85 to Conventional Gasoline), finding the final fuel economy using E85:

$$MPG_{E85} = \frac{MPG * MPG_{DoE,E85}}{MPG_{DoE,CG}} \tag{61}$$

Thus, utilizing the emissions factors for E85, the analysis determines the emissions profiles as a function of the E85 emission factor ($f_{emission,E85}$ [g/gfuel]) and the density of E85 (ρ_{E85} [g/gal]):

$$m_{em,E85} = \frac{f_{emission,E85} * \rho_{E85}}{MPG_{E85}} \tag{62}$$

Finally, the third table included in this worksheet includes the total yearly emissions (Table 14) and fuel costs (Table 15). This is a simple evaluation based on the total yearly miles driven by the fleet and the number of vehicles in the fleet:

$$m_{em,year} = m_{em,mile}\, d_{year}\, N \tag{63}$$

where $m_{em,year}$ is the total emissions produced per year [g], $m_{em,mile}$ is the mass of emissions produced per mile [g/mile], d_{year} is the number of miles driven per year [miles], and N is the number of vehicles in the fleet [-]. Similarly, the analysis calculates the total fuel cost of driving this vehicle per year:

$$C_{year} = C_{mile}\, d_{year}\, N \tag{64}$$

where C_{mile} is the fuel cost of driving the vehicle per mile [$/mile], and C_{year} is the fuel cost of driving the vehicle per year [$/year].

Table 14: Yearly WtW emissions of the Baseline Vehicle Fleet.

	Yearly Emissions [kg]									
Vehicle	**VOC**	**CO**	**NO_x**	**PM_{10}**	**$PM_{2.5}$**	**SO_x**	**CH_4**	**N_2O**	**CO_2**	**GHG**
Chevy Impala	217	3352	305	33	19	100	505	9	3.61E+05	3.76E+05
	297	4588	417	45	27	136	691	12	4.94E+05	5.15E+05
	291	3092	557	192	73	238	973	120	5.93E+05	6.53E+05
	398	4233	763	262	100	326	1332	164	8.12E+05	8.94E+05
Chevrolet Silverado 1/2-Ton	2156	35472	4114	354	214	1022	5257	114	3.70E+06	3.87E+06
	1730	28454	3300	284	172	820	4217	91	2.97E+06	3.10E+06
	2886	30652	5522	1901	727	2362	9645	1188	5.88E+06	6.47E+06
	2315	24588	4430	1525	583	1895	7737	953	4.72E+06	5.19E+06
Chevrolet Silverado 3/4-Ton	1329	21871	2536	218	132	630	3241	70	2.28E+06	2.38E+06
	1521	25028	2903	250	151	721	3709	80	2.61E+06	2.73E+06
Chevrolet Uplander	581	9554	1108	95	58	275	1416	31	9.97E+05	1.04E+06
	680	11182	1297	112	67	322	1657	36	1.17E+06	1.22E+06
Line Truck [x10^3]	2766	7449	8811	856	550	2332	12283	205	8.28E+06	8.65E+06

Table 15: Annual driving fuel cost.

Vehicle	Liquid Fuel Cost [$]	Driving Cost [$/mile]
Chevy Impala	124600.80	0.148
	170538.64	0.203
	150667.06	0.179
	206215.01	0.245
Chevrolet Silverado 1/2-Ton	1277737.20	0.257
	1024957.32	0.206
	1493418.25	0.301
	1197969.32	0.241
Chevrolet Silverado 3/4-Ton	787826.00	0.322
	901525.26	0.368
Chevrolet Uplander	344157.60	0.209
	402789.23	0.244
Line Truck	3975990.48	0.581

4.2: New Vehicle Fleet (WtW)

The New Vehicle Fleet worksheet is similar to the Baseline Vehicle sheet in its layout and included statistics, with the absence of known fuel amounts due to a more recent inclusion of these electrified vehicles in the fleet. Table 16 shows the first table in this worksheet, which includes the vehicle, the model year, the vehicle it is replacing, the number of vehicles in the fleet, and the total yearly miles traveled. The second table containing information on the fuel economy and per-mile emissions profile (Table 17) is slightly different from the Baseline Vehicle counterpart, as this table includes the

influence of electric vehicle charging, changing the emissions profile, in some cases, quite significantly.

Table 16: Yearly driving specifications of the New Vehicle Fleet.

Vehicle Type	Model Year	Baseline Vehicle Replaced	Driving Fuel Type	Miles Traveled	# Vehicles In Fleet
Chevy Volt	2011	2006 Impala	CG/Electricity	21000	4
Nissan Leaf	2011	2006 Impala	Electricity	21000	4
Toyota Prius	2008	2003 Impala	CG	21000	9
Ford Fusion Hybrid	2012	2006 Impala	CG	21000	6
Silverado Hybrid	2011	2004 Silverado 1/2 T	CG	18400	6
Ford Transit EV	2011	2004 Astro Van	Electricity	27500	4

Table 17: Per-mile emissions profile and fuel economy of the New Vehicle Fleet.

Vehicle	MPG	MPGe	Electric Medium	Emissions [g/mile]									
				VOC	CO	NOx	PM_{10}	$PM_{2.5}$	SO_x	CH_4	N_2O	CO_2	GHG
Chevy Volt	104.8	69.2	Wind	0.064	0.993	0.090	0.010	0.006	0.029	0.149	0.003	107	111
	104.8	69.2	Coal	0.091	1.308	0.453	0.573	0.154	0.752	0.607	0.006	443	460
	104.8	69.2	2010GMix	0.082	1.159	0.323	0.267	0.075	0.381	0.665	0.006	302	321
Nissan Leaf	N/A	125.8	Wind	0.000	0.000	0.000	0.000	0.000	0.000	0.000	0.000	0	0
	N/A	125.8	Coal	0.026	0.299	0.345	0.535	0.141	0.686	0.435	0.003	320	332
	N/A	125.8	2010GMix	0.017	0.158	0.221	0.244	0.066	0.334	0.490	0.003	186	199
Toyota Prius	46.0	46.0	N/A	0.146	2.257	0.205	0.022	0.013	0.067	0.340	0.006	243	253
Ford Fusion Hybrid	39.0	39.0	N/A	0.172	2.663	0.242	0.026	0.015	0.079	0.401	0.007	287	299
Silverado Hybrid	21.0	21.0	N/A	0.320	4.945	0.450	0.049	0.029	0.147	0.745	0.013	532	555
Ford Transit EV	N/A	66.1	Coal	0.049	0.570	0.656	1.018	0.268	1.307	0.828	0.006	609	632
	N/A	66.1	Wind	0.000	0.000	0.000	0.000	0.000	0.000	0.000	0.000	0	0
	N/A	66.1	2010GMix	0.032	0.301	0.421	0.465	0.126	0.635	0.932	0.005	354	379

One should note the high level of emissions from the electricity generation mix. In particular, the high levels of sulfur oxides and particulate matter are due to the large amount of coal-fired electricity used. Likewise, this accounts for the higher levels of CO, CO_2, and GHG in the generation mix. This trend illustrates the relatively low production levels of renewable energy in the US. Furthermore, this difference causes higher SO_x and PM emissions in the Nissan LEAF and Chevrolet Volt than in the Toyota Prius. This is due to a combination of the high levels of coal- and natural gas-fired electricity, combined with the fact that the Toyota Prius obtains a relatively high gasoline fuel economy. Finally, recent regulations on sulfur levels in gasoline further reduce these

SO_x emission levels. It is important to note that the latest regulations and technological improvements to coal- and oil-fired plants will lead to lowered WtW electricity emissions in the future. Section 4.3 describes how new technologies will influence the emissions profiles of electricity sources.

Similar to the Baseline Vehicle worksheet, the final table contains the yearly emissions and cost analysis. Table 18 contains the final emissions profiles based on electricity mix and fuel type, and Table 19 shows the cost analysis of these vehicles. For additional review, Appendix A5 contains the remaining tables depicting the WtP and PtW analyses for each of these vehicles.

Table 18: Yearly emissions profile of the New Vehicle Fleet

	Total Emissions									
	VOC	**CO**	**NO_x**	**PM_{10}**	**$PM_{2.5}$**	**SO_x**	**CH_4**	**N_2O**	**CO_2**	**GHG**
	[g]	[g]	[g]	[g]	[g]	[g]	[g]	[g]	[kg]	[kg]
Chevrolet Volt	5392	83401	7581	818	481	2474	12542	225	8976	9357
	7648	109865	38052	48103	12920	63165	51005	505	37254	38679
	6888	97356	27132	22428	6300	32004	55860	504	25397	26944
Nissan Leaf	0	0	0	0	0	0	0	0	0	0
	2144	25142	28949	44923	11817	57658	36541	267	26865	27858
	1394	13255	18581	20530	5536	28022	41118	235	15601	16699
Toyota Prius	27608	426642	38822	4191	2466	12681	64278	1150	45933	47882
Ford Fusion Hybrid	21709	335479	30527	3295	1939	9972	50544	905	36118	37651
Silverado Hybrid	35325	545895	49673	5362	3155	16226	82245	1472	58772	61266
Ford Transit EV	5345	62695	72187	112020	29468	143777	91119	665	66990	69466
	0	0	0	0	0	0	0	0	0	0
	3485	33055	46332	51194	13805	69872	102531	583	38904	41641

Table 19: Cost analysis of the New Vehicle Fleet worksheet.

	Liquid Fuel Cost [$]	Electricity Fuel Cost [$]	Driving Cost [$/mile]
Chevrolet Volt	3094.30	1225.67	0.051
Nissan Leaf	0.00	1988.78	0.024
Toyota Prius	15859.57	0.00	0.084
Ford Fusion Hybrid	12470.76	0.00	0.099
Silverado Hybrid	24227.54	0.00	0.219
Ford Transit EV	0.00	4959.22	0.045

4.3: Differences Worksheet

The third worksheet present in the fleet analysis workbook depicts an easy-to-read comparison of new vehicles versus their baseline counterparts. This sheet gives the emissions and cost savings of one year of driving each of the vehicles based on a user-entered number of vehicles and yearly miles traveled. The default values show the differences of one vehicle at the distance driven of the baseline vehicle in the comparison. For example, Tables 20 and 21 show the comparison between a Chevrolet Volt and the Chevrolet Impala based on one vehicle, driven 21000 miles in one year. One should note the high levels of PM, SO_x, and CH_4 emissions due to the high amount of coal-fired power plants (explaining the PM and SO_x increases) and the use of NG-fired power plants (explaining the CH_4 increase) in the 2010 US Electricity Generation Mix. However, there are drastic improvements in the VOC, CO, NO_x, N_2O, CO_2, and GHG emissions, as well as boasting an over $2000 decrease in fuel costs in just one year. The use of gasoline in the Chevrolet Volt also increases CH_4 levels;

however, due to the lack of gasoline in the LEAF and Transit EV, the CH_4 levels never overcome the rates by the Impala or the Uplander.

Table 20: Emissions comparison between a Chevrolet Volt and a Chevrolet Impala driven 21000 miles.

Vehicle	VOC	CO	NO_x	PM_{10}	$PM_{2.5}$	SO_x	CH_4	N_2O	CO_2	GHG
	[g]	[g]	[g]	[g]	[g]	[g]	[g]	[g]	[kg]	[kg]
Chevy Impala	5423	83798	7625	823	484	2491	12625	226	9022	9405
Chevy Volt	1722	24339	6783	5607	1575	8001	13965	126	6349	6736
DIFFERENCE	**3701**	**59459**	**842**	**(4784)**	**(1091)**	**(5510)**	**(1340)**	**100**	**2672**	**2669**

Table 21: Fuel cost comparison between a Chevrolet Volt and a Chevrolet Impala driven 21000 miles.

Vehicle	Driving Cost	Liquid Fuel Cost	Electricity Fuel Cost	Total Driving Cost
	[$/mile]	[$]	[$]	[$]
Chevy Impala	0.148	3115	0	3115
Chevy Volt	0.051	774	306	1080
DIFFERENCE	**0.097**	**2341**	**(306)**	**2035**

For more information, Appendix A6 contains tables for comparisons between the Nissan LEAF, Toyota Prius, Ford Fusion Hybrid, Chevrolet Silverado Hybrid, and Ford Transit EV and their baseline counterparts including the Chevrolet Impala, Chevrolet Silverado 1/2-Ton, Chevrolet Silverado 3/4-Ton, and the Chevrolet Uplander.

4.4: Potential Future Improvements to WtW Analysis

Regulations and improvements to current coal and natural gas extraction and use will lower future PM, SO_x, NO_x, and CH_4 emissions. In particular, a recent amendment by the EPA to the Clean Air Act in 2012 requires coal- and oil-fired electric utility steam generating units to meet more stringent hazardous air pollution standards [72]. Research into the technology needed to meet these standards results in low sulfur levels, particulate size, and ash levels, as shown by Steel and Patrick's study of the production of clean coal through chemical demineralization [73]. Furthermore, a study performed by Franco and Diaz describes a number of technologies utilized in reducing NO_x, SO_x, PM, and mercury levels through both pre- and post-combustion measures. For example, selective catalytic reduction post-combustion reduces NO_x levels by 75 to 85%, and chemical and biological cleaning can reduce sulfur levels prior to combustion by up to 90% [74]. Likewise, electrostatic precipitators, filters, and wet scrubbers reduce PM emissions by up to 99% [74].

A study by Tingley and Fernandez of the EPA outlines a number of technologies implemented in reducing methane emissions from natural gas systems. These technologies result in system improvements for two reasons: directly reducing emissions and attaining higher extraction efficiency due to lowered losses [75]. For example, low-bleed pneumatics, flash tank separators, and vapor recovery units (among others) reduced yearly emissions by 31 million tons of CO_2-equivalent in the production process alone. Furthermore, improvements in the processing, transmission, and distribution of natural gas resulted in an emissions reduction of over 94 million tons

of CO_2-equivalent Nation-wide between yearly emissions measured in 1995 and 2000 [75].

Finally, research is taking significant steps towards improving the sustainability of nuclear electricity production through technologies such as breeder reactors and thorium use as a fertile fuel, capable of breeding the fissile uranium-233 [76, 77]. The widespread use of these types of technologies and many others will result in a far lower electricity emissions profile than is currently calculated by GREET. Thus, future emissions levels will reduce these differences in favor of EVs.

Another important item is the reduction in maintenance costs and PM emissions as the use of regenerative braking reduces wear on brake pads and rotors. This reduction in maintenance costs is even more drastic when considering the Nissan LEAF and the Ford Transit EV, as these vehicles do not require maintaining oil or replacing coolant as often as they do not utilize an internal combustion engine.

4.5: Cost Comparison Worksheet

The final worksheet of the fleet analysis compares the overall costs of all of the baseline vehicles and electrified vehicles. Of particular importance are two metrics: calculating the break-even point of the two vehicles based on the principal cost and fuel costs per year, evaluated in years and in miles required to overcome the difference. The analysis finds the break-even point in years ($t_{break\text{-}even}$ [years]) as a function of the principle cost ($C_{p1,2}$ [$]), the cost of driving per mile ($C_{mile\ 1,2}$ [$/mile]), and the distance driven per year in miles (d_{year} [miles]):

$$t_{break\ -even} = \frac{C_{P1} - C_{P2}}{\left(C_{mile\ ,1} - C_{mile\ ,2}\right) d_{year}} \tag{65}$$

Likewise, the break-even point in miles ($d_{break\text{-}even}$[miles]) is a function of the principle cost (C_P[$]), and the cost of driving per mile ($C_{mile1,2}$ [$/mile]):

$$d_{break\ -even} = \frac{C_{P1} - C_{P2}}{\left(C_{mile\ ,1} - C_{mile\ ,2}\right)} \tag{66}$$

The worksheet displays this comparison visually via a linear graph as a function of years and miles. Figure 14 shows the comparison of a Chevrolet Impala with a principle cost of $25,760, the Nissan LEAF with a principle cost of $35,200, and the Chevrolet Volt with a principle cost of $31,465, each driven 21,000 miles per year. The figures show a break-even point of 3.63 years at 76,129 miles. One must note the added difference between the maintenance costs, not calculated in this analysis. The Nissan LEAF will have much lower maintenance costs due to the lack of an ICE, thus not requiring engine oil or engine coolant, as well as the reduced need for replacing brake pads and rotors due to the utilization of regenerative braking.

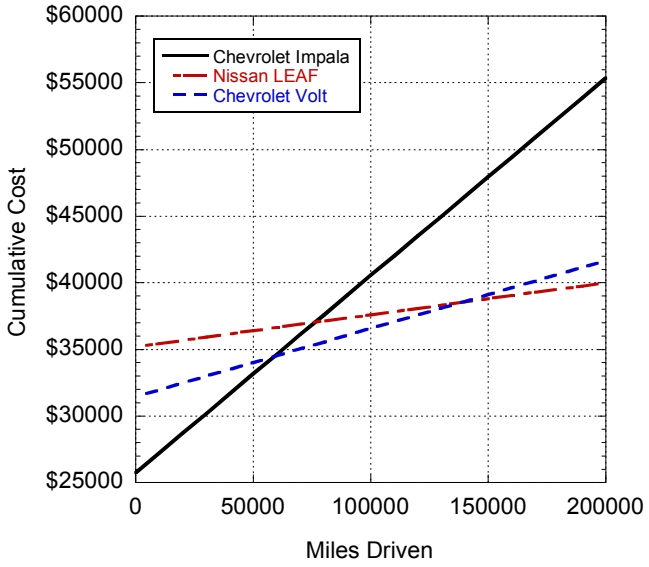

Figure 14: Cost Comparison of the Impala, LEAF, and Volt as a function of miles driven.

5.0: Conclusion

This chapter describes the methodology behind performing a WtW fuel, emissions, and cost analysis based on ten vehicle dynamics models formulated from Newton's Second Law of Motion. The vehicles modeled include the 2011 Chevrolet Impala, 2005 Chevrolet Silverado 1/2-Ton, 2009 Chevrolet Silverado 3/4-Ton, 2011 Chevrolet Uplander, 2011 Chevrolet Volt, 2011 Nissan LEAF, 2008 Toyota Prius, 2012 Ford Fusion Hybrid, 2011 Chevrolet Silverado Hybrid, and 2011 Ford Transit EV. These models allow for vehicular studies based on the different driving cycles of a particular individual, company fleet, or government entity. Furthermore, the models provide a detailed analysis of the vehicles studied, calculating the fuel economy and emissions resulting from dissimilar driving scenarios.

The fleet analysis performed in this study shows the effects of replacing conventional ICE vehicles with electrified counterparts. In particular, it describes the effects of utilizing coal-fired power plants as the primary electricity fuel source, and the subsequent increases in PM and SO_x emissions. Furthermore, this study shows the effects on fuel costs due to the high efficiency of the new electrified vehicles and the consumption of electricity, which is far less expensive than petrol fuels. For example, the replacement of one Chevrolet Impala by a Nissan LEAF driven for 21000 miles in one year results in a reduction of CO_2 of just over 5 metric tons, as well as a cost savings of $2618. However, due to the high level of coal-fired electricity use in the US, PM_{10} increases by over 4.6 kg, $PM_{2.5}$ increases by just under 1 kg, and SO_x emissions increase by over 4.9 kg. These trends are similar to that of the Ford Transit EV, although the lower fuel economy of the Transit versus the LEAF reduces the overall

savings. However, technological advancements towards reducing PM, SO_x, NO_x, and CH_4 emissions from coal- and natural-gas fired electric utility plants will decrease the harmful emissions profile of electricity. This will cause subsequent updates to MOVES and GREET.

The study includes a full WtP, PtW, and WtW calculation of the emissions produced at each step of fuel production and consumption. This analysis shows the effects of the US Electricity Generation mix on the subsequent emissions of BEVs, commonly considered zero emissions vehicles. This further supports the idea that it is important to investigate the entire fuel cycle as opposed to simply fuel usage at the vehicle. A vast majority of emissions from liquid fuel involve the combustion of the fuel in the vehicle, while all of the emissions from electricity come from the production of the fuel.

Moreover, the study shows the effects of extended idling on fuel consumption and vehicle fuel economy, as shown by the Chevrolet Silverado 1/2-Ton. The Silverado boasts a fuel efficiency of 18.7 mpg corresponding to the drive cycle performed and logged for the purposes of this study. However, when considering the total average fuel consumption and miles traveled by the Silverado fleet, the fuel economy lowers to 15 mpg. This is largely due to idling while the work trucks are stopped while on the job.

Finally, the fleet analysis boasts two simple-to-use consumer metrics, including an emissions and cost comparison, which compares two vehicles against one another based on the number of miles driven and vehicles replaced. The second consumer metric shows a cost analysis, calculating the time and distance required in order for two

vehicles to attain an equal cumulative cost when considering the principle cost of the vehicles, the number of miles driven, and the cost of driving one mile.

6.0: Future Work

Considerations for future work include the implementation of improved data logging, an increase in drive cycles considered in model optimization, further improvement of the PtW analysis performed by MOVES, individual vehicle emissions measurements, the utilization of specific emissions results from power plants, improved model algorithms for the Toyota Prius and other parallel hybrids based on their individual control algorithms, and the inclusion of a materials Life Cycle Analysis similar to the efforts in Chapter 3 of this thesis.

Improving data logging requires the use of a different data logger than the AutoEnginuity ScanTool. This equipment was able to log fuel use; however, it had difficulty remaining connected for complete drive cycles. Moreover, it could not log the fuel use and the motor and engine speeds simultaneously. This information is useful for calculating the exact efficiencies at each time step based on the individual *bsfc* and motor efficiency maps. Furthermore, fuel use data was often inaccurate, producing erroneous data not useful to the model. Improved decoding of the vehicle communications CAN strings would improve this data logging, providing a broader knowledge base used in developing and optimizing the vehicle models.

The logging of more drive cycles with each vehicle will help accurately calculate the fuel use in a number of scenarios other than the one drive cycle performed by each of the vehicles. The data produced by the Chevrolet Impala model would be vastly improved with the addition of a heavily highway-driving based drive cycle, attaining a

fuel economy closer to the average suggested by the yearly fuel use and distance driven by these vehicles.

The author improved the PtW analysis performed by GREET using the EPA's MOVES. However, the analysis of diesel-powered cars and trucks produced erroneous data due to a lack of statistical data on these vehicles. Future developments in EPA's MOVES may improve these estimates. Furthermore, the calculation of the PtW fuel emissions improves with direct measurement of the individual vehicles' emissions profiles. This measurement would allow for the optimization of the fuel burn emissions profile based on the specific engine's emissions production, as well as the vehicle's aftertreatment system. Likewise, measurement of individual power plant emissions profiles improves the accuracy of electricity emissions profiles. Furthermore, the inclusion of new, more accurate profiles would more accurately depict the electricity emissions profiles.

Due to a lack of information available on the engine control algorithms of parallel hybrids, this study utilizes simplified algorithms based on broad assumptions. Further knowledge and research into the control algorithms used in the vehicles would result in increased accuracy, and thus, more accurate energy use and emissions profiles. However, much of this information is confidential, and thus a public model is not likely. In this area, more detailed control algorithms have been developed, such as in Arata et al.'s development of a simulation of the Toyota HEV powertrain [15] and can be reviewed for additional improvements.

Finally, the inclusion of a material LCA similar Chapter 3 of this thesis would lead to a better view of the total emissions when using of electrified vehicles. This involves

the consideration of building the HV battery pack, the use of lightweight, complex materials, the construction of the various powertrains and control systems, and the use of lubrication and coolant systems required in ICE versus electric motors.

7.0: References

1. Research and Innovative Technology Association., *Table 1-19: Sales of Hybrid Vehicles in the United States.* 2012.
2. Clean Air Trust, *Sulfur Dioxide.* 1999.
3. U.S. Environmental Protection Agency, *Nitrogen Dioxide (NO2).* 2012.
4. U.S. Environmental Protection Agency, *An Introduction to Indoor Air Quality (IAQ): Volatile Organic Compounds (VOCs).* 2012.
5. Ramanujan, K., *Methane's Impacts on Climate Change May Be Twice Previous Estimates.* 2005.
6. Wang, M., *Argonne National Lab's Greenhouse Gases, Regulated Emissions, and Energy Use in Transportation Model.* Center for Transportation Research, Energy Systems Division, Argonne National Laboratory, Iowa, 2011.
7. U.S. Energy Information Administration, *Figure 2.0: Primary Energy Consumption by Source and Sector, 2011.* 2011.
8. U.S. Department of Energy, *EPA Approves California's Zero Emissions Vehicle Program.* 2007.
9. Sullivan, J. and E. Cobas-Flores. *Full vehicle LCAs: a review*. 2001.
10. Hondo, H., *Life cycle GHG emission analysis of power generation systems: Japanese case.* Energy, 2005. **30**(11): pp. 2042-2056.
11. Hausmann, A., *Advances in Electric Drive Vehicle Modeling with Subsequent Experimentation and Analysis*, in *Department of Mechanical Engineering*2012, University of Kansas. p. 171.
12. Grathwaite, J., *Range Anxiety: Fact or Fiction?* 2011.
13. Hall, L.E., *Nissan Leaf.* 2012.
14. Voelcker, J., *Extended range electric Chevy Volt gets electric range extended to 38 miles.* 2012.
15. Arata, J., et al., *Backward-Looking Simulation of the Toyota Prius and General Motors Two-Mode Power-Split HEV Powertrains.* SAE Int. J. Engines, 2011. **4**(1): pp. 1281-1297.
16. Auterra. *DashDyno SPD*. 2012 10/22/2012]; Available from: http://www.auterraweb.com/dashdynoseries.html.
17. Garmin, *Garmin GPS 18x OEM.* 2012.
18. GPSVisualizer.com, *Find "Missing" Elevations with GPS Visualizer.* 2012.
19. DashDyno, A., *Gallery.* 2012.
20. Giddings, G., *Nissan LEAF CAN-do*, 2011, Gary Giddings: MyNissanLEAF.com.
21. GpsGate, F., *GpsGate Client*, 2011.
22. Software, E., *RS232 Data Logger*, 2012.
23. AutoEnginuity, L.L.C., *AutoEnginuity ScanTool.* 2011.
24. AutoEnginuity, L.L.C., *AutoEnginuity OBD-II Diagnostic ScanTool User Guide.* 2012.
25. Wang, M., Y. Wu, and A. Elgowainy, *Operating manual for GREET: Version 1.7.* Center for Transportation Research, Energy Systems Division, Argonne National Laboratory, Iowa, 2007: p. 119.
26. U.S. Energy Information Administration, *Monthly Energy Review: Primary Energy Consumption by Source.* 2012. **June 2012**.
27. U.S. Energy Information Administration, *Table 8.2a: Electricity Net Generation: Total (All Sectors), 1949-2011.* 2012.
28. Tunnel, A.W., *Appendix: Aerodynamic Forces.* 2012.
29. Xiaoling, H. and J.W. Hodgson, *Modeling and simulation for hybrid electric vehicles. I. Modeling.* Intelligent Transportation Systems, IEEE Transactions on, 2002. **3**(4): pp. 235-243.
30. Chevrolet, K.T., *Used Vehicle Brochures: Specifications.* 2011.
31. Tuthill, B., *Coefficient of Drag: Web Forum Entry.* 2007.

32. New-Cars.com, *2005 Chevy Silverado Specs.* 2009.
33. DecodeThis.com, *2009 Chevrolet Silverado 2500 HD Work Truck Extended Cab Long Box 4WD.* 2012.
34. Manufacturers, T., *2009 Chevrolet Silverado 2500HD Crew Cab Tech Specs.* 2009.
35. Edmunds.com, *2009 Chevrolet Silverado 2500HD Features & Specs.* 2012.
36. Edmunds.com, *2008 Chevrolet Uplander Features & Specs.* 2012.
37. Profess, *2007 Chevrolet Uplander Specifications.* 2012.
38. GM-Volt.com, *Chevy Volt Specs.* 2012.
39. Motor, F., *2012 Ford Fusion Hybrid Technical Specifications.* 2012.
40. Motors, G., *Battery Chemistries: An Introduction.* 2012.
41. Motors, G., *2012 Silverado Specs.* 2012.
42. Hall, L.E., *Chevrolet Silverado Hybrid.* 2012.
43. Motors, G., *Chevrolet Silverado Hybrid - 2012.* 2012.
44. Microsoft, *2008 Toyota Prius Specs & Features.* 2012.
45. Connection, T.C., *2008 Toyota Prius - Specifications.* 2012.
46. Meisel, J., *An Analytic Foundation for the Toyota Prius THS-II Powertrain with a Comparison to a Strong Parallel Hybrid-Electric Powertrain*, 2006, SAE International.
47. Muta, K., M. Yamazaki, and J. Tokieda, *Development of New-Generation Hybrid System THS II - Drastic Improvement of Power Performance and Fuel Economy*, 2004, SAE International.
48. Hernandez, E., *Nissan LEAF electric motor and transmission.* 2010.
49. LeafTalk UK, *LEAF - Technical Specs (EUR LHD).* 2010.
50. Dynamics, A., *Transit Connect Electric Specifications & Ordering Guide.* 2012.
51. Automobile-Catalog.com, *2012 Ford Transit Connect XLT Premium Wagon.* 2012.
52. PassionPerformance.cr, *2012 Nissan LEAF Technical Specs.* 2012.
53. Genta, G., *Motor vehicle dynamics: modeling and simulation*. Vol. 43. 1997: World Scientific Publishing Company Incorporated.
54. Kotwicki, A.J., *Dynamic models for torque converter equipped vehicles*1982: Society of Automotive Engineers.
55. Heywood, J.B., *Internal combustion engine fundamentals.* 1988.
56. Depcik, C., *Open-ended thermodynamic cycle simulation.* Unpublished master thesis, University of Michigan, Ann Arbor, 2000.
57. Sato, Y.; Ishikawa, S.; Okubo, T.; Abe, M.; Tamai, K.; *Development of High Response Motor and Inverter System for the Nissan LEAF Electric Vehicle*, 2011, SAE International.
58. Jones, R., *TechDig 2.0*, 1998.
59. AndyH. *My Nissan Leaf Discussion Forum*. [Discussion Forum] 2010 April 23, 2010 [cited 2012; Available from: http://www.mynissanleaf.com/viewtopic.php?p=50645.
60. Doerffel, D. and S.A. Sharkh, *A critical review of using the Peukert equation for determining the remaining capacity of lead-acid and lithium-ion batteries.* Journal of Power Sources, 2006. **155**(2): p. 395-400.
61. Peukert, W., *An equation for relating capacity to discharge rate, Electrotech.* Vol. Z, 1897. **18**: p. 287-288.
62. Cikanek, S.R. and K.E. Bailey. *Regenerative braking system for a hybrid electric vehicle*. in *American Control Conference, 2002. Proceedings of the 2002*. 2002.
63. Gao, Y., L. Chen, and M. Ehsani, *Investigation of the Effectiveness of Regenerative Braking for EV and HEV*, 1999, SAE International.
64. Miller, M.A.; Holmes, A.G.; Conlon, B.M.; Savagian, P.J.; *The GM "Voltec" 4ET50 Multi-Mode Electric Transaxle.* SAE Int. J. Engines, 2011. **4**(1): p. 1102-1114.

65. ontherun. *ecomodder.com BSFC Map Discussion Forum*. [Discussion Forum] 2011 10-13-2011 [cited 2012; Available from: http://ecomodder.com/forum/showthread.php/bsfc-chart-thread-post-em-if-you-got-1466-20.html.
66. U.S. Department of Energy. *www.fueleconomy.gov Find-A-Car*. 2012 [cited 2012; Available from: http://www.fueleconomy.gov/feg/findacar.shtml.
67. Witzenburg, G. *Ford 2.5L I-4 Hybrid: Unprecedented Efficiency, Refinement*. [News Article] 2010 June 25, 2010 [cited 2012 10-11-2012]; Available from: http://wardsauto.com/news-amp-analysis/ford-25l-i-4-hybrid-unprecedented-efficiency-refinement.
68. Ansell, B., *2007 Vortec 6.0L V8 (LQ4).* 2007.
69. EPA Office of Transportation and Air Quality (OTAQ), *Fact Sheet: New Fuel Economy and Environment Labels for a New Generation of Vehicles.* 2011.
70. U.S. Department of Energy, *Clean Cities Alternative Fuel Price Report*, 2012.
71. United States Energy Information Administration, *Table 6: Class of Ownership, Number of Consumers, Sales, Revenue, and Average Retail Price by State and Utility: Residential Sector, 2010.* 2011.
72. U. S. Environmental Protection Agency, *National Emission Standards for Hazardous Air Pollutant Emissions From Coal- and Oil-Fired Electric Utility Steam Generating Units and Standards of Performance for Fossil-Fuel-Fired Electric Utility, Industrial-Commerical-Institutional, and Small Industrial-Commercial-Institutional Steam Generating Units*, U. S. Environmental Protection Agency, Editor 2012: Federal Register Online.
73. Steel, K.M. and J.W. Patrick, *The production of ultra clean coal by chemical demineralisation.* Fuel, 2001. **80**(14): p. 2019-2023.
74. Franco, A. and A.R. Diaz, *The future challenges for "clean coal technologies": Joining efficiency increase and pollutant emission control.* Energy, 2009. **34**(3): p. 348-354.
75. Fernandez, K.A.T.a.R.L., *Methods for Reducing Methane Emissions from Natural Gas Systems.* 2000.
76. World Nuclear Association, *Thorium.* 2011.
77. Hoglund, B., *Thorium Nuclear Fuel Cycle.* 1997.

Small Scale Smart Grid Construction and Analysis

Bryan Strecker, Nicholas Surface, Jonathan Mattson, Chris Depcik

Department of Mechanical Engineering - University of Kansas, Lawrence, Kansas (United States)

Abstract

The current electrical grid cannot maintain the rising energy demand of the digital age without the construction of new power plants. In addition, this increasing need requires upgrading a large number of components within the aging energy infrastructure. Furthermore, with the advent and commercialization of electrified vehicles (EVs), energy demand has the capacity to climb dramatically. A sustainable solution via renewable energy technologies can act to offset this increased demand; however, transformers and meters across the country do not currently account for this option. As a result, a wholesale revision of the electrical grid into an intelligent communication pathway (energy and information) is required in order to ensure the energy security of the United States. Moreover, this system must integrate the onset of EV technology, allowing for two-way transfer of energy and information between the vehicle fleet and the grid.

To this end, the University of Kansas EcoHawks have constructed a scale smart grid integrating solar and wind energy, energy storage, EVs, and the current energy infrastructure demonstrating the capabilities of, and a proposed control method for, the system. Within this system, the grid has been broken into four main groups: energy sources, sinks, storage, and control, while keeping the focus on five defined E's of sustainability: energy, economics, environment, education, and ethics. Through the design of a small-scale grid, the technology in modeling a large-scale grid was explored in detail through a trial-and-error methodology at a reduced cost. *Words: 239.*

1.0: Background and Problem Definition

Designed with a singular purpose, the electrical grid currently used in the United States (US) is formed around the purpose to “keep the lights on”. It is a centrally planned and controlled system with relatively little flexibility to fluctuations in energy demand. As the nation and the economy become increasingly digital, energy demand is growing rapidly. For example, it is estimated that by 2015 around 60% of the total electrical load will be from chip technologies and automated manufacturing versus 10% of the total in the 1990s [1].

While the automotive industry is presently dependent on petroleum sources, the growing presence of Plug-in Hybrid Electric (PHEV) and Battery Electric Vehicles (BEV) will begin to act as a stress upon the electrical grid by drawing resources during times of peak energy demand. A study from Oak Ridge National Laboratory finds that charging vehicles during off-peak hours (after 10 pm) would result in only slight increases in total energy requirements, but charging after work could require around 160 new power plants [2]. Of importance, taking a sustainable approach towards these vehicles can act to lower greenhouse-gas emissions, improve urban air quality, save consumers money, bolster power-grid reliability and reduce oil imports [3]. Toward this objective, the University of Kansas EcoHawks senior design program focuses on investigating the linkage of the vehicle to the grid for improved efficiencies in both arenas. In the next few paragraphs, the background of the EcoHawks is given in order to provide the proper context as to how the authors came to construct a sustainable scale Smart Grid.

Upon starting the EcoHawks in Fall 2008, the faculty mentor (Christopher Depcik) met with interested students and outlined a sustainable architecture as the

approach to projects within the program. The students' definition of sustainability draws from others mentioned in the literature [4-6] and illustrates the application of engineering techniques to solving real-world problems by holistically approaching the situation from five vectors of success, the five E's of sustainability: energy, environment, education, economics and ethics. Each of these concepts individually addresses specific aspects of sustainability, shaped by the confluence of the ideals of people, planet, and prosperity. Moreover, it is through the application of the vectors of success that the students have developed the means to face the challenges of a sustainable approach to automobiles and its associated energy infrastructure.

The initial efforts of interested students began by recycling a 1974 Volkswagen Beetle into a fuel neutral series hybrid [7]. The modular nature of the students' design, as depicted in Figure 1, provides future students the flexibility to enhance efficiency by replacing the current diesel generator with a fuel cell, additional battery bank, or any power plant that provides the most sustainable solution. Moreover, sustainability is further evident by using 100% biodiesel fuel created from on campus dining services waste cooking oil. This fuel is created by a Biodiesel Initiative run through the Chemical and Petroleum Engineering Department at the University of Kansas, demonstrating interdisciplinary interaction. Furthermore, other departments, such as Environmental Engineering and Biology, are investigating other feedstock sources like rapeseed oil in this generator for improved efficiency and reduced emissions as shown in Figure 2. Note that Figure 2 depicts the brake-specific fuel consumption (bsfc) and nitrous oxide (NOx) emissions from a number of diesel feedstocks, including the conventional ultra-

low sulfur diesel (ULSD), as well as the renewable sources including used canola oil, rapeseed oil, olive oil, and palm oil.

Figure 1: 100% biodiesel generator integrated in a 1974 VW Super Beetle.

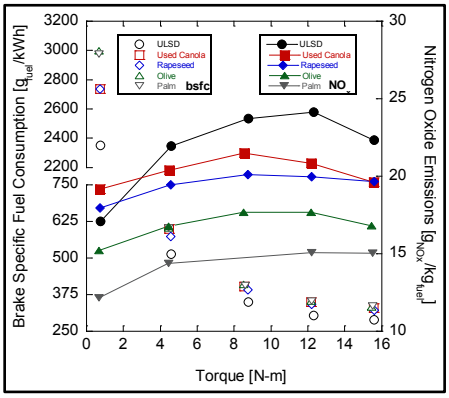

Figure 2: Generator results investigating unique oil feedstocks for efficiency and reduced emissions.

In the second year, the EcoHawks added plug-in charging capability to the Beetle along with building an expandable solar array, shown in Figure 3, powering a renewable energy filling station, highlighting their commitment to promoting sustainable energy. This transition of the Beetle to a PHEV design enables modeling and testing of grid integration, which will be one focus of this paper as described later. This occurs by storing energy from the sun in a battery bank that allows the Beetle, or any other electrified vehicle, to charge based on renewable resources at any time of day. Hence,

the EcoHawks' design laboratory acts as a storage medium for renewable sources when not immediately needed, demonstrating the future of sustainable energy management.

Figure 6: Solar array on the roof of the EcoHawks' design laboratory.

In the same year, the EcoHawks began providing the ability for students to test new concepts and explore novel technologies on the small-scale. This included teams of students fabricating unique 1/8th scale Remote Control (RC) vehicles utilizing hydrogen fuel cell and parallel hybrid architectures [6] while further investigating the theory behind renewable energy as evident through the student built solar panel in Figure 4. Using smaller components significantly reduces the cost of advanced designs while providing students the opportunity to explore theory, test the equipment and fail. Through information gathered in this effort, future successes have been realized (as Sitkin predicted [8]), and current endeavors save design time and research costs. For example, during this year, students utilize nickel cadmium, nickel metal hydride, lithium cobalt and lithium iron batteries in their RC cars in order to learn about advanced battery technologies. The lessons learned from this effort led directly to a current BEV construction (described later) and one of the battery storage mediums for renewable energy employed in this paper. Furthermore, efforts on the reduced scale allow a

common thread within the curriculum as interdisciplinary cooperation became more feasible due to reduced cost and a mobile design [9].

Figure 7: Student built solar panel used to explore solar technology.

As this information was learned, students actively published and presented their knowledge in order to enable others to take similar sustainable paths [10]. Moreover, university acknowledgement of the success of the program is illustrated through the University of Kansas Center for Sustainability Academic Project and Faculty Sustainability Leadership Awards, as well as Student Organization of the Year Award. In addition, students facilitated educational objectives at the K-12 level by actively searching for partner educators [11-13]. Targeted K-12 activities introduced young students to the theory and practice of building of electric vehicles and solar cells [14] with an emphasis on sustainable construction [15, 16]. Encouraging and developing exploration of sustainability, as early as elementary school, provides students the necessary foundation to become well-rounded scientists.

Current efforts on the vehicular side involve recycling a 1997 GMC Jimmy into a modern BEV for the University of Kansas Libraries in their use on campus for daily delivery of materials. Since the library system's driving cycle is repeatable, moderate in length (30 miles), and package weight decreases along with the State of Charge (SOC),

this provides a perfectly targeted application for advanced vehicle technologies demonstrating a sustainable solution. Increasing the battery sophistication to $LiFeYPO_4$ chemistry (beyond the lead-acid battery technology of the Beetle using the knowledge learned through the RC car approach) provides a larger capacity for vehicle use as a storage medium of energy from renewable sources. Hence, not only does the EcoHawks' design laboratory provide energy storage, the vehicle will act as a source of energy for the grid reducing its potential issue as a stress on the energy infrastructure.

At this point, there were many individual projects underway; however, there was not one system acting to tie the various projects together. In keeping with the spirit of the EcoHawks program, it was decided that any control system would have to integrate all of the existing elements while providing for the capability of adding further projects. This system would ideally be able to monitor the flow of energy throughout and between the EcoHawks' component projects, such as between roof-mounted solar panels and the Beetle, while calculating the efficiencies of this energy transfer. The solution was the implementation of a Smart Grid system.

To this end, the EcoHawks applied for and received an EPA grant (P^3: People, Prosperity and the Planet [17]) to build a stand-alone model of a scale Smart Grid, schematically shown via Figure 5, in order to demonstrate both the laboratory and vehicle as methodologies to enhance renewable energy usage in a sustainable manner. This final design, shown in Figure 6, was then taken to an EPA competition on the National Mall in Washington, D.C. in order to compete against other universities for additional funding. In the following sections, this model Smart Grid architecture is described along with future efforts to implement it on the large scale.

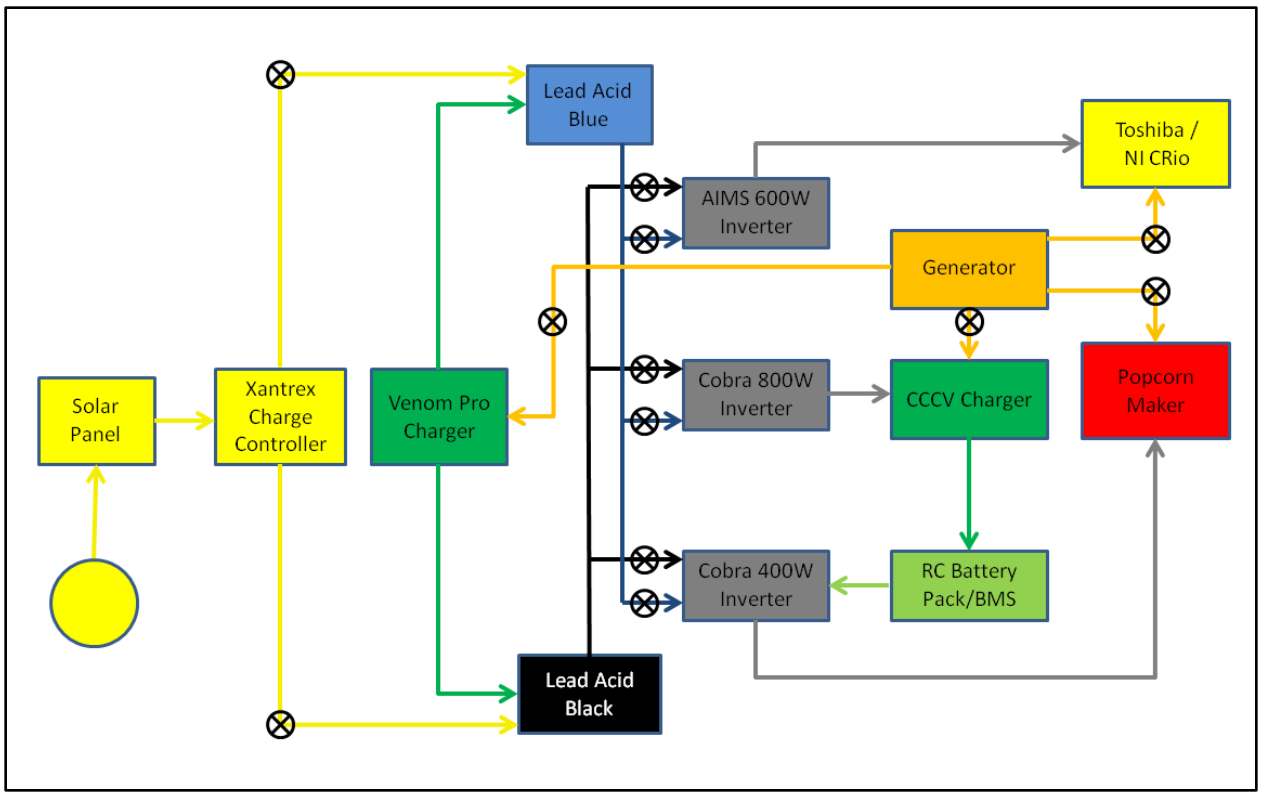

Figure 8: Energy flow diagram of scale Smart Grid model.

Figure 6: Final Smart Grid design.

2.0: Purpose, Objectives, Scope

A Smart Grid is a new approach to the field of energy infrastructure. It allows for a safer and more secure energy grid, and it has the capability to be more efficient, economical, and environmentally friendly than the current energy grid system used in the US. As a new technology, the definition of a Smart Grid has not been universally agreed upon, leading to various competing definitions. For some, it involves installing smart meters in homes; for others, it requires integrating decentralized energy sources into the grid. The European Regulators' Group for Electricity and Gas uses the following definition [18]:

"Smart Grid is an electricity network that can cost efficiently integrate the behavior and actions of all users connected to it – generators, consumers and those that do both – in order to ensure an economically efficient, sustainable power system with low losses and high levels of quality and security of supply and safety".

While the above definition provided a suitable basis for the project, the authors additionally investigated the definition provided by the US Department of Energy (DoE), which has a slightly differing vision of a Smart Grid, involving the [19]:

- Decentralization of energy production and storage, and
- Two-way communication from end users or appliances and the energy network.

Decentralizing energy production occurs by incorporating renewable energy as distributed generation via home or local solar panels, wind turbines, and other forms. Furthermore, part-time use of PHEV and BEV battery packs as storage banks coupled with renewable generation, and conversion into other usable forms, facilitates decentralized storage.

Interactive customer involvement provides an additional energy resource. Consumers will have the capability to match their demand for electricity with the system's ability to meet those requirements. For example, a person may choose to consume energy overnight when energy demand and price is lower by charging their vehicle and selling that energy back for a profit during peak-hours when energy demand and price is high. As the study by Oak Ridge elucidates, no new power plants would be required while fostering efficiency through maintaining current power plant load without cycling reactors and grounding unneeded energy [2].

The current iteration of the scale Smart Grid built by the authors (as described in the next section) moves energy efficiently based on sources and sinks, decentralizing energy production and storage through a switchboard. A student-constructed National Instruments (NI) system monitors information on available energy, production rates, and usage rates. This control system and information measured by the NI setup links energy customers to producers creating new electricity markets in bidding, selling, and using electricity. On-demand information about power quality is vital to mitigate business losses in the digital economy; for example, $100 billion is lost each year due to slow response to power outages [20]. Active monitoring and automated control of energy sources will predict outages before they occur and speed recovery from unexpected disturbances by rerouting electricity and notifying human responders instantly. Furthermore, this leads to identification of improvements for inefficiencies and previously unknown power losses. The greater volume and quality of information available from the Smart Grid will lead to enhancements in maintenance, asset utilization, and efficiency. Moreover, the adaptability of the Smart Grid to record,

disseminate and make decisions from any energy source or sink provides the ultimate flexibility. The structure of the Smart Grid and inherent information-sharing qualities will significantly encourage each producer and consumer of energy to reduce his/her costs while lessening overall waste and emissions.

In short, this paper will demonstrate the major aspects of using a scale Smart Grid; namely the recording of energy transfer, dynamic pricing, active monitoring and control, and efficiency analysis. Before illustrating the use of the scale Smart Grid in capturing this information, a detailed narrative of the system's architecture is first given.

3.0: System Setup

The Smart Grid contains four main categories: *sources* (renewable and non-renewable), *storage* (bulk and dynamic), *sinks* (both static and dynamic), and the *control system* (sensing and control). The next subsections will cover the purpose of each of these areas. This is accomplished by simulating a large-scale grid with small-scale components. Of particular importance, the technology between the two scales is similar, providing insight into potential problematic areas, efficiency losses, and overall energy usage. Moreover, issues during design and implementation are quickly alleviated on the smaller scale, facilitating a faster attainment of the desired end result.

3.1: Sources

Currently in the US, 85% of the provided energy comes from non-renewable sources, such as coal-fired power plants [21]. On the small scale of this project, a Generac iX800 800W gasoline generator acts as this analog. In general, this source powers household appliances that hold a relatively constant state of energy usage (such as refrigerators). Moreover, the existing energy grid uses reserve power sources

in order to balance the peaks and valleys of a daily power usage cycle. This backup power can come from a number of sources, such as the large diesel generators used in hospitals or other vital civic buildings. For this effort, a sustainable approach to reserve power comes from solar energy, due to it being a zero emissions, and thus an ethically sound, source of energy.

Solar energy is possible as a bulk source of energy, but it is more often implemented as an auxiliary reserve source of power. When using solar energy strategically, the potential impact upon the grid can vary greatly, becoming more or less of a reliable source [22]. An HQRP monocrystalline flexible solar panel has been chosen as the proxy for this photovoltaic reserve source. This panel is able to provide up to 20.7 VDC and 1.783 A in an open-circuit setup for a total potential output of 36.9 W. Efficiency calculations can be made based upon the size of the solar panel and the average solar irradiance of the area where this work was accomplished. In order to measure the instantaneous solar irradiance, the authors have utilized an Apogee SP-215 pyranometer that outputs a zero to 4.4 V signal corresponding to a potential solar irradiance of zero to 1100 W/m^2. This signal is read by the NI hardware and translated in a student-built LabVIEW system. Because solar energy varies depending on the strength of the solar irradiance, regulation of its output to the grid must occur in order to provide a steady energy flow while preventing an overcharge of potential storage mediums like batteries. To this end, the scale setup utilizes a Xantrex C35 charge controller that is capable of handling a 12 VDC load at a current up to 35 A.

Control of power flow was achieved through the implementation of a switchboard consisting of various toggle switches. From this switchboard, the user can choose to

divert power from the renewable or grid analog sources based on simulated customer demand or to batteries acting as storage mediums. Hence, the authors have direct control over power as desired by the DoE vision for a Smart Grid. Note that future efforts include automating the process, decreasing response time to required changes in the system.

3.2: Storage

Two distinctive battery banks store the renewable energy for immediate or later usage. One bank consists of two 12 VDC lead acid batteries: an Optima Blue Top deep cycle lead acid (Lead Acid Blue, 75 Ah in Figure 5), and an AAE Marine deep cycle lead acid battery (Lead Acid Black, 90 Ah in Figure 5). Wiring of these batteries in parallel provides optimal freedom of control of various storage units possible within a large-scale application.

The second battery bank consists of a lithium iron phosphate battery pack composed of A123 26650 M1 cells that are the same battery brand as found in the Chevy Volt vehicle (RC Battery Pack/BMS in Figure 5). This bank acts as the small-scale representation of a PHEV or BEV while operating additionally as a storage medium rather than a singular sink as the current grid now dictates. Two battery packs will serve this purpose: a four-cell pack has been used in initial testing, and a second eight-cell battery pack is currently being constructed. The test pack is composed of four 3.3 VDC cells wired in series for a nominal voltage of 13.2 VDC and capacity of 3.6 Ah. The larger pack will be wired with four cells in series, two strings in parallel in order to increase the storage capacity to 7.2 Ah.

3.3: Sinks

Conventional or renewable sources can deliver power to three distinct sinks in the system. The PHEV/BEV pack discussed in the Storage section acts in dual capacity as a sink representing the necessity of consumers to charge their vehicles when pack voltage is low. Moreover, a popcorn maker acts as an analog appliance for energy usage in the home, business or industry setting. The last sink involves powering the control system (Toshiba/NI/Apogee in Figure 5) in order to monitor, measure and manage the flow of energy. It is important to mention that the Venom Pro Charger indicated in Figure 5 is included as a method to recharge the Blue and Black lead acid batteries from the conventional grid in case the system is without sunlight for a significant amount of time.

In order to use power from the conventional grid, all three sinks can plug directly into the gasoline generator. Two Cobra inverters and a higher quality AIMS inverter (indicated in Figure 5) convert 12 VDC battery energy into 120 VAC. The two Cobra inverters are less efficient modified sine wave inverters, while the AIMS power inverter produces a higher-efficiency pure sine wave to allow for a comparative analysis. The popcorn maker appliance requires approximately 300 W of energy as measured; hence, the 400 W inverter provides enough capacity to handle any potential energy losses in this system connection.

Charging the PHEV/BEV pack is a Constant Current, Constant Voltage (CCCV in Figure 5) device that represents a standard power supply from the wall (120 VAC input). It outputs a voltage of 14.61 VDC, a constant charging current of 0.7 A and is controlled by a Battery Management System (BMS). The draw from the CCCV is well below the

capability of the indicated 400 W inverter; however, the authors chose to use the same brand inverter as the popcorn maker, albeit at a higher-power (800 W) in order to allow for higher energy draw should the need arise if other devices are added to the system. When rectifying renewable energy stored in the lead-acid batteries to 120 VAC, this PHEV/BEV pack acts as a storage medium through CCCV charging; however, when charging via the generator, this pack acts as a sink.

Finally, in order to provide sufficient power for the laptop, the NI system and sensors, the 600 W AIMS Pure Sine Wave Inverter provides high quality AC power in order to run the sensory system and to meet future energy demands. For a large-scale application where the individual components are more expensive, use of a pure sine wave inverter is preferred in order to protect the components. However, modified sine wave inverters suffice for the basic power needs of this smaller scale application at a reduced cost.

Of significant importance, the choice of building a 13.2 VDC PHEV/BEV pack allows the authors to demonstrate and analyze a Vehicle-to-Grid (V2G) scenario. As Figure 5 shows, a connection exists between the pack, a 400 W inverter and the popcorn maker. Proving this V2G concept is important for a working Smart Grid as this technology can be used strategically in order to reduce the strain on the existing power grid due to variability in consumer energy requirements throughout the course of the day. For example, a fleet of electrified vehicles can store energy produced at night when it is plentiful and inexpensive, releasing this power to the grid during the 5 PM energy surge [23].

3.4: Control System

As Figure 5 demonstrates, a Smart Grid is a complex structure of energy flow with the flexibility to maximize energy efficiency. The scale Smart Grid handles AC and DC power with currents ranging from less than 1 A up to 30 A. As stated, a manual switchboard consisting of single pole double throw (SPDT) and double pole double throw (DPDT) toggle switches was implemented to isolate energy pathways, while maintaining safety and desired system control. NI modules record voltage and current measurements that feed into a LabVIEW program as high-resolution digital readings. Due to a 5 A limit for NI modules, Hawkeye hall-effect current sensors were implemented to allow measurement of high current AC pathways, while current shunts have been utilized to measure the high-current DC pathways (more information on these sensors is covered in the next section). These sensors produce a voltage output directly proportional to the magnitude of the current read by an NI module. Power consumption and efficiency losses are calculated from raw voltage and current readings.

A LabVIEW Graphical User Interface (GUI) facilitates communication between the user and the data acquisition system. An example of the LabVIEW block diagrams created is given in Figure 7 below, showing some of the complexity in the program. The main display consists of the flowchart diagram (Figure 5) with power and efficiency indicators overlaid, allowing the user to read the magnitude and direction of energy flow throughout the system. Moreover, recently collected data in graphical form is available through sub-GUIs accessible from the main display. The program can be installed as a stand-alone application on any PC, requiring only an Ethernet connection to the data

acquisition chassis. Finally, in order to facilitate more automated control over the system, the LabVIEW program will replace the switchboard through implementation of digital relays after more thorough testing of the system has been completed.

Controlling the charging and discharging of the PHEV/BEV pack is an Elithion Lithiumate BMS consisting of circuit (aka cell) boards attached to each parallel set of cells in the series, a Hall Effect current sensor and a controller. The BMS measures each individual cell's voltage using the cell boards and monitors the current flowing into or out of the pack using the sensor. Each PHEV and BEV vehicle on the market has a unique battery pack; hence, a BMS acts to charge and balance the cells properly in order to protect the battery pack and prolong its lifetime. More information on the operation of this battery pack and BMS is available in the Results section.

The BMS uses relays to control the charging and discharging of the battery pack while protecting against over-voltage, under-voltage and maximum charging and discharging currents. Relays can either disconnect the battery charger from power, or disconnect the load from the battery pack. The two relays used are off-the-shelf automotive headlight and horn relays designed for a coil voltage of 12 VDC and rated for a current of 40 A. The BMS triggers the relays using a 12 VDC output signal based on sensor readings. The control of this pack is significantly important in order to prolong the lifespan of the batteries and make the vehicle more affordable to the average consumer over the life of the automobile [24].

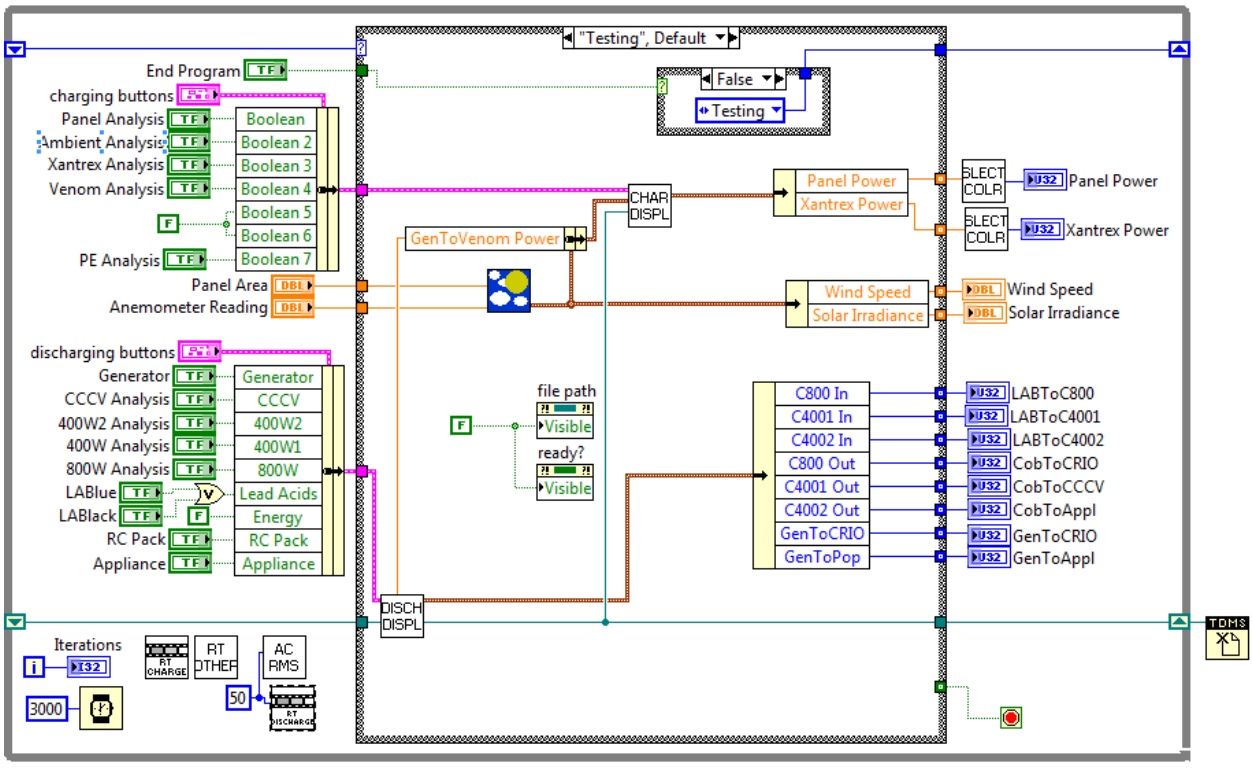

Figure 7: LabVIEW block diagram used in the student-created software.

3.5: Sensors

An array of sensory equipment has been implemented to work in tandem with the NI modules. In particular, three Hawkeye 723HC hall-effect current sensors measure the AC current flowing from the generator, as well as from the DC-AC inverters. Moreover, three 50 A current shunts are being used to measure the DC current supplied to the DC-AC inverters. The Hawkeye current sensors have an adjustable signal range able to sense between zero and 50, 100, or 200 A currents. The 0-50 A range was selected providing a 5:1 adjustment factor between the 1-10 mV output and the current being measured. In order to obtain a more precise measurement, the wire was looped through each Hawkeye six times giving a final conversion factor of 5/6:1, or 5/6 A per mV. The current shunts output a 0-50 mV signal corresponding to a 0-50 A current measurement; hence, there is no conversion factor required for these sensors.

4.0: Smart Grid Testing Results

The authors completed scale Smart Grid testing in each area as it was constructed. This provided a structured methodology in order to debug the grid and diagnose problems. In the following sections, a few test results are presented in order to illustrate concepts of the Smart Grid along with the issues that occurred and how these problems were alleviated. After improvements were made, final testing was performed in order to ascertain inefficiencies in the system and to provide a basis for future large-scale implementation. Many of the power and efficiency measurements are displayed in Figure 8 in a visualization of the system's capabilities.

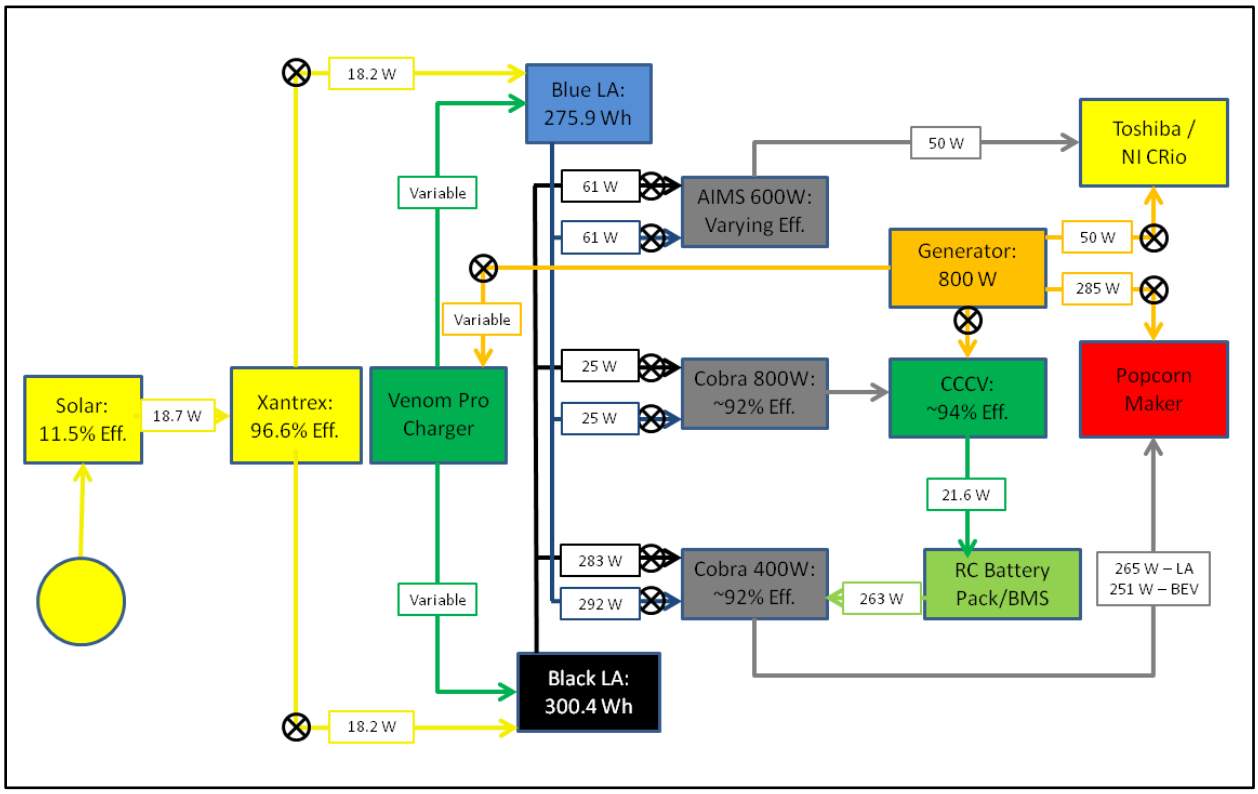

Figure 8: Smart Grid flow diagram with average or approximate efficiencies and power ratings.

4.1: Solar Panel Source and Lead Acid Storage

The solar panel was deployed in slightly hazy conditions for a 29-minute test, providing a varying output ranging from 6.66 to 18.74 W. At the maximum power output of 18.74 W, the pyranometer indicated a reading of 138.37 W/m^2 that corresponds to an efficiency of 13.54% based on the measured panel area of 0.34 m^2. Likewise, at the minimum power output of 6.66 W, the pyranometer measured 73.24 W/m^2 resulting in an efficiency of 9.1%. Since a typical monocrystalline solar panel attains a maximum efficiency of 18 to 24%, the solar panel employed is achieving approximately one-half of that power. However, this particular monocrystalline panel has a large amount of empty space, with the cells adhered to a flexible sheet of insulated aluminum intended to be employed on the roof of an automobile (the authors wanted to test this particular panel for potential use with the GMC Jimmy BEV conversion efforts mentioned earlier). This allows the panel to be malleable, reducing the chance of cell cracking. Typical solar panels utilize as much space on the panel as possible in order to increase the area-based efficiency [25].

A second cause of inefficiency for this power source acting as an auxiliary reserve for the grid was from the Xantrex charge controller. The Xantrex is vital to the protection of the lead acid battery bank, preventing over-charging of the battery; however, it does require a power input in order to run the controller. At the maximum solar power output of 18.74 W, the power reading after the Xantrex was 18.18 W with a subsequent efficiency of 97.01%. Likewise, during the minimum power output of 6.66 W, the power reading after the Xantrex was 6.26 W for an efficiency of 93.87%.

Overall, when the solar panel output was at its maximum, the efficiency was equal to 13.13%. In comparison, when the panel output was at a minimum, the efficiency was only 8.54%. During this test, the voltage increase for the lead acid battery totaled 0.27 VDC. Over all the solar tests performed to date, the average Xantrex efficiency was 96.6% with the average pyranometer-based efficiency at 11.5% resulting in a final efficiency of the solar energy auxiliary system for the Smart Grid of 11.1%.

4.2: Lead Acid Storage and Home Appliance Sink

Testing with the popcorn maker demonstrates renewable energy as a source for the customer on the grid. In this examination, renewable energy stored in the lead acid batteries running through a 400 W Cobra inverter powered the popcorn maker. Using these tests, the efficiency losses through the inverters were compared to the energy usage from running the popcorn maker off the generator. The Blue lead acid battery was able to run the popcorn maker for 18 batches, drawing a total of 276 Wh. However, the Black lead acid battery only created 13 batches, drawing a total of 300 Wh. Note that the complete runs were accomplished starting from a fully charged battery until the inverter shuts off when the voltage of the battery falls below 11.5 VDC.

More power was drawn during testing on the Black lead acid battery because a brief down-time was taken between batches in order to store individual tests, which caused the system to cool slightly. Whereas, during Blue testing, the batches were switched out more rapidly, leaving the program running, reducing heat lost between batches and requiring less power from the battery to reheat the appliance. This was

accomplished in order to simulate the difference of customer approach to appliance usage.

Over all of the tests, the average power draw from the Blue lead acid battery was 291.7 W; whereas, it was reduced to 283.3 W from the Black lead acid battery. When using the Blue lead acid battery, the average power draw after the inverter was 267.1 W, resulting in an efficiency of 91.6% for the inverter. However, the Black lead acid battery system was slightly more efficient with the average power draw after the inverter equal to 263.6 W, corresponding to an efficiency of 93.0%. This relatively small difference in efficiency is the result of variances in the testing environment: for example, changes ambient temperature. During each of the tests with the popcorn maker, the voltage drop on the lead acid bank being utilized was measured and recorded. From this data, the average voltage drop was 0.115 VDC, with a maximum and minimum drop of 0.225 VDC and 0.070 VDC respectively when drawing from the Blue lead acid battery. When drawing from the Black lead acid battery, the average voltage drop was 0.231 VDC, with a maximum and minimum now equal to 0.334 VDC and 0.156 VDC. The average voltage drop corresponding to a cold-start popcorn batch was 0.280 VDC while for a warm start the value was 0.111 VDC.

In addition, a number of popcorn batches were run drawing power from the generator in order to perform a comparative analysis. During these batches, the average cumulative energy draw was 13.8 Wh, with a maximum of 24.3 Wh for a cold-start batch, and a minimum of 9.0 Wh for a warm-start batch. The maximum instantaneous power draw from all of the generator batches was 284.5 W, while the minimum power draw was 281.0 W. Because the generator outputs AC power, it does

not suffer the same efficiency loss from the implementation of a separate inverter. Here, the quality of the inverters comes into play as well. The less efficient modified sine wave created by the Cobra inverters caused a lower power draw for a longer batch duration, hence the 20 W draw difference. Despite this difference in instantaneous power draw, the overall energy use per batch was similar as the batches powered through the Cobra inverter took slightly longer to finish. However, the generator does suffer overall (aka cradle-to-grave) efficiency losses due to the conversion from chemical to mechanical to electrical power in the generator. Moreover, this conversion will result in the production of hazardous and greenhouse gas emissions through the burning of fuel. Hence, while the power quality is better, the environment does suffer from the emissions released (provided later in this paper).

4.3: PHEV and BEV Storage and Sinks

In order to demonstrate the PHEV/BEV battery pack in a V2G scenario, the control system computer was powered from the A123 battery pack by sending energy through a 400 W inverter. The power consumption of the laptop was measured at approximately 50 W with the initial battery pack voltage at 13.28 VDC. The battery pack was able to power the laptop for eight minutes with the minimum, average and maximum of the different battery voltages (cells) indicated by the BMS displayed in Figure 9. The BMS was programmed to disconnect the energy draw from the pack when the average voltage dropped below 3.0 VDC. Successful disconnection occurred with a minimum cell voltage equal to 2.91 VDC, and a maximum cell voltage at 3.12 VDC. Although three of the cells still held a significant charge, the single low voltage

cell caused premature disconnection in order to protect the battery, prolonging its life and satisfying customer expectations.

Using the setup, another V2G scenario involves running the appliance (e.g., popcorn maker) off the PHEV/BEV battery pack. Unfortunately, the small capacity of the test pack (3.6 Ah) only operated the appliance for 35 seconds at a power draw of approximately 288 W. This was several minutes shorter than initial estimates. As a result, a second battery pack using four Headway 8 Ah cells was built in order to perform a comparative analysis. This new pack has a larger capacity and a higher available discharge rate, making it more appealing in a V2G situation. In testing this battery pack, three full batches of popcorn were completed, discharging a total of 66.7 Wh over 16 minutes before the BMS cut off the discharge current due to a low pack voltage of 11.5 V. During these tests, the BMS was able to keep the individual cells within 0.02 V of their average voltage.

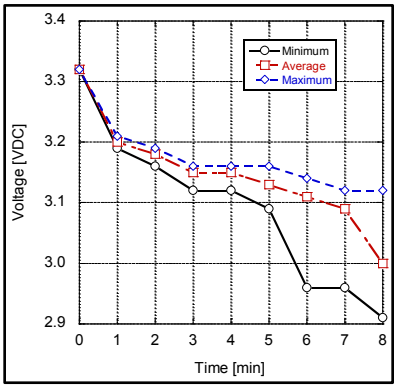

Figure 9: V2G scenario powering laptop off PHEV/ BEV battery pack.

When using batteries in a sink or source scenario from the grid based on conventional or renewable energy sources, the BMS acts to balance the pack for cell consistency while preventing over-charging in order to prolong the lifetime of the batteries and allow the customer a better return on investment for electrified vehicles.

In order to validate the control of the scale Smart Grid, a couple charging trials were accomplished. The first charging trial began with initial cell voltages of 3.22, 3.25, 3.25 and 2.85 VDC. Data was taken every thirty seconds for 20 minutes from the BMS for the minimum, average and maximum cell voltages as shown in Figure 10. The BMS operated as desired, charging and balancing the cells to 3.31, 3.32, 3.31 and 3.30 VDC, respectively. A second trial began with initial cell voltages of 3.25, 3.24, 3.24 and 2.65 VDC. For this trial, data was taken once per minute for twenty minutes and then less periodically for the next 75 minutes as illustrated in Figure 11. As expected, the BMS stopped charging after 56 minutes when the maximum voltage limit was reached by one of the batteries. The large change in voltage after 40 minutes relates to the charge curve profile of $LiFeYPO_4$ batteries (flat from 10-90% SOC with steep changes at 0-10% and 90-100%) that demonstrates the necessity of proper charging control.

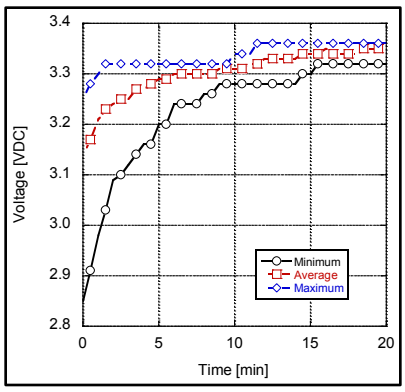

Figure 10: BMS cell balancing example

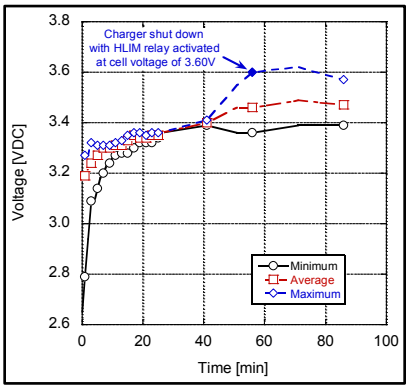

Figure 11: BMS over-charging relay test.

4.4: Control Sink

In keeping with the spirit of the Smart Grid project, the control system and attached sensory banks would have to be powered from the same varying sources as the rest of the system. However, this control system required a source of high quality power from the battery banks that the Cobra inverters were unable to supply. The AIMS inverter did manage to successfully the pure sine wave power needed to power the control system, but operated at a higher cost. The inverter required 19.9 watts to operate, but only supplied 9.2 watts to the sensory equipment, giving an apparent loss of 10.7 watts through the AIMS inverter for an efficiency of 46.3%.

However, this efficiency is not a constant value. If the inverter was switched on, but not connected to any output load, the inverter still drew around 10 watts of power, indicating that the high quality AIMS inverter requires 10 watts of power to run. Testing showed that this 10 watt power draw appeared to be constant, regardless of the output load. Because of this constant draw, the efficiency of the inverter would increase significantly as the load was increased (for example; by powering the laptop computer that was running the control system off of the AIMS inverter as well).

4.5: Control System

After successful debugging, the final iteration of the LabVIEW program consists of a GUI with the original block diagram (Figure 5) and color-coded indicators representing the location and magnitude of power transmission. Clicking on a single block brings up a sub-GUI with several graphical displays describing the status of the given component. This typically includes voltage, current and power readings plotted over time. For the renewable energy component, solar irradiance is indicated and maximum potential solar power is plotted based on the size of the photovoltaic panel.

In order to calculate AC voltage, an algorithm takes the root mean square of 50 raw readings and converts it into a readable output. To provide enough time to perform this calculation and all other computations, the program updates itself once every three seconds. Hence, every voltage, current, power and efficiency value is logged, plotted and stored at this frequency. Moreover, the code includes data recording and archiving organized into several channels with each channel representing a grid component. After the program is loaded, the user's first task is to select a location to store the results file. Upon successful completion of a test, the program is terminated by clicking

on an “End Program” block after which the program saves all recorded data to a National Instruments technical data management solution (TDMS) file at the given location. Using a free downloadable LabVIEW add-on (available from ni.com) the file can be opened in Microsoft Excel. The data is then presented in spreadsheet form with each sheet representing a channel containing columns of recorded data.

4.6: Emissions and Cost Analysis

If all available sources were run simultaneously, the renewable solar source in the scale Smart Grid makes up approximately 2.3% of the energy potential, which parallels US renewable energy production of 6.9% [26]. Inopportunely, solar energy potential is reduced by the inefficiencies involved with the Xantrex charge controller, as well as the inherent inefficiencies of the panel itself. However, the ability to store 582Wh of renewable energy in battery banks increases this end use potential. Using Argonne National Laboratory’s Greenhouse Gases, Regulated Emissions, and Energy Use in Transportation Model (GREET) to perform a full emissions and energy use analysis, the emissions reduced by using this stored renewable energy as opposed to petroleum, coal, and other conventional sources are shown in Table 1 [27]. Moreover, this table includes estimates for the amount of emissions offset per day based on the average local solar irradiance over the course of 15 years [28]. Thus, although the deployment of renewable energy does have some inherent inefficiencies, it avoids the toxic emissions caused by using conventional power sources currently the foundation of the energy grid infrastructure. This expansion of the influence of renewable energy influence is made possible by using a Smart Grid architecture as demonstrated.

Table 1: Grams of emissions from common energy sources per storage bank capacity.

	Solar		Petroleum		Coal		Natural Gas		Nuclear	
	[g/bank]	[g/day]	[g/bank]	[g/day]	[g/bank]	[g/day]	[g/bank]	[g/day]	[g/bank]	[g/day]
NO_x	0	0	1.338	0.324	0.749	0.181	0.486	0.118	0.017	0.004
SO_x	0	0	3.697	0.895	1.492	0.361	0.062	0.015	0.014	0.003
Particulates	0	0	0.073	0.018	1.468	0.335	0.037	0.009	0.013	0.003
CO_2	0	0	589.8	142.8	695.1	168.3	347.7	84.2	8.7	2.1
GH Gas	0	0	607.6	147.1	722.0	174.8	415.6	100.6	9.4	2.3

A further look into the effects of using renewable energy sources versus conventional driving schemes can be performed using the GREET model in comparing a conventional vehicle (2011 Chevrolet Impala) to two instances of an electric vehicle (2011 Nissan LEAF) using a coal utility, or stored solar energy source. Table 2 shows this emissions comparison for each of these three vehicles driven 10,000 miles over the course of one year.

Table 2: Grams of emissions per 10,000 miles of two vehicles with various energy sources.

	2011 Chevrolet Impala	2011 Nissan LEAF	2011 Nissan LEAF
	Conventional Gasoline	Coal-Fire Utility	Stored Solar Utility
NO_x	4,514	3,463	0.0
SO_x	1,572	6,898	0.0
Particulates	863	6,788	0.0
CO_2	5,507,519	3,213,959	0.0
GH Gas	5,770,305	3,332,758	0.0

The average cost of electricity in the United States as of August 2011 was 10.6 cents/kWh. By utilizing the solar panel consistently during the year, users would save just under 1.5 cents per day per solar panel deployed. Given the initial cost of $161.68 for the solar panel, the return on investment (RoI) is approximately 30 years. However, if dynamic pricing is deployed as described in Borenstein et al.'s research [29, 30], a Smart Grid equipped with the ability to track the cost of electricity would be able to decrease this RoI significantly by storing energy when it is inexpensive, and discharging energy as the price rises. This is one of the main benefits of a V2G system in that it allows for an emissions offset when referring to transportation while additionally reducing emissions and energy cost through tracking dynamic pricing and utilizing energy in the most efficient manner. Again, the scale Smart Grid built by the authors demonstrates this capability.

5.0: Discussion

In this work, the authors evaluated the performance of a student-built scale Smart Grid based on five defined tenets of sustainability: energy, environment, education, economics and ethics. Moreover, the scale Smart Grid constructed attains the goals as stated by the DoE; e.g., decentralization of energy production and storage

while maintaining an effective two-way communication between end-users and the energy network [31]. In specific, the scale Smart Grid presented includes the integration of renewable energy resources, PHEV/BEV technology, dynamic power generation and communication in order to maximize efficiency and optimize power distribution. It analyzes the entire energy cycle from initial production to final consumption while enabling customer interaction.

The Smart Grid design aims to utilize energy from renewable sources and optimize the usage of existing centralized power generation in order to reduce the environmental impact from fossil fuel emissions and substantially improve overall power generation efficiency. This is a more ethically sustainable approach to increasing the capabilities of the energy infrastructure than the construction of 160 new conventional power plants. The preliminary data gained from testing renewable power generation and storage is promising. The solar panel charge control operation was successful, as the Xantrex controller adjusted the panel's output voltage for optimum charging under any weather conditions. Hence, the solar panel has successfully charged the battery banks both individually and simultaneously, proving the integration of several renewable energy generation methods into a Smart Grid system. Through using dynamic pricing, this ability to store collected renewable energy will significantly reduce the RoI on the solar panel itself, as well as the Smart Grid as a whole.

A switchboard enables the user to distribute the energy throughout the network to maximize efficiency. With the BMS controlled A123 battery pack, the Smart Grid demonstrates both V2G and G2V technologies, as the PHEV/BEV can effectively sell the power back as desired or draw energy from the Smart Grid. This two-way flow of

energy creates additional storage for renewable energy distributed throughout the grid. A LabVIEW DAQ system and sensor network supports communication of all energy flow. NI hardware assembles and transmits all data collected through its voltage and current modules to the LabVIEW program that processes and displays grid energy information in a convenient user-friendly manner. An organized graphical GUI and several sub-GUIs keep the user up-to-date with grid status. Finally, the addition of convenient data recording allows for comprehensive analysis and post-processing.

Through the implementation of a Smart Grid, the authors have demonstrated lower emissions and increased renewable energy deployment. This work demonstrates that electrified vehicles, renewable energy and control schemes are feasible as alternatives to conventional power sources. The reduction of harmful emissions improves the long-term health and quality of life. Although greenhouse gases, particularly carbon dioxide, remain a major global concern, greater use of PHEV/BEV technology will reduce roadside toxic emissions including carbon monoxide, carbon dioxide, and nitrous oxides. Through using renewable sources of electricity, one can also reduce particulate matter and sulfuric acid emissions. Moreover, the implementation of the demonstrated G2V and V2G technology through the electrified vehicle battery pack will aid in reducing harmful emissions due to inefficient use of energy across the grid. As global energy demand and oil prices rise, the cost of living will increase making it harder for future generations to maintain modern living standards without the implementation of Smart Grid technology.

6.0: Future Work

Future efforts with the scale Smart Grid include testing various alternative battery chemistries, higher efficiency components, and other renewable energy sources like wind. A major improvement currently underway is the automation of the entire system through the replacement all switches and manual control schemes with relays modulated by amendments to the LabVIEW program. Furthermore, current work involves replacing faulty wiring in order to provide a safe research base for future work and research with the Smart Grid. This wiring substitution includes the creation of a full wiring diagram, currently absent in the Smart Grid design and necessary for future extrapolation. This work will provide the foundation for the construction of a full-scale adaptation of the Smart Grid beginning with complete knowledge of the system's strengths and weaknesses. In addition, this system will tie together other student projects, including the large-scale solar array and the synthetic gas test rig already in place at the EcoHawks barn facility. Finally, the use of a large-scale Smart Grid is conducive to further research into widespread PHEV/BEV integration, including exploration into full-scale V2G technology. The final steps of future work include determining suggested components for large-scale implementation directly based on the strengths and weaknesses of the small-scale Smart Grid, providing a strong base for efficient extrapolation with minimal waste.

7.0: Acknowledgements

The authors of this paper would like to thank National Instruments, Argonne National Labs, the United States Environmental Protection Agency, the University of Kansas, our faculty advisor Dr. Christopher Depcik, as well as the remaining members

of the 2010 Smart Grid team, including Andrew Moore, Mickey Clemon, Shelton Heilman, and Len Necefer, who were instrumental in creating the Smart Grid, but were not involved in the writing of this report.

8.0: References

1. Office of Electricity Delivery and Energy Reliability, *The Smart Grid: An Introduction."* Department of Energy, Editor 2008.
2. Vyas, A.D., Santini, D.J., and Johnson, L.R., *Plug-In Hybrid Electric Vehicles' Potential for Petroleum Use Reduction: Issues Involved in Developing Reliable Estimates.* 2009.
3. Voelcker, J., *Can plug-in hybrid electric vehicles keep the electric grid stable?* IEEE Spectrum, 2007.
4. United States Environmental Protection Agency, *Sustainability - Basic Information.* 2011.
5. American Society of Interior Designers, *Sustainable Design.* 2011.
6. Christopher Depcik PhD, Austin Hausmann, Jessica Lamb, Bryan Strecker, Chris Billinger, Will Pro, Melanie Gray, *Incorporating Sustainable Automotive and Energy Design into the Engineering Curriculum using Remote Control Cars.* International Journal of Engineering Education, 2010.
7. Fagan, M., *Sustainability drives KU engineers*, 2009, Lawrence Journal World.
8. Sitkin, S.B., *Learning through failure: The strategy of small losses.* Organizational Learning, 1996.
9. C. Depcik, A. Hausmann, J. Lamb, B. Strecker, C. Billinger, W. Pro, M. Gray, *Incorporating Sustainable Automotive and Energy Design into the Engineering Curriculum using Remote Control Cars.* International Journal of Engineering Education, 2011. **27**(2): p. 1-16.
10. Depcik, C., L. McKown, and M. LeGresley, *A Sustainable Approach to Advanced Energy and Vehicular Technologies at the University of Kansas.*, in *ASME International Mechanical Engineering Congress & Exposition*2009: Lake Buena Vista, FL, USA.
11. Howard, C. *Teachers learn about cutting-edge engineering from KU faculty - KU News*. 2010; Available from: http://www.news.ku.edu/2010/july/12/engineering.shtml.
12. Depcik, C., L. McKown, and M. LeGresley, *University of Kansas EcoHawks: Sustainable Automotive Engineering.*, in *Tenth Annual Kansas Environmental Education Conference*2009: Lawrence, KS.
13. Howard, C., *99th annual Engineering Expo set for Feb. 19-20 - KU News*, 2010.
14. Gleue, A.D., *Building a Gratzel Solar Cell.* 2008.
15. Engineering Student Council *KU Engineering Expo*. 2011; Available from: http://groups.ku.edu/~kuesc/cgi-bin/?q=expo-003.html.
16. EcoHawks, K. *KU EcoHawks - K-12 Student Competitions*. 2011; Available from: http://groups.ku.edu/~ecohawks/k12.htm.
17. U.S. Environmental Protection Agency. *P3: People, Prosperity and the Planet Student Design Competition for Sustainability*. 2012 09/12/2012 12/6/2012]; Available from: http://www.epa.gov/P3/.
18. Clastres, C., *Smart grids: Another step towards competition, energy security and climate change objectives.* Energy Policy, 2011.
19. Department of Energy Office of Electricity Delivery and Energy Reliability, *A Vision for the Smart Grid*, D.o. Energy, Editor 2009.
20. Booze Allen Hamilton; Horizon Energy Group; Renz Consulting, L., *Understanding the Benefits of the Smart Grid*, D.o. Energy, Editor 2010, National Energy Technology Laboratory.
21. ENERGY.GOV, *Department of Energy - Fossil Fuels.* 2011.
22. Halamay, D., et al., *Reserve Requirement Impacts of Large-Scale Integration of Wind, Solar, and Ocean Wave Power Generation.* Sustainable Energy, IEEE Transactions on, 2011. **PP**(99): p. 1-1.
23. Clement-Nyns, K., E. Haesen, and J. Driesen, *The impact of vehicle-to-grid on the distribution grid.* Electric Power Systems Research, 2011. **81**(1): p. 185-192.

24. Peterson, S.B., J. Apt, and J.F. Whitacre, *Lithium-ion battery cell degradation resulting from realistic vehicle and vehicle-to-grid utilization.* Journal of Power Sources, 2010. **195**(8): p. 2385-2392.
25. Investor, G.W., *Efficiency of Solar Cells made of Silicon (Monocrystalline, Multicrystalline), Thin Film (CIGS, CIS, aSi, CdTe, CZTS), Multijunction.* Green World Investor, 2011.
26. Administration, U.S.E.I., *Renewable Energy Consumption and Electricity Preliminary Statistics 2009.* 2010.
27. Argonne National Laboratory, *The Greenhouse Gases, Regulated Emissions, and Energy Use in Transportation Model.* 2011.
28. Kansas Corporation Commission: Energy Programs, *Photovoltaic Electrical Energy Production in Kansas.* 2005.
29. Borenstein, S., M. Jaske, and A. Rosenfeld, *Dynamic pricing, advanced metering, and demand response in electricity markets.* 2002.
30. Borenstein, S., *Electricity Pricing that Reflects Its Real-Time Cost*, 2009, NBER Reporter.
31. Smart Grid Analysis *Government Policy Determines Smart Grid Development*. The Smart Grid: Terminology and History 2010 [cited 2010 November 8]; Available from: http://smartgridanalysis.com/articles/article/government_policy_determines_smart_grid_development/.

Appendix A.1: Current and Historical Emissions Regulations

Table A1-1: EPA emission standards: historical [3].

		Emission Limits at Half Useful Life (50,000 miles) Maximum Allowed Grams per Mile				
Model Year / Standard	**Vehicles**	**NO_x**	**NMHC**	**CO**	**PM**	**THC**
1987-1993 / Tier 0	LDV	1.0	-	3.4	0.2	0.41
1985-1986	LDV	1.0	-	3.4	0.6	0.41
1984	LDV	1.0	-	3.4	0.6	0.41
1983	LDV	1.0	-	3.4	0.6	0.41
1982	LDV	1.0	-	3.4	0.6	0.41
1981	LDV	1.0	-	3.4	-	0.41
1980	LDV	2.0	-	7	-	0.41
1978-1979	LDV	2.0	-	15	-	1.5
1977	LDV	2.0	-	15	-	1.5
1975-1976	LDV	3.1	-	15	-	1.5
1973-1974	LDV	3.0	-	39	-	3.4
Pre-Control Levels (Pre-1968)	LDV	3.5	-	87	-	8.8
1988-1993 / Tier 0	LDT 1	1.2	-	10	0.26	0.8
1988-1993 / Tier 0	LDT 2-4	1.7	-	10	0.26	0.8
1987	LDT	2.3	-	10	0.26	0.8
1984-1986	LDT	2.3	-	10	0.6	0.8
1982-1983	LDT	2.3	-	18	0.6	1.7
1981	LDT	2.3	-	18	-	1.7
1979-1980	LDT	2.3	-	18	-	1.7
1978	LDT	3.1	-	20	-	2
1975-1977	LDT	3.1	-	20	-	2
1973-1974	LDT	3	-	39	-	3.4
Pre-Control Levels (Pre-1968)	LDT	3.6	-	39	-	6.5

Table A1-2: EPA Tier 1 and Tier 2 emission standards [3] with only LDV, LDT1, and LDT2 added to the table.

			Emission Limits at Full Useful Life (100,000 to 120,000 miles) Maximum Allowed Grams per Mile				
Standard	**Model Year**	**Vehicles**	**NO_x**	**NMOG**	**CO**	**PM**	**HCHO**
Tier 1 Program (1994 - 2003)							
LDV	1994-2003	LDV	0.6	0.31	4.2	0.10	-
LDT1	1994-2003	LDT1	0.6	0.31	4.2	0.10	0.8
LDV diesel	1994-2003	LDV	1.25	0.31	4.2	0.10	-
LDT1 diesel	1994-2003	LDT1	1.25	0.31	4.2	0.10	0.8
LDT2	1994-2003	LDT2	0.97	0.40	5.5	0.10	0.8
Tier 2 Program (2004+)							
Bin 1	2004+	LDV, LDT	0.00	0.00	0.00	0.00	0.00
Bin 2	2004+	LDV, LDT	0.02	0.010	2.1	0.01	0.004
Bin 3	2004+	LDV, LDT	0.03	0.055	2.1	0.01	0.011
Bin 4	2004+	LDV, LDT	0.04	0.070	2.1	0.01	0.011
Bin 5	2004+	LDV, LDT	0.07	0.090	4.2	0.01	0.018
Bin 6	2004+	LDV, LDT	0.10	0.090	4.2	0.01	0.018
Bin 7	2004+	LDV, LDT	0.15	0.090	4.2	0.02	0.018
Bin 8a	2004+	LDV, LDT	0.20	0.125	4.2	0.02	0.018
Bin 9a	2004-2006	LDV, LDT1	0.30	0.090	4.2	0.06	0.018
Bin 9b	2004-2006	LDT2	0.30	0.130	4.2	0.06	0.018
Bin 10a	2004-2006	LDV, LDT	0.60	0.156	4.2	0.08	0.018

Table A1-3: CARB light-duty vehicle emission standards [3] with only LDV, LDT1, and LDT2 added to the table.

			Emission Limits at Full Useful Life (100,000 – 120,000 miles)				
LEV I Program (2001 - 2006)							
ULEV I diesel	2001-2006	LDV, LDT 1	0.30	0.55	2.1	0.04	0.011
ULEV I	2001-2006	LDV, LDT 1	0.30	0.55	2.1	N/A	0.011
LEV I diesel	2001-2006	LDV, LDT 1	0.30	0.090	4.2	0.08	0.018
LEV I	2001-2006	LDV, LDT 1	0.30	0.090	4.2	N/A	0.018
ILEV		LDV, LDT 1	0.30	0.090	4.2	0.08	
ILEV	2001-2006	LDT 2	0.50	0.130	5.5	0.08	
LEV I diesel	2001-2006	LDT 2	0.50	0.130	5.5	0.10	0.023
LEV I	2001-2006	LDT 2	0.50	0.130	5.5	N/A	0.023
TLEV I diesel	2001-2003	LDV, LDT 1	0.60	0.156	4.2	0.08	0.018
TLEV I	2001-2003	LDV, LDT 1	0.60	0.156	4.2	N/A	0.018
TLEV I diesel	2001-2006	LDT 2	0.90	0.200	5.5	0.10	0.023
TLEV I	2001-2006	LDT 2	0.90	0.200	5.5	N/A	0.023
LEV II Program							
Standard	**Model Year**	**Vehicles**	**NO_x**	**NMOG**	**CO**	**PM**	**HCHO**
ZEV	2004+	LDV, LDT	0.0	0.0	0.0	0.0	0.0
PZEV	2004+	LDV, LDT	0.02	0.010	1.0	0.01	0.004
SULEV II	2004+	LDV, LDT	0.02	0.010	1.0	0.01	0.004
ULEV II	2004+	LDV, LDT	0.07	0.055	2.1	0.01	0.011
LEV II	2004+	LDV, LDT	0.07	0.090	4.2	0.01	0.018
LEV II option 1	2004+	LDV, LDT	0.10	0.090	4.2	0.01	0.018

Appendix A.2: Diesel Emissions Trends

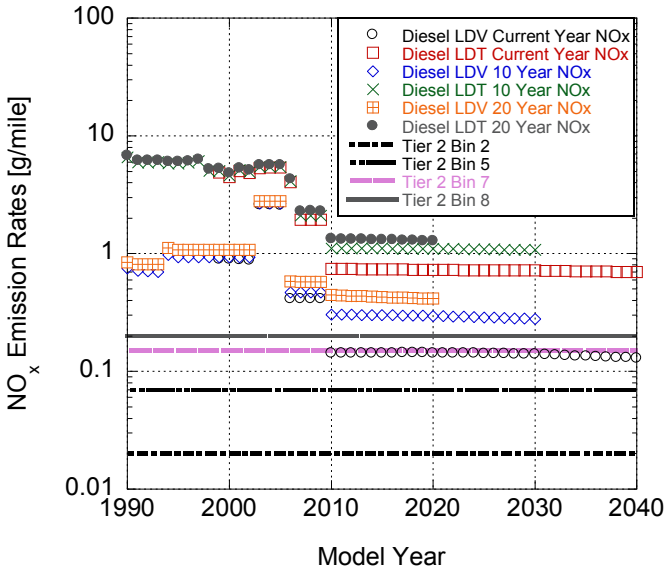

Figure A2.1: Diesel NO_x emission levels for new, ten-year, and twenty-year old LDV and LDT.

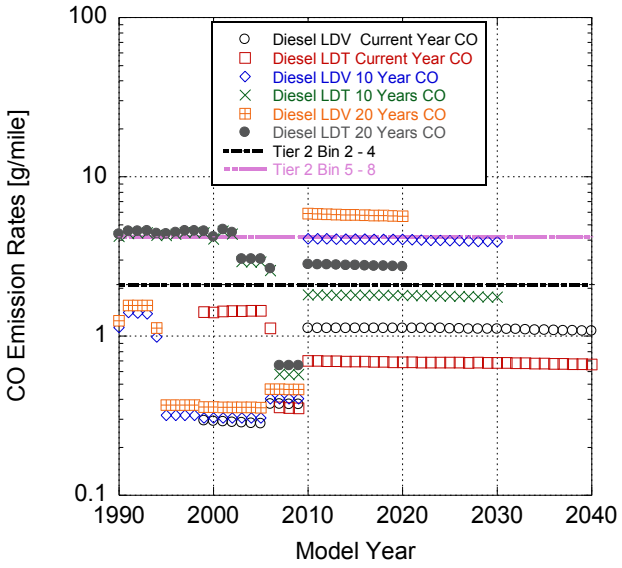

Figure A2.2: Diesel CO emission levels for new, ten-year, and twenty-year old LDV and LDT.

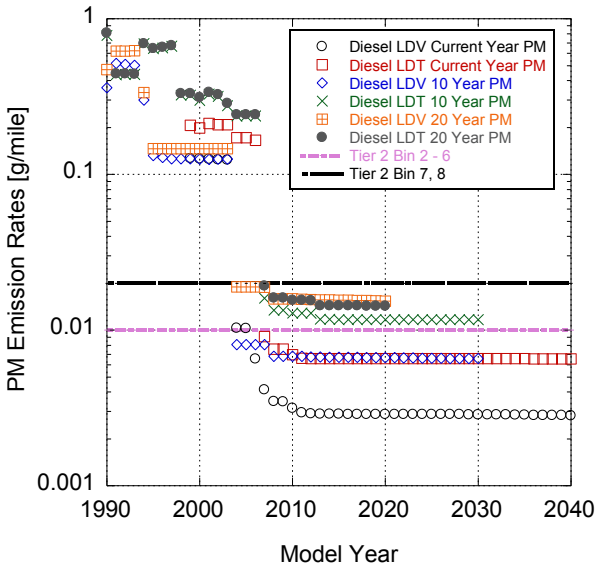

Figure A2-3: Diesel PM emission levels for new, ten-year, and twenty-year old LDV and LDT.

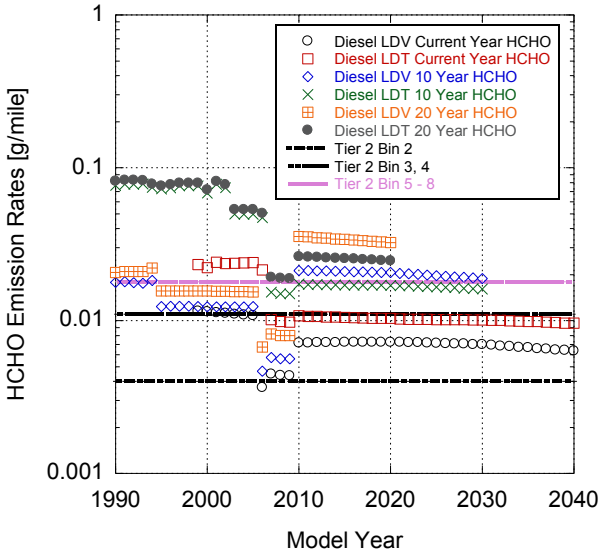

Figure A2-4: Diesel HCHO emission levels for new, ten-year, and twenty-year old LDV and LDT.

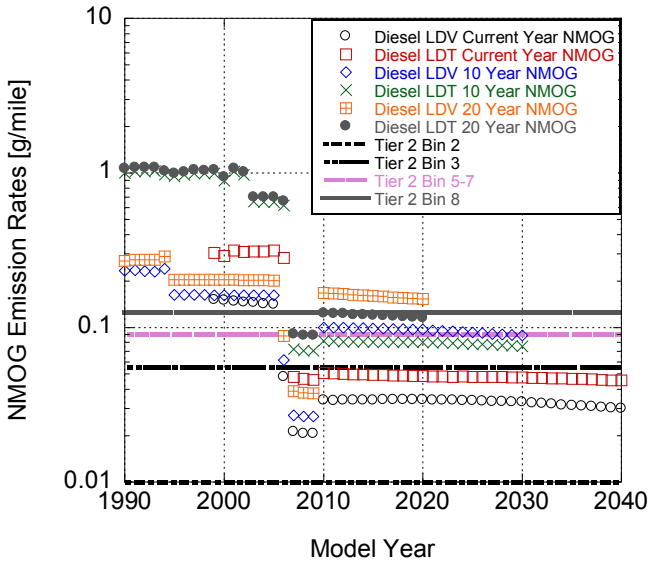

Figure A2-5: Diesel NMOG emission levels for new, ten-year, and twenty-year old LDV and LDT.

Appendix A.3: Diesel Time Sheet Emissions Tables

Table A3: Time sheet for criteria pollutant emissions found in Argonne's GREET2011 model for a Diesel LDV.

Model Year	MPG	VOC (Exhaust)	VOC (Evap.)	CO	NO_x	PM_{10} (Exhaust)	PM_{10} (TBW)	$PM_{2.5}$ (Exhaust)	$PM_{2.5}$ (TBW)	CH_4	N_2O
1990	26.52	0.392	0.000	1.168	0.914	0.1396	0.0205	0.1282	0.0073	0.0118	0.067
1995	26.04	0.198	0.000	0.812	1.074	0.0737	0.0205	0.0679	0.0073	0.0047	0.030
2000	26.40	0.088	0.000	0.817	0.300	0.0719	0.0205	0.0671	0.0073	0.0026	0.012
2005	28.08	0.088	0.000	0.539	0.141	0.0090	0.0205	0.0084	0.0073	0.0026	0.012
2010	29.77	0.060	0.000	0.534	0.080	0.0090	0.0205	0.0084	0.0073	0.0026	0.012
2015	32.64	0.060	0.000	0.534	0.080	0.0090	0.0205	0.0084	0.0073	0.0026	0.012
2020	35.34	0.060	0.000	0.534	0.080	0.0090	0.0205	0.0084	0.0073	0.0026	0.012

Appendix A.4: Diesel Emissions Trends - Climate

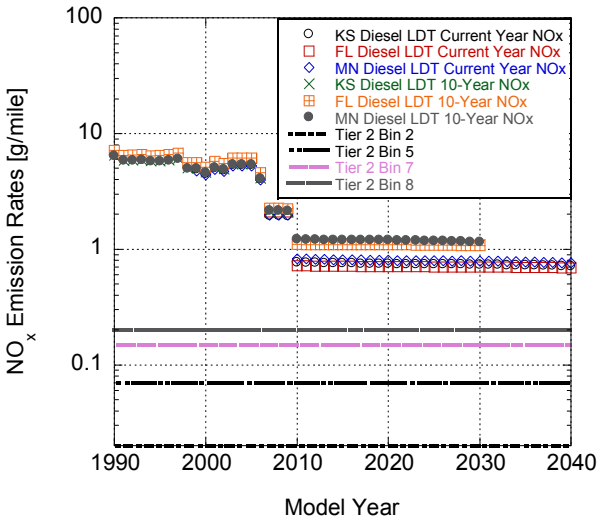

Figure A4.1: Diesel LDT NO_x emission rates as a function of model year and state.

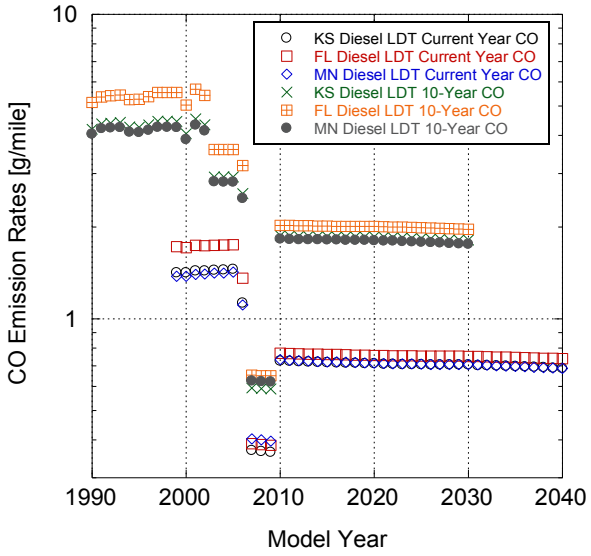

Figure A4.2: Diesel LDT CO emission rates as a function of model year and state.

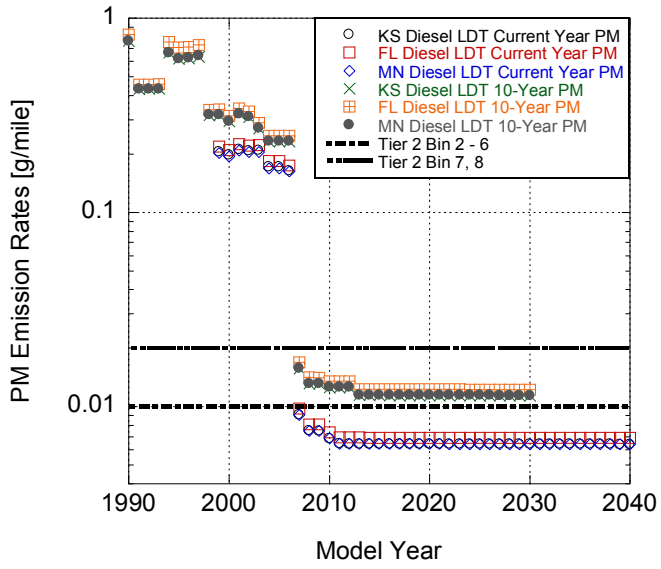

Figure A4.3: Diesel LDT PM emission rates as a function of model year and state.

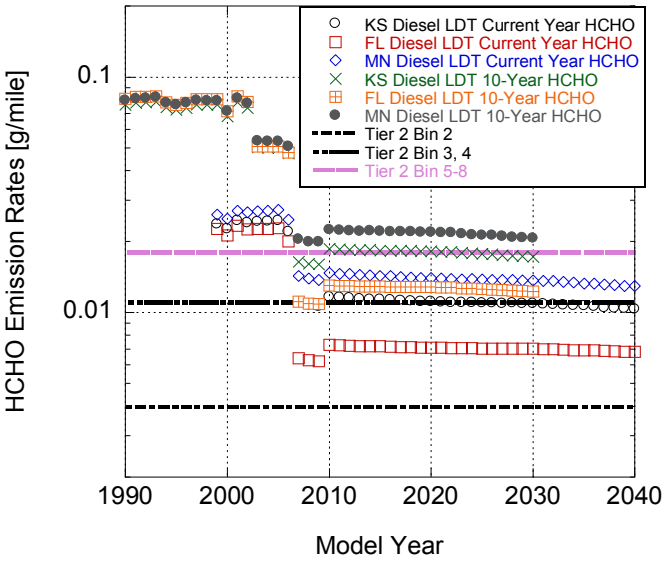

Figure A4.4: Diesel LDT HCHO emission rates as a function of model year and state.

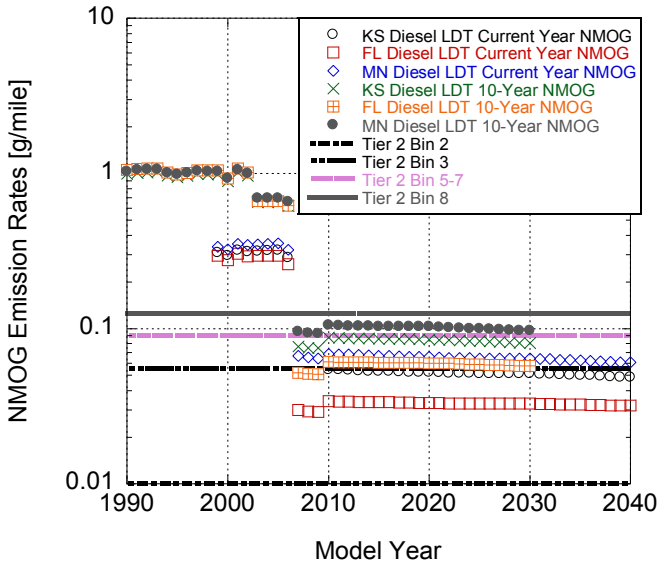

Figure A4.5: Diesel LDT NMOG emission rates as a function of model year and state.

Appendix A.5: WtP and PtW Fleet Analysis Tables

Table A.5.1: WtP per-mile emissions for baseline vehicle fleet.

			Emissions [g/mile]									
Vehicle	**MPG**	**Fuel**	**VOC**	**CO**	**NO_x**	**PM_{10}**	**$PM_{2.5}$**	**SO_x**	**CH_4**	**N_2O**	**CO_2**	**GHG**
Chevrolet Impala	26.02	CG	0.121	0.055	0.211	0.033	0.017	0.112	0.585	0.005	78	94
	19.01	CG	0.166	0.076	0.288	0.045	0.024	0.153	0.801	0.007	107	129
	19.23	E85	0.217	0.159	0.457	0.217	0.077	0.281	1.144	0.132	262	330
	14.05	E85	0.297	0.218	0.626	0.297	0.106	0.385	1.566	0.181	358	451
Chevrolet Silverado 1/2-Ton	15.01	CG	0.070	0.103	0.394	0.058	0.032	0.207	1.108	0.002	144	173
	18.71	CG	0.056	0.083	0.316	0.047	0.026	0.166	0.889	0.002	116	139
	11.48	E85	0.364	0.267	0.766	0.364	0.130	0.472	1.917	0.221	439	553
	14.31	E85	0.292	0.214	0.615	0.292	0.104	0.378	1.538	0.177	352	443
Chevrolet Silverado 3/4-Ton	12.00	CG	0.263	0.120	0.456	0.072	0.038	0.243	1.268	0.011	169	204
	10.49	CG	0.301	0.137	0.522	0.082	0.043	0.278	1.451	0.012	194	234
Chevrolet Uplander	18.51	CG	0.171	0.078	0.296	0.046	0.024	0.158	0.822	0.007	110	132
	15.81	CG	0.200	0.091	0.346	0.054	0.029	0.184	0.963	0.008	129	155
Line Truck	6.99	ULSD	0.151	0.222	0.846	0.125	0.069	0.444	2.377	0.004	310	371

Table A.5.2: PtW per-mile emissions for baseline vehicle fleet.

			Emissions [g/mile]									
Vehicle	**MPG**	**Fuel**	**VOC**	**CO**	**NO_x**	**PM_{10}**	**$PM_{2.5}$**	**SO_x**	**CH_4**	**N_2O**	**CO_2**	**GHG**
Chevrolet Impala	26.02	CG	0.110	3.368	0.127	0.007	0.007	0.006	0.013	0.011	333	337
	19.01	CG	0.150	4.609	0.174	0.010	0.009	0.008	0.018	0.015	456	461
	19.23	E85	0.148	4.556	0.172	0.010	0.009	0.002	0.018	0.015	442	447
	14.05	E85	0.203	6.236	0.235	0.013	0.012	0.003	0.024	0.020	606	612
Chevrolet Silverado 1/2-Ton	15.01	CG	0.166	4.514	0.264	0.014	0.013	0.010	0.018	0.014	580	584
	18.71	CG	0.133	3.621	0.212	0.011	0.010	0.008	0.015	0.011	465	469
	11.48	E85	0.217	5.903	0.345	0.018	0.017	0.004	0.024	0.018	744	750
	14.31	E85	0.174	4.735	0.277	0.015	0.014	0.003	0.019	0.015	597	602
Chevrolet Silverado 3/4-Ton	12.00	CG	0.208	5.644	0.330	0.018	0.016	0.012	0.023	0.017	725	731
	10.49	CG	0.237	6.458	0.378	0.020	0.018	0.014	0.026	0.020	829	836
Chevrolet Uplander	18.51	CG	0.135	3.661	0.214	0.011	0.010	0.008	0.015	0.011	470	474
	15.81	CG	0.158	4.284	0.251	0.013	0.012	0.009	0.017	0.013	550	555
Line Truck	6.99	ULSD	0.387	1.225	0.866	0.041	0.038	0.009	0.009	0.036	1298	1309

Table A.5.3: WtP yearly total emissions for baseline vehicles.

	Total Emissions [g]									
Vehicle	**VOC**	**CO**	**NO_x**	**PM_{10}**	**$PM_{2.5}$**	**SO_x**	**CH_4**	**N_2O**	**CO_2**	**GHG**
	101.90	46.51	176.84	27.77	14.63	94.10	491.30	4.17	65607	79132
	139.46	63.66	242.04	38.01	20.02	128.79	672.44	5.70	89796	108306
Chevrolet	182.32	133.81	384.10	182.56	64.91	236.45	961.04	110.83	219899	276954
Impala	249.54	183.15	525.71	249.87	88.84	323.63	1315.36	151.70	300972	379062
	348.63	512.95	1958.25	289.94	158.66	1028.18	5502.98	9.50	717588	857994
Chevrolet	279.66	411.47	1570.84	232.58	127.27	824.77	4414.30	7.62	575625	688254
Silverado	1807.21	1326.37	3807.22	1809.59	643.38	2343.71	9525.89	1098.59	2179653	2745181
1/2-Ton	1449.68	1063.97	3054.02	1451.59	516.10	1880.05	7641.34	881.25	1748443	2202091
Chevrolet	644.26	294.07	1118.14	175.59	92.48	594.97	3106.42	26.35	414823	500336
Silverado										
3/4-Ton	737.24	336.51	1279.51	200.93	105.82	680.84	3554.74	30.15	474691	572545
Chevrolet	281.44	128.46	488.45	76.70	40.40	259.91	1357.02	11.51	181213	218569
Uplander	329.39	150.35	571.67	89.77	47.28	304.19	1588.21	13.47	212085	255805
Line										
Truck [kg]	775.33	1140.76	4355.00	644.81	352.84	2286.60	12238.21	21.13	1595864	1908115

Table A.5.4: PtW yearly total emissions for baseline vehicles.

	Total Emissions [g]									
Vehicle	**VOC**	**CO**	**NO_x**	**PM_{10}**	**$PM_{2.5}$**	**SO_x**	**CH_4**	**N_2O**	**CO_2**	**GHG**
	92.15	2828.79	106.50	6.12	5.67	4.65	11.03	9.06	279813	282790
	126.13	3871.71	145.77	8.37	7.75	6.36	15.09	12.41	382974	387048
Chevrolet	124.67	3827.07	144.09	8.28	7.66	1.83	14.92	12.26	371668	375695
Impala	170.64	5238.04	197.21	11.33	10.49	2.50	20.42	16.78	508694	514206
	824.64	22425.55	1311.40	69.87	64.14	47.68	91.05	68.72	2880330	2903085
Chevrolet	661.50	17989.01	1051.96	56.04	51.45	38.25	73.04	55.12	2310503	2328756
Silverado	1078.38	29325.89	1714.92	91.36	83.87	18.09	119.07	89.86	3698271	3728027
1/2-Ton	865.04	23524.23	1375.65	73.29	67.28	14.51	95.51	72.09	2966627	2990497
Chevrolet	508.45	13827.12	808.58	43.08	39.55	29.40	56.14	42.37	1775951	1789981
Silverado										
3/4-Ton	581.83	15822.66	925.28	49.29	45.25	33.64	64.24	48.49	2032257	2048312
Chevrolet	222.12	6040.30	353.23	18.82	17.28	12.84	24.53	18.51	775815	781944
Uplander	259.96	7069.35	413.40	22.02	20.22	15.03	28.70	21.66	907985	915158
Line										
Truck [kg]	1990.59	6308.63	4455.85	212.84	197.53	46.14	44.41	183.75	6681829	6737696

Table A.5.5: New Vehicle Fleet WtP per-mile emissions.

				Emissions [g/mile]									
Vehicle	**MPG**	**MPGe**	**Electric Medium**	**VOC**	**CO**	**NO_x**	**PM_{10}**	**$PM_{2.5}$**	**SO_x**	**CH_4**	**N_2O**	**CO_2**	**GHG**
	104.8	69.2	Wind	0.030	0.014	0.052	0.008	0.004	0.028	0.145	0.001	19	23
Chevrolet	104.8	69.2	Coal	0.057	0.329	0.415	0.571	0.152	0.750	0.603	0.005	356	372
Volt	104.8	69.2	2010PMix	0.048	0.180	0.285	0.266	0.074	0.379	0.661	0.004	215	233
	N/A	125.8	Wind	0.000	0.000	0.000	0.000	0.000	0.000	0.000	0.000	0	0
Nissan	N/A	125.8	Coal	0.026	0.299	0.345	0.535	0.141	0.686	0.435	0.003	320	332
LEAF	N/A	125.8	2010PMix	0.017	0.158	0.221	0.244	0.066	0.334	0.490	0.003	186	199
Toyota	46.0	46.0	N/A	0.069	0.031	0.119	0.019	0.010	0.063	0.331	0.003	44	53
Prius	46.0	46.0	N/A	0.069	0.031	0.119	0.019	0.010	0.063	0.331	0.003	44	53
Ford	26.8	26.8	N/A	0.118	0.054	0.205	0.032	0.017	0.109	0.568	0.005	76	92
Fusion													
Hybrid	39.0	39.0	N/A	0.081	0.037	0.140	0.022	0.012	0.075	0.390	0.003	52	63
Chevrolet													
Silverado													
Hybrid	21.0	21.0	N/A	0.150	0.069	0.261	0.041	0.022	0.139	0.725	0.006	97	117
	N/A	66.1	Coal	0.049	0.570	0.656	1.018	0.268	1.307	0.828	0.006	609	632
Ford	N/A	66.1	Wind	0.000	0.000	0.000	0.000	0.000	0.000	0.000	0.000	0	0
Transit EV	N/A	66.1	2010PMix	0.032	0.301	0.421	0.465	0.126	0.635	0.932	0.005	354	379

Table A.5.6: New Vehicle Fleet PtW per-mile emissions.

			Electric	Emissions [g/mile]									
Vehicle	**MPG**	**MPGe**	**Medium**	**VOC**	**CO**	**NO_x**	**PM_{10}**	**$PM_{2.5}$**	**SO_x**	**CH_4**	**N_2O**	**CO_2**	**GHG**
	104.8	69.2	Wind	0.034	0.979	0.038	0.002	0.001	0.002	0.004	0.001	87	88
Chevrolet	104.8	69.2	Coal	0.034	0.979	0.038	0.002	0.001	0.002	0.004	0.001	87	88
Volt	104.8	69.2	2010PMix	0.034	0.979	0.038	0.002	0.001	0.002	0.004	0.001	87	88
	N/A	125.8	Wind	0	0	0	0	0	0	0	0	0	0
Nissan	N/A	125.8	Coal	0	0	0	0	0	0	0	0	0	0
LEAF	N/A	125.8	2010PMix	0	0	0	0	0	0	0	0	0	0
Toyota	46.3	46.3	N/A	0.062	1.891	0.071	0.004	0.004	0.003	0.007	0.006	187	189
Prius	46.3	46.3	N/A	0.062	1.891	0.071	0.004	0.004	0.003	0.007	0.006	187	189
Ford	26.8	26.8	N/A	0.107	3.272	0.123	0.007	0.007	0.005	0.013	0.010	324	327
Fusion													
Hybrid	39.0	39.0	N/A	0.073	2.247	0.085	0.005	0.004	0.004	0.009	0.007	222	225
Chevrolet													
Silverado													
Hybrid	21.0	21.0	N/A	0.136	4.173	0.157	0.009	0.008	0.007	0.016	0.013	413	417
Ford	N/A	66.1	Coal	0	0	0	0	0	0	0	0	0	0
Transit	N/A	66.1	Wind	0	0	0	0	0	0	0	0	0	0
EV	N/A	66.1	2010PMix	0	0	0	0	0	0	0	0	0	0

Table A.5.7: New Vehicle Fleet WtP yearly emissions

	Total Emissions [g]									
Vehicle	**VOC**	**CO**	**NO_x**	**PM_{10}**	**$PM_{2.5}$**	**SO_x**	**CH_4**	**N_2O**	**CO_2**	**GHG**
	2530	1155	4392	690	363	2337	12201	104	1629277	1965148
Chevrolet	4787	27619	34863	47975	12802	63027	50664	384	29906731	31287833
Volt	3998	15112	23948	22302	6191	31836	55482	353	18051205	19543280
	0	0	0	0	0	0	0	0	0	0
Nissan	2144	25142	28949	44923	11817	57658	36541	267	26864738	27857750
LEAF	1394	13255	18581	20530	5536	28022	41118	235	15601320	16699360
Toyota	12970	5920	22509	3535	1862	11977	62535	530	8350718	10072156
Prius	28821	13155	50020	7855	4137	26616	138966	1179	18557152	22382570
Ford	14849	6778	25771	4047	2131	13713	71596	607	9560693	11531558
Fusion										
Hybrid	10198	4655	17699	2779	1464	9418	49173	417	6566372	7919980
Chevrolet										
Silverado										
Hybrid	16595	7574	28801	4523	2382	15325	80014	679	10684876	12887482
	5345	62695	72187	112020	29468	143777	91119	665	66989967	69466142
Ford	0	0	0	0	0	0	0	0	0	0
Transit EV	3485	33055	46332	51194	13805	69872	102531	583	38903700	41640709

Table A.5.8: New Vehicle Fleet PtW yearly emissions.

	Total Emissions [g]									
Vehicle	**VOC**	**CO**	**NO_x**	**PM_{10}**	**$PM_{2.5}$**	**SO_x**	**CH_4**	**N_2O**	**CO_2**	**GHG**
	2862	82246	3189	128	118	138	341	121	7346772	7391399
	2862	82246	3189	128	118	138	341	121	7346772	7391399
Chevrolet Volt	2862	82246	3189	128	118	138	341	121	7346772	7391399
	0	0	0	0	0	0	0	0	0	0
	0	0	0	0	0	0	0	0	0	0
Nissan LEAF	0	0	0	0	0	0	0	0	0	0
	11641	357347	13454	773	716	587	1393	1145	35347340	35723386
Toyota Prius	25869	794105	29898	1717	1590	1305	3095	2545	78549645	79385302
	13429	412228	15520	891	826	677	1607	1321	40775893	41209691
Ford Fusion Hybrid	9223	283122	10660	612	567	465	1104	907	28005259	28303195
Chevrolet Silverado Hybrid	15008	460699	17345	996	923	757	1796	1476	45570454	46055259
	0	0	0	0	0	0	0	0	0	0
	0	0	0	0	0	0	0	0	0	0
Ford Transit EV	0	0	0	0	0	0	0	0	0	0

Appendix A.6: Fleet Analysis Differences Tables

Table A.6.1: Nissan Leaf/Chevrolet Impala cost comparison at 21000 miles.

Vehicle	Driving Cost	Liquid Fuel Cost	Electricity Fuel Cost	Total Driving Cost
	[$/mile]	[$]	[$]	[$]
Chevrolet Impala	0.148	3115	0	3115
Nissan LEAF	0.024	0	497	497
DIFFERENCE	**0.125**	**3115**	**(497)**	**2618**

Table A.6.2: Nissan Leaf/Chevrolet Impala emissions comparison at 21000 miles.

Vehicle	VOC	CO	NO_x	PM_{10}	$PM_{2.5}$	SO_x	CH_4	N_2O	CO_2	GHG
	[g]	[g]	[g]	[g]	[g]	[g]	[g]	[g]	[kg]	[kg]
Chevrolet Impala	5423	83798	7625	823	484	2491	12625	226	9022	9405
Nissan LEAF	349	3314	4645	5132	1384	7006	10280	59	3900	4175
DIFFERENCE	**5074**	**80484**	**2980**	**(4309)**	**(900)**	**(4515)**	**2346**	**167**	**5121**	**5230**

Table A.6.3: Toyota Prius/Chevrolet Impala cost comparison at 21000 miles.

Vehicle	Driving Cost	Liquid Fuel Cost	Electricity Fuel Cost	Total Driving Cost
	[$/mile]	[$]	[$]	[$]
Chevrolet Impala	0.148	3115	0	3115
Toyota Prius	0.084	1762	0	1762
DIFFERENCE	**0.064**	**1353**	**0**	**1353**

Table A.6.4: Toyota Prius/Chevrolet Impala emissions comparison at 21000 miles.

Vehicle	VOC	CO	NO_x	PM_{10}	$PM_{2.5}$	SO_x	CH_4	N_2O	CO_2	GHG
	[g]	[g]	[g]	[g]	[g]	[g]	[g]	[g]	[kg]	[kg]
Chevrolet Impala	5423	83798	7625	823	484	2491	12625	226	9022	9405
Toyota Prius	3068	47405	4314	466	274	1409	7142	128	5104	5320
DIFFERENCE	**2355**	**36393**	**3312**	**357**	**210**	**1082**	**5483**	**98**	**3918**	**4084**

Table A.6.5: Ford Fusion Hybrid/Chevrolet Impala cost comparison at 21000 miles.

Vehicle	Driving Cost	Liquid Fuel Cost	Electricity Fuel Cost	Total Driving Cost
	[$/mile]	[$]	[$]	[$]
Chevy Impala	0.148	3115	0	3115
Ford Fusion Hybrid	0.099	2078	0	2078
DIFFERENCE	**0.049**	**1037**	**0**	**1037**

Table A.6.6: Ford Fusion Hybrid/Chevrolet Impala emissions comparison at 21000 miles.

Vehicle	VOC	CO	NO_x	PM_{10}	$PM_{2.5}$	SO_x	CH_4	N_2O	CO_2	GHG
	[g]	[g]	[g]	[g]	[g]	[g]	[g]	[g]	[kg]	[kg]
Chevy Impala	5423	83798	7625	823	484	2491	12625	226	9022	9405
Ford Fusion Hybrid	3618	55913	5088	549	323	1662	8424	151	6020	6275
DIFFERENCE	**1804**	**27885**	**2537**	**274**	**161**	**829**	**4201**	**75**	**3002**	**3130**

Table A.6.7: Chevrolet Silverado Hybrid/Chevrolet Silverado 1/2-Ton cost comparison at 18400 miles.

Vehicle	Driving Cost	Liquid Fuel Cost	Electricity Fuel Cost	Total Driving Cost
	[$/mile]	[$]	[$]	[$]
Chevrolet Silverado 1/2-Ton	0.257	4732	0	4732
Chevrolet Silverado Hybrid	0.219	4038	0	4038
DIFFERENCE	**0.038**	**694**	**0**	**694**

Table A.6.8: Chevrolet Silverado Hybrid/Chevrolet Silverado 1/2-Ton emissions comparison at 18400 miles.

Vehicle	VOC	CO	NO_x	PM_{10}	$PM_{2.5}$	SO_x	CH_4	N_2O	CO_2	GHG
	[g]	[g]	[g]	[g]	[g]	[g]	[g]	[g]	[kg]	[kg]
Chevrolet Silverado 1/2-Ton	7986	131378	15236	1312	793	3784	19469	422	13706	14318
Chevrolet Silverado Hybrid	5887	90982	8279	894	526	2704	13707	245	9795	10211
DIFFERENCE	**2098**	**40396**	**6957**	**418**	**267**	**1080**	**5762**	**177**	**3911**	**4107**

Table A.6.9: Chevrolet Silverado Hybrid/Chevrolet Silverado 3/4-Ton cost comparison at 24500 miles.

Vehicle	Driving Cost	Liquid Fuel Cost	Electricity Fuel Cost	Total Driving Cost
	[$/mile]	[$]	[$]	[$]
Chevrolet Silverado 3/4-Ton	0.322	7878	0	7878
Chevrolet Silverado Hybrid	0.219	5377	0	5377
DIFFERENCE	**0.102**	**2502**	**0**	**2502**

Table A.6.10: Chevrolet Silverado Hybrid/Chevrolet Silverado 3/4-Ton emissions comparison at 24500 miles.

Vehicle	VOC	CO	NO_x	PM_{10}	$PM_{2.5}$	SO_x	CH_4	N_2O	CO_2	GHG
	[g]	[g]	[g]	[g]	[g]	[g]	[g]	[g]	[kg]	[kg]
Chevrolet Silverado 3/4-Ton	13294	218713	25365	2185	1319	6299	32412	702	22817	23837
Chevrolet Silverado Hybrid	7839	121145	11023	1190	700	3601	18252	327	13043	13596
DIFFERENCE	**5455**	**97568**	**14341**	**995**	**619**	**2699**	**14160**	**376**	**9774**	**10240**

Table A.6.11: Ford Transit EV/Chevrolet Uplander cost comparison at 27500 miles.

Vehicle	Driving Cost	Liquid Fuel Cost	Electricity Fuel Cost	Total Driving Cost
	[$/mile]	[$]	[$]	[$]
Chevrolet Uplander	0.209	5736	0	5736
Ford Transit EV	0.045	0	1240	1240
DIFFERENCE	**0.163**	**5736**	**(1240)**	**4496**

Table A.6.12: Ford Transit EV/Chevrolet Uplander emissions comparison at 27500 miles.

Vehicle	VOC	CO	NO_x	PM_{10}	$PM_{2.5}$	SO_x	CH_4	N_2O	CO_2	GHG
	[g]	[g]	[g]	[g]	[g]	[g]	[g]	[g]	[kg]	[kg]
Chevy Uplander	9679	159240	18468	1591	961	4586	23598	511	16613	17355
Ford Transit EV	871	8264	11583	12799	3451	17468	25633	146	9726	10410
DIFFERENCE	**8808**	**150976**	**6885**	**(11208)**	**(2491)**	**(12882)**	**(2035)**	**366**	**6887**	**6945**